POLITECNICO DI MILANO

Facoltà di Ingegneria Industriale

Corso di laurea in Ingegneria Energetica

Heat transfer coefficient and pressure drop in convective boiling and condensation of R134a inside horizontal microfin tubes

Relatore:
Prof. Andrea LUCCHINI

Tesi di Laurea di
Fabio PULCINI
Matr. 858747

Anno Accademico 2017-2018

Questa tesi è dedicata a mio fratello *Mirko*.

Dopo questi lunghi e intensi anni finalmente il giorno è arrivato: scrivere queste frasi di ringraziamento è il tocco finale della mia tesi. È stato un periodo di profondo apprendimento, non solo a livello scientifico, ma anche personale. Vorrei spendere due parole di ringraziamento nei confronti di tutte le persone che mi hanno sostenuto e aiutato durante questo periodo.

Prima di tutto vorrei ringraziare tutti coloro che mi hanno guidato nel progetto di tesi, in particolar modo il professor Andrea Lucchini che mi ha seguito passo dopo passo nella realizzazione di quest'opera, i professori Luigi Colombo e Adriano Muzzio i cui consigli sono sempre stati tanto graditi quanto fondamentali. Un ulteriore ringraziamento va a Thanh Nhan Phan da cui ho imparato molto sull'attività di laboratorio. Mi avete fornito tutti gli strumenti di cui avevo bisogno per intraprendere la strada giusta e portare a compimento la mia tesi.

Un enorme ringraziamento va alla mia famiglia, a mia madre e mio padre che, con il instancabile sostegno, sia morale che economico, mi hanno permesso di arrivare fin qui davanti a voi oggi, contribuendo alla mia formazione personale; a mio fratello, è sempre stato ed è un modello per me e non ci sarà mai un amico più fidato di lui. Un pensiero va a mio nonno Giovanni, spero di averlo reso orgoglioso.

Una caloroso e sincero ringraziamento va alla mia ragazza Giulia, è stata al mio fianco da quando eravamo solo compagni di banco fino a diventare una parte fondamentale della mia vita e del mio futuro. Mi ha sempre sostenuto e spero e confido che continui a farlo a lungo. Tutti i miei amici hanno avuto un peso determinante nel conseguimento di questo risultato, punto di arrivo e contemporaneamente di partenza della mia vita. Grazie per aver condiviso con me in questi anni le esperienze più importanti, vi voglio bene.

Contents

List of Figures

List of Tables

Symbols

Latin symbols

A	$[m^2]$	cross section area
A_k	$[m^2]$	cross section area where k-th phase is present
A_l	$[m^2]$	cross section area occupied by the liquid
A_{ld}		dimensionless liquid cross-sectional area
A_v	$[m^2]$	cross section area occupied by the vapor
A_{vd}		dimensionless vapor cross-sectional area
Bo		boiling number
C_f		friction factor
c_{pl}	$[J/kgK]$	liquid specific heat
c_{pv}	$[J/kgK]$	vapor specific heat
C_s		space correlation coefficient
C_t		time correlation coefficient
c_w	$[J/kgK]$	demineralized water specific heat
d	$[m]$	tube diameter
d_f	$[m]$	maximum internal diameter at the base of the microfin tube
d_i	$[m]$	tube internal diameter
d_i	$[m]$	tube internal mean diameter
D_{kn}	$[m^n]$	n-dimension domain where is present the k-th phase
D_n	$[m^n]$	n-dimension domain
d_r	$[m]$	tube diameter at fin root
d_{tip}	$[m]$	tube diameter at fin tip
$\left(\frac{dp}{dz}\right)_v$	$[Pa/m]$	unit length pressure drop for vapor flow
d_{tip}	$[m]$	inner diameter measured at the fin tip
E		enhancement factor
E		high order terms

e_f	$[m]$	microfin height
E_{fin}		finned tube enhancement factor
f		friction factor
f		generic quantity
$\mathbf{F}$	$[N/kg]$	external forces per unit of mass
F_{fl}		parameter depending on the fluid, it is equal to 1.63 for R134a
f_l	$[kg/m^3]$	liquid friction factor
Fr_l		liquid Froude number
Fr_{lo}		liquid only Froude number
Fr_{om}		homogeneous Froude number
Fr_{So}		Froude number with Soliman notation
Fr_v		vapor Froude number
Fr_{vo}		vapor only Froude number
$f_{tp,m}$		two-phase friction factor for microfin
f_v	$[kg/m^3]$	vapor friction factor
g	$[m/s^2]$	gravity acceleration
G	$[kg/m^2s]$	mass flux
Ga_l		liquid Galileo number
$\dot{g}_i$	$[kg/m^2s]$	mass transfer per unit interface area and per unit of time
h	$[m]$	height of the completely stratified liquid layer
h	$[W/m^2K]$	mean heat transfer coefficient
h	$[J/kg]$	specific enthalpy
h_{cb}	$[W/m^2K]$	convective flow boiling heat transfer coefficient
h_d	$[W/m^2K]$	heat transfer coefficient independent of the dependent zone for microfin
h_{ds}	$[W/m^2K]$	heat transfer coefficient independent of the dependent zone for smooth tube
h_{eb}	$[W/m^2K]$	heat transfer coefficient for static boiling
h_i	$[W/m^2K]$	heat transfer coefficient independent of the independent zone for microfin
h_{is}	$[W/m^2K]$	heat transfer coefficient independent of the independent zone for smooth tube
h_l	$[W/m^2K]$	heat transfer coefficient for single phase liquid flow
h_l	$[J/kg]$	liquid refrigerant enthalpy
h_{ld}		dimensionless height of the completely stratified liquid layer
h_{tp}	$[W/m^2K]$	two-phase heat transfer coefficient

h_{lv}	$[J/kg]$	latent heat of phase change
h_m	$[J/kg]$	inlet mixture enthalpy
h_{mf}	$[W/m^2K]$	local microfin flow boiling heat transfer coefficient
h_{nb}	$[W/m^2K]$	heat transfer coefficient obtained with Cooper dimensional nucleate pool boiling correlation for pure fluids
h_{pb}	$[W/m^2K]$	pool boiling heat transfer coefficient
h_{sl}	$[J/kg]$	saturated liquid enthalpy at the temperature inlet
h_{sl}	$[J/kg]$	saturated liquid refrigerant enthalpy
h_{sl}	$[J/kg]$	saturated liquid specific enthalpy
h_{sv}	$[J/kg]$	saturated vapor specific enthalpy
h_{sv}	$[J/kg]$	saturated vapor refrigerant enthalpy
h_v	$[J/kg]$	vapor refrigerant enthalpy
j		counter denoting the j-th interface passing through $\mathbf{x}$ during the interval T
j_k	[m/s]	local volumetric flux
J_k	[m/s]	superficial velocity of the k-th phase
$j_v^\star$		dimensionless vapor velocity
Ja		Jakob number
Ja_l		liquid Jacob number
j_l^{corr}	$[m/s]$	modified superficial velocity
j_v^{corr}	$[m/s]$	modified superficial velocity
j_l	$[m/s]$	superficial velocity
j_v	$[m/s]$	superficial velocity
J_v		dimensionless vapor velocity
k		phase index
k	$[m]$	surface roughness
k_l	$[W/mK]$	liquid thermal conductivity
k_v	$[W/mK]$	vapor thermal conductivity
L	$[m]$	tube length
l_f		liquid void fraction
$\dot{M}$	$[kg/s]$	refrigerant mass flow rate
$\dot{M}$	$[kg/s]$	total mass flow rate
$\overline{\dot{m}}$	$[kg/s]$	total mass flow rate
$\dot{m}_k$	$[kg/s]$	mass flow rate of k-th phase
$\dot{m}_l$	$[kg/s]$	liquid refrigerant mass flow rate
M_m	$[kg/kmol]$	molecular mass
M_m	$[kg/kmol]$	refrigerant molar mass

$\dot{m}_{ref}$	$[kg/m^2s]$	reference value of mass flux introduced to non-dimensionalize the expression $\dot{m}_{ref} = 500kg/m^2s$
$\dot{m}_w$	$[kg/s]$	demineralized water mass flow rate
$\dot{m}_v$	$[kg/s]$	vapor refrigerant mass flow rate
$\mathbf{n}$		normal unit vector
n		number of independent variables
n_g		number of grooves
n_o		optimal number of grooves
Nu		Nusselt number
Nu_b		Nusselt number for stratified flow
Nu_{cv}		Nusselt number due to convective heat transfer
Nu_f		Nusselt number for convective condensation
Nu_f		Nusselt number due to film condensation
p	$[Pa]$	pressure
P	$[m]$	wet perimeter
p_0	$[Pa]$	mixer inlet pressure
p_c	$[Pa]$	critical pressure
p_f	$[m]$	axial pitch from fin to fin
P_i	$[m]$	length of the phase interface
P_{id}		dimensionless length of the phase interface
p_{in}	$[Pa]$	inlet refrigerant pressure
P_l	$[m]$	wet perimeter of the tube
P_{ld}		dimensionless wet perimeter of the tube
p_r		reduced pressure
Pr_l		liquid Prandtl number
p_{rm}	$[Pa]$	modified reduced pressure
Pr_v		vapor Prandtl number
P_v	$[m]$	dry perimeter in contact with vapor
P_{vd}		dimensionless dry perimeter in contact with vapor
$\mathbf{q}$	$[W/m^2]$	heat flux
q	$[W/m^2]$	heat flux
$\dot{Q}$	$[W]$	heat exchanged
Re		Reynolds number
Re_l		liquid Reynolds number
Re_{lo}		liquid only Reynolds number
Re_v		vapor Reynolds number
Re_{vo}		vapor only Reynolds number

S	$[m^2]$	exchanging surface
S	$[m^2]$	exchanging surface at the fin base
S	$[m^2]$	exchanging surface, referred to the inner diameter
t	$[s]$	time
t_0	$[s]$	reference time
T	$[K]$	mean refrigerant temperature
T	$[K]$	temperature
$\tilde{\mathbf{T}}$	$[Pa]$	stress tensor
T_0	$[K]$	mixer inlet temperature
T_0	$[K]$	reference temperature
T_c	$[K]$	critical temperature
T_{in}	$[K]$	inlet refrigerant temperature
T_{in}	$[K]$	inlet temperature
T_{in}	$[K]$	refrigerant inlet temperature
T_{out}	$[K]$	outlet refrigerant temperature
T_r	$[K]$	refrigerant temperature
T_s	$[K]$	mean surface temperature
T_{sat}	$[K]$	refrigerant saturation temperature at pressure p
T_{sub}	$[K]$	subcooling temperature
T_w	$[K]$	wall temperature
$T_{w,in}$	$[K]$	demineralized water inlet temperature
$T_{w,out}$	$[K]$	demineralized water outlet temperature
u	$[J/kg]$	internal energy per unit of mass
$U_{\Delta T}$	$[K]$	temperature difference absolute uncertainty
$U_{\Delta T_w}$	$[K]$	temperature difference absolute uncertainty
u_f		relative uncertainty
U_f		absolute uncertainty
u_i		relative uncertainty of the i-th quantity
$u_{\dot{m}_l}$		liquid refrigerant mass flow rate relative uncertainty
$u_{\dot{m}_v}$		vapor refrigerant mass flow rate relative uncertainty
U_p	$[Pa]$	pressure transducer absolute uncertainty
$U_{\dot{Q}}$	$[W]$	heat absolute uncertainty
U_S	$[m^2]$	surface absolute uncertainty

U_T	$[K]$	thermocouples absolute uncertainty
$U_{\dot{V_w}}$	$[m^3/s]$	heat absolute uncertainty
U_{x_i}		measured quantity absolute uncertainty
$U_{x_{in}}$		inlet vapor quality absolute uncertainty
U_y		dependent quantity absolute uncertainty
v	$[m/s]$	mean flow velocity
$\overline{v}$	$[m^3/kg]$	mean specific volume
$\mathbf{v}$	$[m/s]$	velocity
$\overline{\dot{V}}$	$[m^3/s]$	total volumetric flow rate
$\mathbf{v}_i$	$[m/s]$	interface velocity
$\dot{V}_k$	$[m^3/s]$	instantaneous volumetric flow rate of k-th phase
$v_{k,a}$	$[m/s]$	axial component velocity of k-th phase
v_l	$[m^3/kg]$	liquid specific volume
v_v	$[m^3/kg]$	vapor specific volume
$\dot{V}_w$	$[m^3/s]$	demineralized water volume flow rate
$\dot{V}_w$	$[m^3/s]$	demineralized water volumetric flow rate
We		Weber number
We_{om}		homogeneous Weber number
$\mathbf{x}$	$[m]$	position vector
x		quality
X		abscissa correction factor
X^2		Lockhart-Martinelli parameter
x_i		independent variables: measured quantity
x_{in}		inlet vapor quality
x_{out}		outlet vapor quality
X_{tt}		Lockhart-Martinelli parameter
y		dependent quantity
Y		ordinate correction factor

Greek symbols

α_f	$[^\circ]$	helix angle of the microfins
β	$[rad]$	apex angle
δ	$[m]$	annular liquid film thickness
Δp	$[Pa]$	pressure drop between inlet and outlet
δp_A	$[Pa]$	acceleration pressure drop
Δt	$[s]$	time interval
ΔT	$[K]$	temperature difference
ΔT_{ml}	$[K]$	logarithmic mean temperature
ΔT_w	$[K]$	demineralized water temperature difference
Δx		quality variation
ϵ		void fraction

ϵ_c		parameter
ϵ_{c1}		parameter
ϵ_{c2}		parameter
ϵ_{in}		inlet void fraction
ϵ_{out}		outlet void fraction
Φ_k^2		two-phase multiplier
Φ_l		liquid two-phase multiplier
Φ_l		liquid two-phase multiplier
Φ_v		vapor two-phase multiplier
λ	$[J/kg]$	latent heat of phase change
μ	$[kg/ms]$	equivalent viscosity
μ	$[kg/ms]$	viscosity
μ_l	$[kg/ms]$	liquid viscosity
μ_v	$[kg/ms]$	vapor viscosity
ρ	$[kg/m^3]$	density
ρ_a	$[kg/m^3]$	air density
ρ_l	$[kg/m^3]$	liquid density
ρ_{om}	$[kg/m^3]$	homogeneous density
ρ_v	$[kg/m^3]$	vapor density
ρ_w	$[kg/m^3]$	demineralized water density
ρ_w	$[kg/m^3]$	water density
σ	$[N/m]$	surface tension
τ_w	$[Pa]$	averaged wall shear stress
ψ	$[W/m^2]$	heat flux density at the wall

Abstract

This thesis consists in an experimental analysis on the heat transfer performances of a circular heat exchanger. The refrigerant R134a flows in a horizontal microfin copper tube, where exchanges thermal power with demineralized water flowing in counter-current. Heat transfer process is evaluated through the heat transfer coefficient and pressure drop.

All the experiments were conducted on two-phase flow, so that the fluid reaching the test section is composed by both liquid and vapor phases. Heat exchange in the test section can be set so that to provide both condensation or evaporation of the refrigerant, the two cases are analyzed in this thesis. Homogeneous and flow pattern models are considered for the analysis.

A further analysis on the heat transfer consists on the comparison between collected data and correlations developed to predict heat transfer coefficient or pressure drop. The last topic of this thesis aims to evaluate correlation capability to predict experimental data.

Chapter 1

Introduction

Nowadays processes where liquid and vapor appear and interact themselves are commonly usual in industry, e.g. refrigeration and air conditioning systems, power engineering and other thermal processing plants. Thus, this kind of flow has an important role in many technological applications and it is necessary a deep study and knowledge of its performance and characteristics. In the last decades two-phase flow in horizontal tubes has been subject of studies aimed to improve the characteristic of the device, the design and the optimization of these systems focuses on:

- improvement of heat transfer rate, to reduce size and cost of heat exchangers;
- reduce the pressure drop inside the pipe, to decrease the pumping power and component stresses.

Compact heat exchangers are beneficial to charge inventory and leakage of refrigerant, and to improve energy efficiency and safety. These targets are all aimed at cost reduction, indeed heat exchanger design is subordinate to economical considerations. For heat exchangers, the heat transfer rate can be computed with the following equation:

$$\dot{Q} = UA\Delta T_{ml} \tag{1.1}$$

where:			
	Q	$[W]$	exchanged thermal power;
	U	$[W/m^2K]$	overall heat transfer coefficient;
	A	$[m^2]$	heat transfer surface area;
	ΔT_{ml}	$[K]$	logarithmic mean temperature difference;

Demand for high-efficiency and compact heat exchangers leads to the development of enhanced surface geometry and refrigerant mixtures, designed in order to increase either or both the heat transfer coefficient and the heat transfer surface area, relative to that given plain surface. In order to evaluate the improvement process, an objective function that considers both exchanged thermal power and pressure drop must be maximized. For examples, the improved design of the heat exchanger may be required for the attainment of the following aims:

1. *Size reduction*: if the thermal power and ΔT_{ml} is kept constant, the heat exchanger size may be reduced thanks to the increase of U $[W/m^2K]$;
2. *Temperature difference reduction*: if thermal power and size are held constant the mean temperature difference may be reduced, this provides increased thermodynamic process efficiency and yields a saving of operating cost;

3. *Exchanged heat increase*: keeping the size and inlet temperatures constant, increase of overall heat transfer coefficient results in increased exchanged thermal power.

Heat transfer inside horizontal tubes is a common application in chemical processes and power industries and heat exchange improvement is subject of studies. Researchers are focusing on different techniques to respond to the challenge:

- production of new enhanced refrigerant fluids, that respect environmental restriction maintaining high thermal exchange properties. **R134a** is one of the most common fluid for refrigeration applications, recently commercial production of *R1234ze* and *R1234zf* has been started. Their properties are still object of studies but they are anticipated to be the refrigerants of choice for high-temperature heat pump systems in industrial applications;
- enhance tubes geometry:
  - to improve energy transport using devices that promote mixing;
  - rough duct surfaces, that increase turbulence without affecting the main flow significantly;
  - fined surfaces.

In the last decades many researchers focused performances improvement, taking into account different aspects, such as global warming potential, chemical stability, safety in working conditions. Hence, the heat exchange process of the fluids has to be deeply analyzed, in particular the focus falls on evaluating the refrigerant performances undergoing phase change.

The refrigerant behavior is affected not only by the characteristics of its molecule, but also by the tube shape. Hence, the choice of tube geometry (micro-fin, rough or conventional) is directly responsible for heat exchangers performances in the same way of the refrigerant choice. Micro-fin tubes are widely used in industrial air-conditioning applications. The reason of the success is that they are more effective than conventional tubes in heat transfer, however they causes an increase of pressure drop so their usage has to be evaluated case by case. It has been demonstrated that the advantages, linked to the enhanced heat transfer, overcome the drawback related to the increase of pressure drop. This condition is obtained under appropriate ranges of operating conditions. The best approach to analyze and distinguish operation condition occurring during two-phase heat exchange is the so called flow regime method: a different model is used to describe the fluid for every different phases distribution (flow pattern) inside the tube.

The aims of the thesis are:

- to evaluate experimentally heat transfer coefficient and pressure drop of two-phase flow in horizontal micro-fin and smooth tube;
- to make a comparison between smooth and micro-fin tubes heat exchange performances, both in evaporation and condensation operating condition;
- to check the capability of correlations to predict heat exchanger behavior;

Chapter 2

Basic two-phase flow theory

2.1 Introduction to boiling and condensation processes

Collier and Thome [1] stated that "convective boiling is defined as the being the addition of heat to a flowing liquid", such that whole the fluid or just a portion is subjected to a phase change. Pressure reduction processes could lead to the same result, but they are excluded from this definition. Condensation is conversely defined as the removal of thermal power from the system, in such a way the vapor is converted into liquid. The heat transfer causes variation in the amount and distribution of each phase, that provokes the flow pattern alteration. Local heat transfer process and, coherently, thermal and physical properties of the fluid are mainly influenced by the flow pattern. Studies reported that, to better analyze heat transfer processes in two-phase flows, it is necessary to develop models that accurately describe flow patterns properties and their relative transition conditions.

2.1.1 Methods of analysis

The analysis of two-phase flow occurs through development and solution of basic equations governing the conservation of mass, momentum, and energy of the considered system. Physical models and assumptions aims to simplify these equations. Three types of assumption have been made:

1. *the 'homogeneous' flow model.* This is the simplest approach, two-phase flow is assumed to be a single-phase flow having weighted average properties between the phases;

2. *the 'separated' flow model.* The two phases are considered separated, so that it is possible to write the equations for both of them. Additional information concerning the interaction with both the phase must be taken into account;

3. *the 'flow pattern' model.* The flow pattern is characterized by phase distribution in the channel, pre-defined geometries are exploited to distinguish a pattern from the others. These geometries are based on configurations or flow patterns in a channel. The basic equations are solved within the framework of each idealized representation.

All the equations are studied starting from the local instantaneous formulation. A mathematical re-arrangement of conservation equations is provided, by means of time and space averaging

operators and appropriate assumptions, in order to get the final set of equations that describes the heat transfer in horizontal two-phase flow.

2.2 Local instantaneous equations

Local balance laws at point **x** are expressed in terms of partial differential equations if point **x** does not belong to a surface of discontinuity, otherwise the local balance laws are then formulated in therms of jump conditions which relate the values of the flow parameters on both sides of the surface of discontinuity [2]. In two-phase flow interfaces can be considered as surfaces of discontinuity.

Denoting with the index k the phases:
k=1 $\Rightarrow$ liquid
k=2 $\Rightarrow$ vapor
The local instantaneous balance equations in each phase are:

- mass:
$$\frac{\partial \rho_k}{\partial t} + \nabla \cdot (\rho_k \mathbf{v}_k) = 0 \tag{2.1}$$

- momentum:
$$\frac{\partial \rho_k \mathbf{v}_k}{\partial t} + \nabla \cdot (\rho_k \mathbf{v}_k \mathbf{v}_k) - \rho_k \mathbf{F} - \nabla \cdot (\tilde{\mathbf{T}}_k) = 0 \tag{2.2}$$

- angular momentum:
$$\tilde{\mathbf{T}}_k = \tilde{\mathbf{T}}_k^t \tag{2.3}$$

- energy:
$$\begin{aligned} &\frac{\partial}{\partial t}\left[\rho_k \left(\frac{v_k^2}{2} + u_k\right)\right] + \nabla \cdot \left[\rho_k \left(\frac{v_k^2}{2} + u_k\right) \mathbf{v}_k\right] + \\ &- \rho_k \mathbf{F} \cdot \mathbf{v}_k - \nabla \cdot (\tilde{\mathbf{T}}_k \cdot \mathbf{v}_k) + \nabla \cdot \mathbf{q}_k = 0 \end{aligned} \tag{2.4}$$

The local instantaneous equations at the interface are:

- mass:
$$\sum_{k=1}^{2} \rho_k (\mathbf{v}_k - \mathbf{v}_i) \cdot \mathbf{n}_k = \sum_{k=1}^{2} \dot{g}_k = 0 \tag{2.5}$$

- momentum (in absence of surface tension):
$$\sum_{k=1}^{2} (\dot{g}_k \mathbf{v}_k - \mathbf{n}_k \cdot \tilde{\mathbf{T}}_k) = 0 \tag{2.6}$$

- energy:
$$\sum_{k=1}^{2} \left[\dot{g}_k \left(\frac{v_k^2}{2} + u_k\right) + \mathbf{q}_k \cdot \mathbf{n}_k - (\mathbf{n}_k \cdot \tilde{\mathbf{T}}_k) \cdot \mathbf{v}_k\right] = 0 \tag{2.7}$$

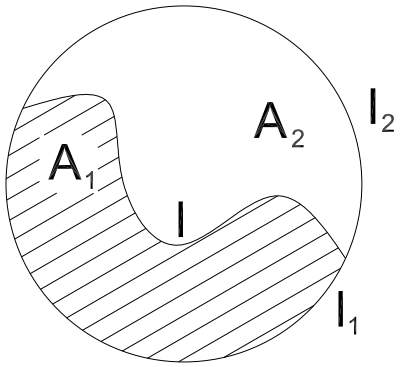

Figure 2.1: Phases in a circular duct

where:	ρ	$[kg/m^3]$	density;
	$\mathbf{v}$	$[m/s]$	velocity;
	$\mathbf{F}$	$[N/kg]$	external forces per unit of mass;
	$\tilde{\mathbf{T}}$	$[Pa]$	stress tensor;
	u	$[J/kg]$	internal energy per unit of mass;
	$\mathbf{q}$	$[W/m^2]$	heat flux;
	$\mathbf{v}_i$	$[m/s]$	interface velocity;
	$\mathbf{n}$		interface unit normal vector outwardly directed;
	$\dot{g}$	$[kg/m^2s]$	mass transfer per unit interface area and unit time;
	k		phase index.

In almost every case the position of the interface is unknown and it is impossible to apply the Navier-Stokes equations because there is no way to give a right formulation of the transport term between the phases. That is such a complex problem that it is not possible a straight solution of the Navier-Stokes problem. It is necessary to formulate the problem in a simpler way. The easiest way to do this is passing from local instantaneous equation to averaged equations.

2.3 Parameters of two-phase flow in a pipe

A two-phase flow is characterized by fluctuating behavior, to simplify Navier-Stokes equations averaging operators, acting on space and time, are required.

2.3.1 Phase density function

The presence or absence of the phase k at a given point $\mathbf{x}$ and a given time t is characterized by the phase density function defined:

$$P_k(\mathbf{x},t) = \begin{cases} 1 & \text{if point } \mathbf{x} \text{ pertains to phase k} \\ 0 & \text{if point } \mathbf{x} \text{ does not pertain to phase k} \end{cases} \tag{2.8}$$

2.3.2 Instantaneous space-averaging operators

Instantaneous field variables may be averaged over a n-dimension domain:
n=1 ⇒ line
n=2 ⇒ area
n=3 ⇒ volume
At a given time, this n-dimension domain can be divided in subdomains such that:

$$\emptyset = D_{n,j} \cap D_{n,k} \qquad j \neq k \tag{2.9}$$

$$D_n = \bigcup_{k=1}^{2} D_{n,k} \tag{2.10}$$

where: D_n n-dimension domain;
$D_{n,k}$ n-dimension domain where is present the k-th phase.

In the following area average quantity will be considered, so the development of averaging operators will be for n equal to 2 Consequently two different instantaneous space averaging operators are introduced:

$$< \cdot >_n = \frac{1}{A} \int_{D_n} \cdot \, dD \tag{2.11}$$

$$< \cdot >_{n,k} = \frac{1}{A_k} \int_{D_{n,k}} \cdot \, dD \tag{2.12}$$

where: A $[m^2]$ cross section area;
A_k $[m^2]$ cross section area where k-th phase is present.
The main quantities coming from the averaging operators defined are:

- instantaneous space fraction

$$\epsilon_k = < P_k(\mathbf{x}, t) >_2 = \frac{A_k}{A} \tag{2.13}$$

- instantaneous volumetric flow rate

$$\dot{V}_k = \int_{D_{2,k}} v_{k,a} dD = A\epsilon_k < v_{k,a} >_{2,k} \tag{2.14}$$

where: $\dot{V}_k$ $[m^3/s]$ volumetric flow rate of k-th phase;
$v_{k,a}$ $[m/s]$ axial component velocity of k-th phase.

- instantaneous mass flow rate

$$\dot{M}_k = \int_{D_{2,k}} \rho_k v_{k,a} dD = A\epsilon_k < \rho_k v_{k,a} >_{2,k} \tag{2.15}$$

where: $\dot{M}_k$ $[kg/s]$ mass flow rate of k-th phase.

2.3.3 Local time-averaging operators

The local field variables can be averaged over a time interval, whose magnitude T must be chosen:

- large enough compared with the time scale of the turbulence fluctuations;
- small enough compared with the time scale of the overall flow fluctuations.

In a given point $\mathbf{x}$ of a two-phase flow, the k-th phase passes this point intermittently and a field variable $f_k(\mathbf{x},t)$ is a piecewise continuous function. Denoting by $T_k(\mathbf{x},t)$ the cumulated time of the k-th phase is within the interval T, it is possible to define two different local time averaging operators:

$$\overline{\cdot} = \frac{1}{T}\int_{t_0}^{t_0+T} \cdot\, dt \tag{2.16}$$

$$\overline{\cdot}^{\,k} = \frac{1}{T_k}\int_{t_0}^{t_0+T_k} \cdot\, dt \tag{2.17}$$

The local time fraction is defined as:

$$\alpha_k(\mathbf{x},t) = \overline{P_k(\mathbf{x},t)} = \frac{T_k(\mathbf{x},t)}{T} \tag{2.18}$$

2.3.4 commutativity of averaging operators

By the definitions, the following identity holds:

$$\overline{P_{n,k} < f_k >_{n,k}} =< \alpha_k \overline{f_k}^{\,k} >_n \tag{2.19}$$

As a consequence, the time-averaged volumetric and mass flow rates can be expressed in the following ways:

$$\overline{\dot{V}_k} = A\overline{\epsilon_k < v_{k,a} >_{2,k}} = A < \alpha_k \overline{v_{k,a}}^{\,k} >_2 \tag{2.20}$$

$$\overline{\dot{M}_k} = A\overline{\epsilon_k < \rho_k v_{k,a} >_{2,k}} = A < \alpha_k \overline{\rho_k v_{k,a}}^{\,k} >_2 \tag{2.21}$$

2.3.5 Qualites

The mass velocity is defined as:

$$\overline{G} = \frac{\overline{\dot{M}}}{A} \tag{2.22}$$

where: G $[kg/m^2 s]$ total mass flux.

The quality is defined as:

$$x = \frac{\overline{\dot{M}_2}}{\overline{\dot{M}}} \tag{2.23}$$

It is impossible to measure or to calculate with high precision the quality of a liquid-vapor mixture flowing in a heated channel and withstanding a phase change. nevertheless, a fictitious quality (equilibrium or thermodynamic quality) can be calculated by assuming that both phases are flowing in saturation conditions.

2.3.6 Volumetric qualities

The volumetric quality is defined as:

$$\beta = \frac{\overline{\dot{V}_2}}{\overline{\dot{V}}} \tag{2.24}$$

where: $\overline{\dot{V}}$ $[m^3/s]$ total volumetric flow rate.
The local volumetric flux is define ad:

$$j_k = \overline{P_k v_{k,a}} = \alpha_k \overline{v_{k,a}}^k \tag{2.25}$$

The superficial velocity is defined as:

$$J_k = < j_k >_2 = \frac{\overline{\dot{V}_k}}{A} = \frac{x_k \overline{\dot{M}_k}}{\rho_k} \tag{2.26}$$

The mixture superficial velocity is defined as:

$$J = \sum_{k=1}^{2} J_k \tag{2.27}$$

2.4 Composite averaged equations

The importance of composite space/time- or time/space- averaged equations is considerable, since all the practical problem of two-phase flow in channels are dealt with using these equations. It is possible to demonstrate the equivalence of the results obtained with one or the other of these methods. The time-average over an interval T of the instantaneous area-averaged balance equations brings to:

- *mass balance*

$$\frac{\partial}{\partial t}\overline{A_k < \rho_k >_{2,k}} + \frac{\partial}{\partial z}\overline{A_k < \rho_k v_{k,a} >_{2,k}} = -\overline{\int_{l(z,t)} \dot{m}_k \frac{dl}{\mathbf{n}_k \cdot \mathbf{n}_{k,l}}} \tag{2.28}$$

- *momentum balance*

$$\begin{aligned} &\frac{\partial}{\partial t}\overline{A_k < \rho_k v_{k,a} >_{2,k}} + \frac{\partial}{\partial z}\overline{A_k < \rho_k v_{k,a}^2 >_{2,k}} - \overline{A_k < \rho_k F_z >_{2,k}} + \\ &\quad + \overline{A_k \frac{\partial p_k}{\partial z}} - \frac{\partial}{\partial z}\overline{A_k < (\mathbf{n}_z \cdot \tilde{\tau}_k) \cdot \mathbf{n}_z >_{2,k}} = \\ &= \overline{\int_{l(z,t)} \mathbf{n}_z (\mathbf{n}_k \cdot \tilde{\tau}_k) \frac{dl}{\mathbf{n}_k \cdot \mathbf{n}_{k,l}}} + \\ &\quad - \overline{\int_{l(z,t)} \mathbf{n}_z (\dot{m}_k \mathbf{v}_k - \mathbf{n}_k \cdot \tilde{\tau}_k) \frac{dl}{\mathbf{n}_k \cdot \mathbf{n}_{k,l}}} \end{aligned} \tag{2.29}$$

- *energy balance*

$$\begin{aligned}
&\frac{\partial}{\partial t}\overline{A_k < \rho_k \left(\frac{v_k^2}{2} + u_k\right) >_{2,k}} + \\
&\quad + \frac{\partial}{\partial z}\overline{A_k < \rho_k \left(\frac{v_k^2}{2} + i_k\right) v_{k,a} >_{2,k}} + \\
&\quad - \overline{A_k < \rho_k \mathbf{F} \cdot \mathbf{v}_k >_{2,k}} + \\
&\quad - \frac{\partial}{\partial z}\overline{A_k < (\tilde{\tau}_k \cdot \mathbf{v}_k) \cdot \mathbf{n}_z >_{2,k}} - \frac{\partial}{\partial z}\overline{A_k < \mathbf{q}_k \cdot \mathbf{n}_z >_{2,k}} = \\
&= -\overline{\int_{l(z,t)} \mathbf{q}_k \cdot \mathbf{n}_k \frac{dl}{\mathbf{n}_k \cdot \mathbf{n}_{k,l}}} + \\
&\quad - \overline{\int_{l(z,t)} \left[\dot{m}_k \left(\frac{v_k^2}{2} + u_k\right) - (\tilde{\mathbf{T}}_k \cdot \mathbf{v}_k) \cdot \mathbf{n}_k + \mathbf{q}_k \cdot \mathbf{n}_k\right] \frac{dl}{\mathbf{n}_k \cdot \mathbf{n}_{k,l}}}
\end{aligned} \tag{2.30}$$

2.5 Frictional pressure drop

The calculation of two-phase pressure drop is an essential issue in many industrial applications. The knowledge of the interaction laws between the phases or between the two-phase mixture and the wall basically relies on experimental evidence. The frictional pressure drop is not usually measured directly, the magiority of the experimental data provides values of the total pressure drop. A void fraction measurement or evaluation is needed to determine the acceleration and gravity pressure drop to be subtracted from the total pressure drop to get the frictional component.

2.5.1 Simplified balance equations

The averaging operators defined over a cross section area (eq. 2.11) and over a time interval (eq. 2.16) give averages of products which can be expressed as a function of the product of the averages by means of correlation coefficient:

$$< fg >= C_s < f >< g > \tag{2.31}$$

where: C_s space correlation coefficient.

$$\overline{fg} = C_t \overline{f}\,\overline{g} \tag{2.32}$$

where: C_t time correlation coefficient.

In the present state of knowledge, the following hypothesis are introduced:

1. the space correlation coefficients are equal to 1;
2. the time correlation coefficients are equal to 1;
3. the equation of state valid for local quantities applies to averaged quantities;
4. longitudinal conduction terms in each phase as well as their derivatives are negligible;
5. the phase viscous stress derivatives and the power of these viscous stresses are negligible;

6. the flow is symmetrical with respect to a straight line.

It follows:

- *mass balance*
  - phase equation

$$\frac{\partial}{\partial t}(\epsilon_k \rho_k) + \frac{\partial}{\partial z}(\epsilon_k \rho_k v_{k,z}) = -\frac{1}{A}\overline{\int_{l(z,t)} \dot{g}_k \frac{dl}{\mathbf{n}_k \cdot \mathbf{n}_{k,l}}} \tag{2.33}$$

  - mixture equation

$$\sum_{k=1}^{2}\left[\frac{\partial}{\partial t}(\epsilon_k \rho_k) + \frac{\partial}{\partial z}(\epsilon_k \rho_k v_{k,z})\right] = 0 \tag{2.34}$$

- *momentum balance*
  - phase equation

$$\begin{aligned}\frac{\partial}{\partial t}(\epsilon_k \rho_k v_{k,z}) + \frac{\partial}{\partial z}(\epsilon_k \rho_k v_{k,z}^2) - \epsilon_k \rho_k F_z + \epsilon_k \frac{\partial p}{\partial z} = \\ = -\frac{1}{A}\overline{\int_{l(z,t)} \mathbf{n}_z \cdot (\dot{g}_k \mathbf{v}_k - \mathbf{n}_k \cdot \tau_k)\frac{dl}{\mathbf{n}_k \cdot \mathbf{n}_{k,l}}} + \\ + \frac{1}{A}\overline{\int_{l_k(z,t)} \mathbf{n}_z \cdot (\mathbf{n}_k \cdot \tilde{\tau}_k)\frac{dl}{\mathbf{n}_k \cdot \mathbf{n}_{k,l}}}\end{aligned} \tag{2.35}$$

  - mixture equation

$$\begin{aligned}\sum_{k=1}^{2}\left[\frac{\partial}{\partial t}(\epsilon_k \rho_k v_{k,z}) + \frac{\partial}{\partial z}(\epsilon_k \rho_k v_{k,z}^2) - \epsilon_k \rho_k F_z\right] + \frac{\partial p}{\partial z} = \\ = \frac{1}{A}\left(\sum_{k=1}^{2}\overline{\int_{l_k(z,t)} \mathbf{n}_z \cdot (\mathbf{n}_k \cdot \tilde{\tau}_k)\frac{dl}{\mathbf{n}_k \cdot \mathbf{n}_{k,l}}}\right)\end{aligned} \tag{2.36}$$

- *energy balance*
  - phase equation

$$\begin{aligned}\frac{\partial}{\partial t}\left[\epsilon_k \rho_k \left(\frac{v_k}{2} + i_k\right)\right] + \frac{\partial}{\partial z}\left[\epsilon_k \rho_k \left(\frac{v_k}{2} + i_k\right) v_{k,z}\right] + \\ - \epsilon_k \rho_k \mathbf{F} \cdot \mathbf{v}_k - \epsilon_k \frac{\partial p}{\partial t} = \\ = -\frac{1}{A}\overline{\int_{l(z,t)} \left[\dot{g}_k \left(\frac{v_k}{2} + i_k\right) - (\tilde{\tau}_k \cdot \mathbf{v}_k) \cdot \mathbf{n}_k + \mathbf{q}_k \cdot \mathbf{n}_k\right] \frac{dl}{\mathbf{n}_k \cdot \mathbf{n}_{k,l}}} + \\ - \frac{1}{A}\overline{\int_{l_k(z,t)} \mathbf{q}_k \cdot \mathbf{n}_k \frac{dl}{\mathbf{n}_k \cdot \mathbf{n}_{k,l}}}\end{aligned} \tag{2.37}$$

– mixture equation

$$\sum_{k=1}^{2}\left\{\frac{\partial}{\partial t}\left[\epsilon_k\rho_k\left(\frac{v_k}{2}+u_k\right)\right]+\frac{\partial}{\partial z}\left[\epsilon_k\rho_k\left(\frac{v_k}{2}+i_k\right)v_{k,z}\right]+ -\epsilon_k\rho_k\mathbf{F}\cdot\mathbf{v}_k-\epsilon_k\frac{\partial p}{\partial t}\right\}= = -\frac{1}{A}\overline{\int_{l_k(z,t)}\mathbf{q}_k\cdot\mathbf{n}_k\frac{dl}{\mathbf{n}_k\cdot\mathbf{n}_{k,l}}} \tag{2.38}$$

2.6 Dimensionless groups

It is useful, for the following treatment, to introduce some dimensionless group:

- *Reynolds number*: for single phase flow it is defined as:

$$Re=\frac{\rho v d}{\mu} \tag{2.39}$$

where:	Re		Reynolds number;
	ρ	$[kg/m^3]$	density;
	v	$[m/s]$	mean flow velocity;
	d	$[m]$	tube diameter;
	μ	$[kg/ms]$	viscosity.

$$Re_l=\frac{G(1-x)d}{\mu_l} \tag{2.40}$$

$$Re_v=\frac{Gxd}{\mu_v} \tag{2.41}$$

where:	Re_l		liquid Reynolds number;
	Re_v		vapor Reynolds number;
	G	$[kg/m^2s]$	mass flux;
	x		quality;
	μ_l	$[kg/ms]$	liquid viscosity;
	μ_v	$[kg/ms]$	vapor viscosity.

Often, dealing with two-phase flows, it is useful to evaluate the Reynolds number of a single phase flow (liquid or vapor) with the same mass flow rate:

$$Re_{lo}=\frac{Gd}{\mu_v} \tag{2.42}$$

$$Re_{vo}=\frac{Gd}{\mu_v} \tag{2.43}$$

where:	Re_{lo}		liquid only Reynolds number;
	Re_{vo}		vapor only Reynolds number;
	G	$[kg/m^2s]$	mass flux;

- *Froude number*: for single phase flow it is defined as:

$$Fr = \frac{v}{\sqrt{gd}} \tag{2.44}$$

where: Fr Froude number;
g $[m/s^2]$ gravity acceleration.

$$Fr_l = \frac{G(1-x)}{\rho_l \sqrt{gd}} \tag{2.45}$$

$$Fr_v = \frac{Gx}{\rho_v \sqrt{gd}} \tag{2.46}$$

$$Fr_{lo} = \frac{G}{\rho_l \sqrt{gd}} \tag{2.47}$$

$$Fr_{vo} = \frac{G}{\rho_v \sqrt{gd}} \tag{2.48}$$

where: Fr_l liquid Froude number;
Fr_v vapor Froude number;
Fr_{lo} liquid only Froude number;
Fr_{vo} vapor only Froude number.

$$Fr_{So} = \frac{G}{\rho_v \sqrt{gd}} \tag{2.49}$$

where: Fr_l liquid Froude number;
Fr_v vapor Froude number;
Fr_{lo} liquid only Froude number;
Fr_{vo} vapor only Froude number.

- *Prandtl number*

$$Pr_l = \frac{\mu_l c_{pl}}{k_l} \tag{2.50}$$

$$Pr_v = \frac{\mu_v c_{pv}}{k_v} \tag{2.51}$$

where: Pr_l liquid Prandtl number;
Pr_v vapor Prandtl number;
c_{pl} $[J/kgK]$ liquid specific heat;
c_{pv} $[J/kgK]$ vapor specific heat;
k_l $[W/mK]$ liquid thermal conductivity;
k_v $[W/mK]$ vapor thermal conductivity.

- *Nusselt number*

$$Nu = \frac{hd}{k_l} \tag{2.52}$$

where: Nu Nusselt number;
h $[W/m^2K]$ heat transfer coefficient.

- *Jakob number*

$$Ja = \frac{c_{pl}(T_{sat} - T_{sub})}{h_{lv}} \tag{2.53}$$

where: Ja Jakob number;
T_{sat} $[K]$ saturation temperature;
T_{sub} $[K]$ subcooling temperature;
h_{lv} $[J/kg]$ latent heat of phase change.

- *Weber number*

$$We = \frac{\rho_l v^2 d}{\sigma} \tag{2.54}$$

where: We Weber number;
σ $[N/m]$ superficial tension.

- *Boiling number*

$$Bo = \frac{q}{G h_{lv}} \tag{2.55}$$

where: Bo Boiling number;
q $[W/m^2]$ heat flux.

- *Galileo number*

$$Ga_l = \frac{g\rho_l^2 d^3}{\mu_l^2} \tag{2.56}$$

- *Laplace number*

$$La = \frac{\sqrt{\sigma/g(\rho_l - \rho_g)}}{D} \tag{2.57}$$

2.7 Homogeneous model

The homogeneous model considers the two phases to flow as a single phase, which properties are assumed to be the mean of the actual phases ones. This model is based on the following assumptions:

- equal vapor and liquid velocities;
- the attainment of thermodynamic equilibrium between the phases;
- the use of appropriate single-phase friction factor for two-phase flow.

In particular, following approach focuses on the steady state condition, such that a flat velocity and time fraction profile has been considered. This leads to the following relationships:

$$\overline{v_{k,z}}^k = v_z \qquad k = 1, 2 \tag{2.58}$$

$$\overline{T_k}^k = T_{sat}(p) \qquad k = 1, 2 \tag{2.59}$$

where: T $[^\circ C]$ temperature.

It follows that:

$$\epsilon_2 = \epsilon = \beta = \frac{x\rho_1}{x\rho_1 + (1-x)\rho_2} \tag{2.60}$$

Considering:

$$\rho = \epsilon\rho_2 + (1-\epsilon)\rho_1 \tag{2.61}$$

it is possible to derive the simplified balance equations written for the mixture.

- *mass balance*

$$\frac{\partial \rho}{\partial t} + \frac{\partial \rho v_z}{\partial z} = 0 \tag{2.62}$$

In steady state condition:

$$\rho v_z = G = \text{constant} \tag{2.63}$$

where: G $[kg/m^2 s]$ mass flux.

- *momentum balance*

$$\frac{\partial \rho v_z}{\partial t} + \frac{\partial \rho v_z^2}{\partial z} = -\frac{\partial p}{\partial z} + \rho F_z - \frac{P}{A}\tau_w \tag{2.64}$$

where: P $[m]$ wet perimeter;
τ_w $[Pa]$ averaged wall shear stress.
taking into account the mass balance eq. 2.62 the eq. 2.64 becomes:

$$\rho\frac{\partial v_z}{\partial t} + \rho v_z\frac{\partial v_z}{\partial z} = -\frac{\partial p}{\partial z} + \rho F_z - \frac{P}{A}\tau_w \tag{2.65}$$

for steady state conditions:

$$\frac{dp}{dz} = -\rho v_z\frac{dv_z}{dz} + \rho F_z - \frac{P}{A}\tau_w = \left(\frac{dp}{dz}\right)_A + \left(\frac{dp}{dz}\right)_G + \left(\frac{dp}{dz}\right)_F \tag{2.66}$$

$$\left(\frac{dp}{dz}\right)_A = -\rho v_z\frac{dv_z}{dz} \tag{2.67}$$

$$\left(\frac{dp}{dz}\right)_G = \rho F_z \tag{2.68}$$

$$\left(\frac{dp}{dz}\right)_F = -\frac{P}{A}\tau_w \tag{2.69}$$

where: $\left(\frac{dp}{dz}\right)_A$ $[Pa/m]$ acceleration pressure drop;
$\left(\frac{dp}{dz}\right)_G$ $[Pa/m]$ gravity pressure drop;
$\left(\frac{dp}{dz}\right)_F$ $[Pa/m]$ frictional pressure drop.

- *energy balance* assuming the hypothesis:

1. the heat flux at the wall is applied on the whole perimeter of the cross section area;
2. the kinetic energy is negligible;
3. the potential energy is negligible.

defining:

$$u = xu_2 + (1+x)u_1 \tag{2.70}$$

$$i = xi_2 + (1+x)i_1 \tag{2.71}$$

where i $[J/kg]$ enthalpy.
The energy balance becomes:

$$\frac{\partial \rho u}{\partial t} + \frac{\partial \rho v_z i}{\partial z} = \frac{P}{A} q \tag{2.72}$$

In steady state flow:

$$\frac{d \rho v_z i}{dz} = \frac{P}{A} q \tag{2.73}$$

In the homogeneous model the following behavior is assumed:

1. *Mechanical equilibrium* the equality of the local velocities along with the assumption of flat profiles lead to the void relation eq. 2.60.

2. *Thermal equilibrium* eq. 2.59 leads to:

$$i_k = i_{sat,k}(p) \qquad k = 1, 2 \tag{2.74}$$

2.7.1 Final set of equations

The set of six equations for the homogeneous model of a steady two-phase flow is formed by the three mixture balance equations for steady state (eq. 2.63, eq. 2.66, eq. 2.73), and the three constrains on the solution (eq. 2.60, eq. 2.74) which specify the flow evolution given by eq. 2.58 and eq. 2.59. In an adiabatic flow the quality is constant and it is considered a parameter whereas in a diabatic flow the quality is directly determined by energy equation (eq. 2.73).

2.7.2 Frictional pressure drop modeling

The friction factor can be defined in the same way for a single phase flow:

$$f = \frac{\tau_w}{\frac{\rho v_z^2}{2}} \tag{2.75}$$

where: f friction factor.
The frictional pressure drop thus reads:

$$\left(\frac{dp}{dz}\right)_F = \frac{4 \tau w}{D} = \frac{2 f \rho v_z^2}{D} \tag{2.76}$$

The friction factor for two-phase flow can be computed as in a single phase flow, with the same mass flow rate of the two-phase flow. The reference phase that is taken into account depends on the quality of the actual flow: if a low quality two-phase flow is considered, the friction factor is approximated to the one of a liquid single phase flow; if a high quality two-phase flow is considered, the friction factor is approximated to the one of a vapor single phase flow.

A turbulent law for single phase flow can be used with a Reynolds number based on an equivalent viscosity μ and a total mass velocity G of the actual two-phase flow:

$$f = f(Re) \tag{2.77}$$

$$Re = \frac{GD}{\mu} \tag{2.78}$$

where: μ $[kg/ms]$ equivalent viscosity.
In his study of water mixture vaporizing in a pipe Owens took an equivalent viscosity equal to the liquid viscosity:

$$\mu = \mu_1 \tag{2.79}$$

Duckler and al. proposed an equivalent viscosity based on the viscosity of each phase weighted by their respective volumetric quality:

$$\mu = \beta\mu_2 + (1-\beta)\mu_1 \tag{2.80}$$

2.7.3 Applicability of the homogeneous model

The homogeneous model approaches two-phase flow by replacing the two-phase flow with an equivalent single phase stream, with the same thermodynamical properties. This assumption can be considered valid if momentum and energy transfer are rapid enough for the local time-averaged velocities and temperatures of the two-phase to be equal. This would imply high stability of flow parameters and that the thermal non-equilibrium has no great influence on the flow. Usually the reported conditions are found if one of the phases is finely dispersed. The homogeneous model has been frequently used to study problems in oil extraction, steam generation and refrigeration. The higher the pressures and velocities, the more realistic the homogeneous model.

2.8 Two-fluid models

In this approach the two-fluid model equations are written in terms of three simplified balance equations for the mixture and three specified evolutions, two of these expressing the thermal equilibrium and the third one being a void correlation.

2.8.1 Balance equations

The simplified balance equations for the mixture (eq. 2.34, eq. 2.36, eq. 2.38) for the mixture in steady state are:

- *mass balance*

$$\frac{d}{dz}[\epsilon\rho_2 v_{z,2} + (1-\epsilon)\rho_1 v_{z,1}] = 0 \tag{2.81}$$

  which leads to:

$$\epsilon\rho_2 v_{z,2} + (1-\epsilon)\rho_1 v_{z,1} = G = \text{constant} \tag{2.82}$$

- *momentum balance*

$$\frac{d}{dz}[\epsilon\rho_2 v_{z,2}^2 + (1-\epsilon)\rho_1 v_{z,1}^2] - [\epsilon\rho_2 + (1-\epsilon)\rho_1]F_z + \frac{dp}{dz} + \frac{4\tau_w}{D} = 0 \tag{2.83}$$

which can be written as:

$$G^2\frac{d}{dz}\left[\frac{x^2}{\epsilon\rho_2} + \frac{(1-x)^2}{(1-\epsilon)\rho_1}\right] - [\epsilon\rho_2 + (1-\epsilon)\rho_1]F_z + \frac{dp}{dz} - \left(\frac{dp}{dz}\right)_F = 0 \tag{2.84}$$

- *momentum energy*

$$\frac{d}{dz}[\epsilon\rho_2 i_2 v_{z,2} + (1-\epsilon)\rho_1 i_1 v_{z,1}] = \frac{4\psi}{D} \tag{2.85}$$

which can be expressed as:

$$G\frac{d}{dz}[xi_2 + (1-x)i_1] = \frac{4\psi}{D} \tag{2.86}$$

2.8.2 Specified evolutions

In many practical cases the fluids flow at saturations and the mechanical non equilibrium is given by an experimental void correlation. It follows:

- *Mecanical nonequilibrium*

$$\epsilon = f(x, p, ...) \tag{2.87}$$

- *Thermal equilibrium*

$$i_k = i_{sat,k}(p) \qquad k = 1, 2 \tag{2.88}$$

The three constraints on the solution (eq. 2.87, eq. 2.88) added to the three mixture balance equations for steady state (eq. 2.82, eq. 2.84, eq. 2.86), form the set of six equations of the two-fluid model of a steady two-phase flow. In an adiabatic flow the quality is constant and it is considered a parameter whereas in a diabatic flow the quality is directly determined by the energy equation (eq. 2.86).

The set of equations (2.82), (2.84), (2.86), (2.87), (2.88) is entirely closed if the wall shear stress τ_w is known.

2.8.3 Lockhart-Martinelli correlations

The first method to determine void fraction and pressure drop in two-phase flows was proposed by Lockhart and Martinelli. Further study brought other methods.

For two component, two-phase flow in horizontal tubes the acceleration pressure drop can be neglected whereas the gravity pressure drop is zero. Consequently the measured pressure drop is equal to the frictional pressure drop.

The following conditions are taken into account:

1. a two-phase mixture flows in a pipe with total mass flow rate such that:

$$\dot{M} = \sum_{k=1}^{2} \dot{M}_k \tag{2.89}$$

where: $\dot{M}$ $[kg/s]$ total mass flow rate;
the frictional pressure drop is denoted by $\left(\frac{dp}{dz}\right)_F$;

Flow Regime	Re	A	n
laminar	< 1000	16	1
turbulent	> 2000	0.046	0.20

Table 2.1: Friction law coefficient

2. the k-th phase flows alone in the same pipe with mass flow rate equal to $\dot{M}_2$, the frictional pressure drop is then denoted by $\left(\frac{dp}{dz}\right)_{F,k}$.

Lockhart and Martinelli introduced the following parameters:

$$\Phi_k^2 = \frac{\left(\frac{dp}{dz}\right)_F}{\left(\frac{dp}{dz}\right)_{F,k}} \tag{2.90}$$

where: Φ_k two-phase multiplier of k-th phase.

$$X^2 = \frac{\left(\frac{dp}{dz}\right)_{F,1}}{\left(\frac{dp}{dz}\right)_{F,2}} \tag{2.91}$$

where: X Lockhart-Martinelli parameter.

As the pressure drop in the single phase flow can be calculated for both turbulent and laminar regimes, there are four possible combinations for calculating X:

1. turbulent liquid and turbulent vapor: index tt is used for X;
2. laminar liquid and turbulent vapor: index lt is used for X;
3. turbulent liquid and laminar vapor: index tl is used for X;
4. laminar liquid and laminar vapor: index ll is used for X.

Lockhart and Martinelli assumed the following friction law to be used in eq. 2.91:

$$f = A\, Re^{-n} \tag{2.92}$$

The expression of the Lockhart-Martinelli parameter is:

- when both liquid and vapor flows are turbulent ($n = 0.2$)

$$X_{tt} = \left(\frac{\mu_1}{\mu_2}\right)^{0.1} \left(\frac{1-x}{x}\right)^{0.9} \left(\frac{\rho_2}{\rho_1}\right)^{0.5} \tag{2.93}$$

- when both liquid and vapor flows are laminar ($n = 1$)

$$X_{ll} = \left(\frac{\mu_1}{\mu_2}\right)^{0.5} \left(\frac{1-x}{x}\right)^{0.5} \left(\frac{\rho_2}{\rho_1}\right)^{0.5} \tag{2.94}$$

The Lockhart-Martinelli method consists in plotting ϵ and Φ_k ($k = 1, 2$) versus the Lockhart-Martinelli parameter X.

Lockhart-Martinelli Parameter	X_{tt}	X_{lt}	X_{tl}	X_{ll}
C	20	12	10	5

Table 2.2: Values of parameter C for the two-phase multiplier

2.8.4 Void correlation

ϵ can be approximated by the equation:

$$\epsilon = 1 - \frac{X}{\sqrt{X^2 + 20X + 1}} \tag{2.95}$$

The curve represents the mechanical nonequilibrium of eq. 2.87.

2.8.5 Frictional pressure drop correlation

Φ_1 and Φ_2 can be approximated by the equations:

$$\Phi_1^2 = 1 + \frac{C}{X} + \frac{1}{X^2} \tag{2.96}$$

$$\Phi_2^2 = 1 + CX + X^2 \tag{2.97}$$

Comments on the Lockhart-Martinelli method are:

- the two-phase multipliers Φ_k depend not only on X but also on the liquid mass flow rate;
- the experimental curves of the two-phase multiplier versus the Lockhart-Martinelli parameter X display several changes of slope indicating definite changes in the two-phase flow patterns.

2.9 Flow patterns in heated channel

Depending on pressure, flow, heat flux and channel geometry a two-phase flow exhibits a specific *flow pattern*. These configurations are recognizable both in evaporation and in condensation processes, so they are very useful to design heat exchangers. It is desirable to know the heat transfer characteristic of each flow pattern to design the heat exchanger to operate in the most favorable conditions.

This thesis focuses only on horizontal two-phase flow inside circular ducts. Engineers have developed many different heat exchangers' geometry, they are all omitted except with the mentioned case since they are not directly relevant to the development of the subject treated in the thesis.

The flow patterns observed in two-phase flow in horizontal circular channels are complicated by asymmetry of the phases resulting from the influence of gravity. They are:

- *Bubbly flow*: the vapor forms discrete bubbles in a continuous liquid phase. Dimensions of the bubbles can vary in a range of diameters that are, although, much smaller with respect to the channel diameter. The different densities of liquid and vapor phase leads to the tendency of bubbles to travel in the upper part of the pipe;

- *Plug flow*: In this case the diameter of the bubbles approaches the pipe diameter. The nose of the bubbles has a characteristic spherical cap and the gas in the bubble is separated form the pipe wall by a slowly descending film of liquid. As already anticipated, the bubbles tend to flow in the upper part of the pipe, so the liquid film above the bubble is thinner than the lower one;

- *Stratified flow*: it occurs at very low liquid and vapor velocities. The two phases flow separately with a relatively smooth interface;

- *Wavy flow*: it occurs at higher vapor velocities than those characterizing stratified flow. The discrepancy between phase velocity generates waves of liquid traveling in the direction of the flow;

- *Slug flow*: a further increase of vapor velocity causes the waves to completely fill the cross-section of the duct. They form a slug, which is propagated along the channel at high velocity;

- *Annular flow*: it exhibits the presence of a gas core with a liquid film around the periphery of the channel. The thickness of the film can be discontinuous and it is major at the base of the tube, due to gravity effects on the flow. A drop flow region can be delineated where the majority of the flow was entrained in the gas core and dispersed as droplets.

The presented flow patterns are depicted in fig. 2.2. The sequence of exhibited flow patterns depends on the flow rate, fluid properties, distribution and magnitude of the heat flux and the channel characteristics. During phase change process it is possible to observe and distinguish the patterns visually, they characterize a portion of the total length of the accounted channel. Depending on the the heat flux direction, phase change can occur from liquid to vapor (boiling, heat flux is directed into the flow) or from vapor to liquid (condensation, heat flux is directed out of the flow). This affects drastically the variation of flow pattern presented in the process, the sequence of flow regimes observed in an horizontal co-current flow is indicated in fig. 2.3.

In particular, three different cases are distinct: (a) evaporation; (b) condensation with high liquid loading; (c) condensation with low liquid loading. Accounting a low enough, uniform heat flux in evaporation case, intermittent drying and re-wetting of the upper surface of the tube in slug and wavy flow are observed. The progressive drying out occurs at the upper circumference due to gravity forces. With the increase of inlet velocities the effect of gravity is less affecting the flow patterns. Considering condensation, the liquid film is formed near to the tube walls, generating an annular flow. As condensation continues, gravity forces increases, so that stratified flow or bubble flow are formed with a high tendency of the residual vapor to flow in the upper half of the tube. The flow rate and the magnitude of heat flux are the main responsible for the presence of stratified or bubble flow.

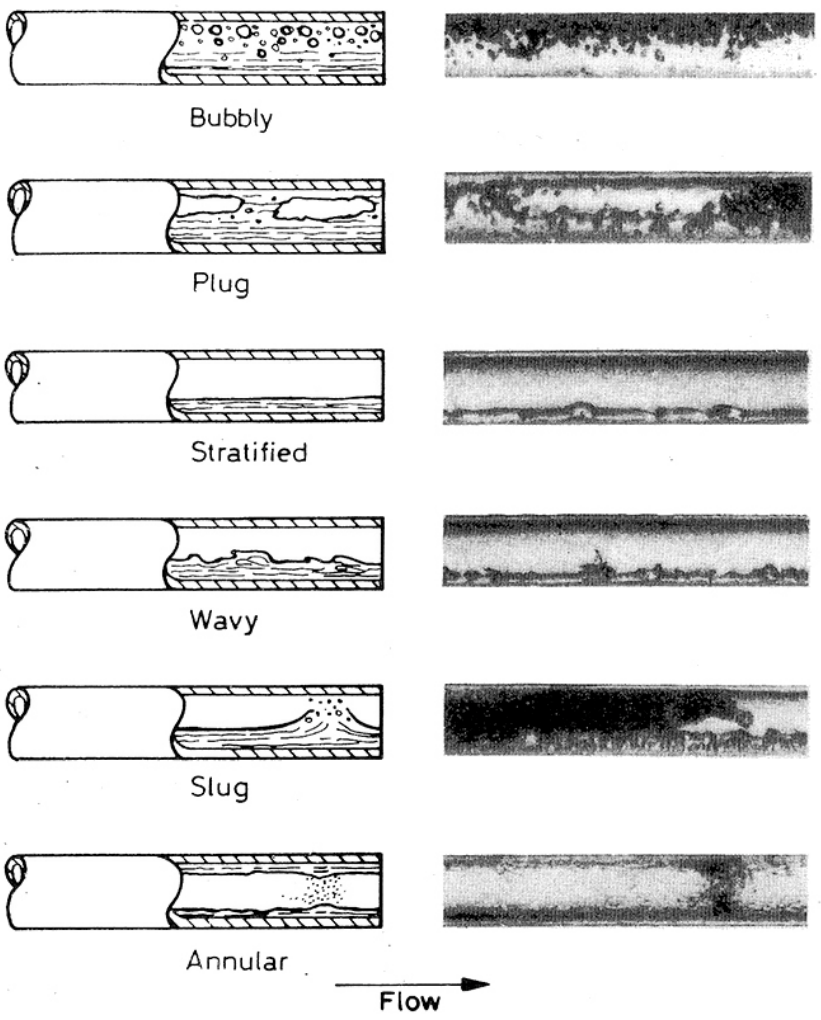

Figure 2.2: Flow regimes in horizontal tube, adiabatic conditions.

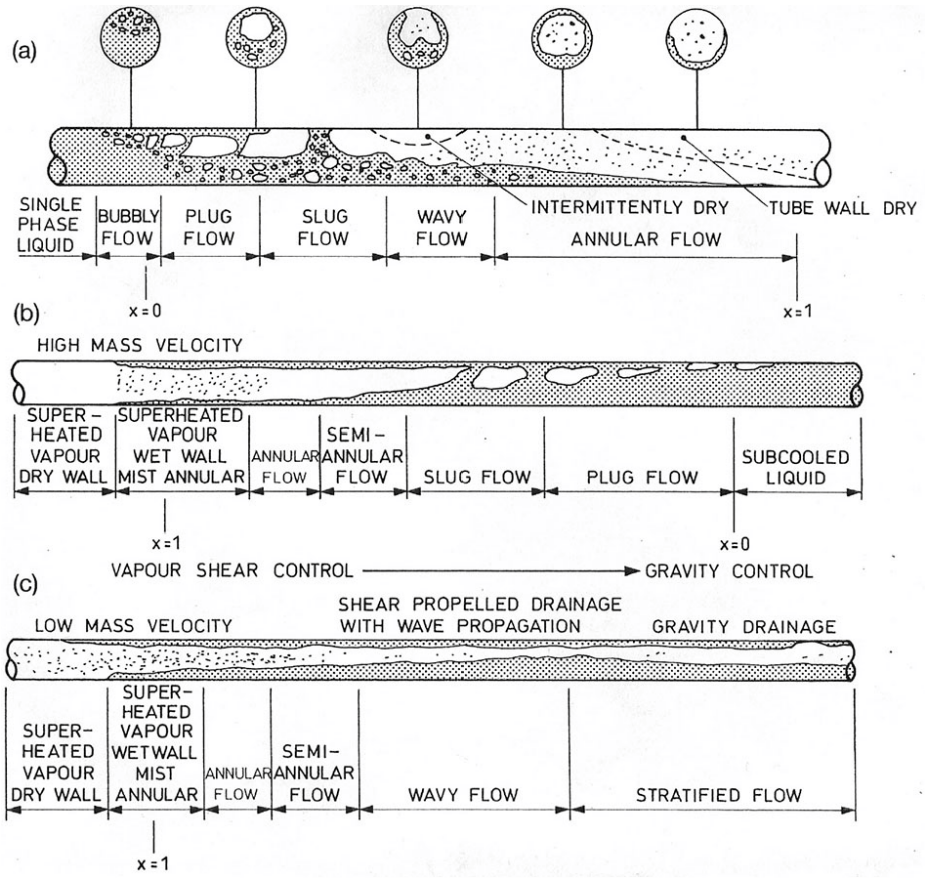

Figure 2.3: Flow regimes in horizontal tube, during evaporation and condensation.

Chapter 3

Pressure drop empirical correlations

3.1 General formulation

Pressure drop is composed by three terms:

1. geodesic component;
2. acceleration component;
3. friction component.

$$\left(\frac{dP}{dz}\right)_{total} = \left(\frac{dP}{dz}\right)_{geodesic} + \left(\frac{dP}{dz}\right)_{acceleration} + \left(\frac{dP}{dz}\right)_{friction} \tag{3.1}$$

1. The geodesic component of the pressure drop can be neglected for an horizontal duct.
2. For the separated flow models, the acceleration pressure drop due to density variation follows the equation proposed by Collier and Thome:

$$\left(\frac{dP}{dz}\right)_{acceleration} = G^2 \frac{d}{dz}\left[\frac{x^2}{\rho_g \epsilon} + \frac{(1-x)^2}{\rho_l(1-\epsilon)}\right] \tag{3.2}$$

   Where ϵ is the void fraction. For this thesis aims, the following expression for the void fraction has been chosen:

$$\epsilon = \frac{1}{1 + (\frac{1-x}{x})(\frac{\rho_g}{\rho_l})^{2/3}} \tag{3.3}$$

   This pressure drop term cannot be neglected since the variation of vapor quality during boiling and condensation affects both the density and void fraction.

3. The frictional pressure drop can be computed through experimental correlations. Correlations are developed for specific cases, so the geometrical parameters of heat exchanger, physical conditions of the test or the analyzed fluid can vary. This affects the output correlation, so that it is possible to obtain high deviation between the predicted data and the experimental ones, in particular if the analyzed case differs from the ones that are objects

of this thesis. The main distinction that affects the applicability range of a specific correlation regards the choice of the performed tests, which are divided in condensation and boiling conditions. In the following treatment frictional pressure drop evaluation methods are presented, with a focus on correlation developed for conditions similar to the one used in this project.

A majority of correlations were propounded on the basis of the two-phase friction multipliers proposed by Lockhart and Martinelli and the fitting correlation of the multipliers from Chisholm, which are both based on separated flow model.

Lockhart and Martinelli proposed the definition of two phase multipliers ϕ_l^2 and ϕ_g^2, defined as the ratio of the two-phase frictional pressure gradient to the frictional pressure gradient which would exists if the considered single phase is assumed to flow alone:

$$\phi_l^2 = \frac{(\frac{\Delta p}{\Delta L})_{tp}}{(\frac{\Delta p}{\Delta L})_l} \tag{3.4}$$

$$\phi_g^2 = \frac{(\frac{\Delta p}{\Delta L})_{tp}}{(\frac{\Delta p}{\Delta L})_g} \tag{3.5}$$

where: $(\frac{\Delta p}{\Delta L})_{tp}$ two-phase frictional pressure gradient per unit length;
$(\frac{\Delta p}{\Delta L})_l$ liquid frictional pressure gradient per unit length;
$(\frac{\Delta p}{\Delta L})_g$ vapor frictional pressure gradient per unit length.

Single phase frictional pressure gradients can be computed with a single-phase friction factor correlation using single-phase properties and mass flux, as follows:

$$\left(\frac{\Delta p}{\Delta L}\right)_l = \frac{[G_{tp}(1-x)]^2}{2d\rho_l} f_l \tag{3.6}$$

$$\left(\frac{\Delta p}{\Delta L}\right)_g = \frac{[G_{tp}x]^2}{2d\rho_g} f_g \tag{3.7}$$

where:

G_{tp}	$[kg/m^2s]$	two-phase flow mass flux;
x		vapor quality;
ρ_l	$[kg/m^3]$	density of the liquid phase;
ρ_g	$[kg/m^3]$	density of the vapor phase;
d	$[m]$	characteristic diameter;
f_l		single phase friction factor (only liquid);
f_g		single phase friction factor (only vapor).

Where the friction factor has been computed by using the Fang et al. [3], which provides a mean absolute relative deviation of 0.02%:

$$f = 0.25\left[log\left(\frac{150.39}{Re^{0.98865}} - \frac{152.66}{Re}\right)\right]^{-2} \tag{3.8}$$

where: Re Reynolds number.

Friction multipliers are function of dimensionless variable X defined as

$$X = \sqrt{\frac{(\frac{\Delta p}{\Delta L})_l}{(\frac{\Delta p}{\Delta L})_g}} \tag{3.9}$$

Hence, it is possible to relate directly X and ϕ_l^2:

$$\phi_l^2 = 1 + \frac{C}{X} + \frac{1}{X^2} \tag{3.10}$$

A similar approach takes into account different friction multipliers:ϕ_{lo}^2 and ϕ_{go}^2. They are defined as the ratio of the two-phase frictional pressure gradient to the frictional pressure gradient which would exists if the whole mass flow rate were liquid or vapor, so they can be computed analogously to the previous multipliers and the values of pressure gradient vary to:

$$\left(\frac{\Delta p}{\Delta L}\right)_{lo} = \frac{G_{tp}^2}{2D\rho_l} f_{lo} \tag{3.11}$$

$$\left(\frac{\Delta p}{\Delta L}\right)_{go} = \frac{G_{tp}^2}{2D\rho_g} f_{go} \tag{3.12}$$

where: f_{lo} single phase friction factor (liquid only);
f_{go} single phase friction factor (vapor only).

Basing on this approaches, the following experimental correlation has been selected to compare actual data with the predicted ones. Selection has been performed following the analysis of Fang-Chen et al. [4], that compares the uncertainty of different experimental correlations. Selected correlations have been computed in conditions similar to the ones that this thesis focuses on, and exhibit the best performances in terms of mean standard absolute and relative deviations from the analyzed data. Depending on the considered correlation the applicable case can vary depending on the parameter that the correlation has been developed for. In particular, if a correlation has been developed basing only on condensation tests, so that correlation cannot be exploited to predict evaporation pressure drop. Analogously, if evaporation tests only are considered for a specific correlation, so condensation conditions cannot be used to compare experimental data with the predicted ones. However, different fluids and tubes geometries are used in correlation databases, this could generate a deviation from the tests conditions this thesis focuses on.

3.2 Sun and Mishima

Sun and Mishima correlation [5] is based on a database including *R134a* and other refrigerants, flowing in horizontal smooth and corrugated channels with diameter range of $[0.506 - 12]mm$. The database refers to both condensation and evaporation experiments. It exploits the relation expressed in eq. 3.10 where C parameter is a function of dimensionless groups:

- if the flow is laminar ($Re_l < 2000$ or $Re_g < 2000$):

$$C = 26\left(1 + \frac{Re_l}{1000}\right)\left[1 - exp\left(\frac{-0.153}{0.27La + 0.8}\right)\right] \tag{3.13}$$

- if the flow is turbulent ($Re_l > 2000$ and $Re_g > 2000$):

$$C = 1.79\left(\frac{Re_g}{Re_l}\right)^{0.4}\left(\frac{1-x}{x}\right)^{0.5} \tag{3.14}$$

where: Re_l Reynolds number of the liquid phase;
Re_g Reynolds number of the vapor phase
La Laplace number.
While the value of ϕ_l^2 is computed as:

$$\phi_l^2 = 1 + \frac{C}{X^n} + \frac{1}{X^2} \tag{3.15}$$

where

- $n = 1$ for laminar condition ($Re_l < 2300$);
- $n = 1.19$ for turbulent condition ($Re_l > 2300$).

The proposed correlation fits with the authors' experimental data with the following uncertainty:

Parameter	MRD [%]	MARD [%]
0 < x < 0.2	-12.8	29.7
0.2 < x < 0.4	-19.3	25.7
0.4 < x < 0.6	-24.7	29.7
0.6 < x < 0.8	-30.3	32.5
0.8 < x < 1	-25.9	27.6
Evaporation	-26.5	31.2
Condensation	-20.6	28.1
Refrigerant	-21.4	27.9

Table 3.1: Sun and Mishima correlation performances, depending on applied case,[].

where:

$$MRD = \frac{1}{N}\sum_{i=1}^{N}\frac{y(i)_{pred} - y(i)_{exp}}{y(i)_{exp}} \tag{3.16}$$

$$MARD = \frac{1}{N}\sum_{i=1}^{N}|\frac{y(i)_{pred} - y(i)_{exp}}{y(i)_{exp}}| \tag{3.17}$$

where: N total number of analyzed data;
$y(i)_{pred}$ predicted value of i-th operating condition;
$y(i)_{exp}$ experimental value of i-th operating condition.
It is possible to notice that the deviation of the correlation is lower for low mean quality of the flow. According to the authors, the correlation can be used both for evaporation and condensation, as these operating conditions do not affect the percentage errors.

3.3 Muller-Steinhagen and Heck

This correlation data includes different fluids, such as water refrigerants and argon, in particular experiments on refrigerant fluids has been performed in horizontal $14mm$ outer diameter duct with a mass flux range of $[50 - 246]Kg/m^2s$. It is essentially an empirical two-phase extrapolation

between liquid only and vapor only [6]. The variations of the thermal properties of the fluid due to different experiment condition is not taken into account. Smooth and relative rough tubes were used for both the evaporation and condensation.

This correlation is based on ϕ_{lo}^2 model, so the dimensionless parameter Y is defined as:

$$Y^2 = \frac{(\Delta p/\Delta L)_{go}}{(\Delta p/\Delta L)_{lo}} \tag{3.18}$$

and the friction multiplier is computed following the the equation:

$$\phi_{lo}^2 = Y^2 x^3 + (1-x)^{1/3}[1 + 2x(Y^2 - 1)] \tag{3.19}$$

where x is the mean vapor quality of the flow. The frictional pressure gradient of the two-phase flow is computed by multiplying the equation result for the frictional pressure gradient of the flow, assumed as liquid only:

$$\left(\frac{\Delta p}{\Delta L}\right)_{tp} = \phi_{lo}^2 \left(\frac{\Delta p}{\Delta L}\right)_{lo} \tag{3.20}$$

The liquid frictional pressure gradient is computed as shown in eq. 3.11.

The proposed correlation exhibits the following performances:

Parameter	MRD [%]	MARD [%]
$0 < x < 0.2$	-13.8	29.7
$0.2 < x < 0.4$	-5.3	25.2
$0.4 < x < 0.6$	-1.2	24.3
$0.6 < x < 0.8$	3.4	26.1
$0.8 < x < 1$	14.7	28.3
Evaporation	-8.8	25.9
Condensation	-2.2	22.1
Refrigerant	-2.6	25.7

Table 3.2: Muller-Steinhagen and Heck correlation performances, depending on applied case.

The table shows clearly better performances with respect to Sun and Mishima correlation, however fluids, mass flux and duct geometry can be different from the ones applied in this project.

3.4 Bandarra Filho et al.

This study [7] deals with pressure drop of refrigerant R134a under convective boiling condition in horizontal smooth and microfin copper tubes. Hence, evaporation conditions are the only acceptable tests which this correlation can be analyzed for. Experiments have been carried out on test section made out of 7.0, 7.93 and $9.52mm$ external diameter. Mass flux and refrigerant qualities vary in the following ranges:

- mass flux range $[70 - 1100] kg/m^2 s$;
- mean quality range $[0.05 - 0.95]$.

It is based on ϕ_l^2 approach, which depends on X_{tt} parameter, defined through the equation:

$$X_{tt} = \left(\frac{1-x}{x}\right)^{0.9} \left(\frac{\rho_v}{\rho_l}\right)^{0.5} \left(\frac{\mu_l}{\mu_v}\right)^{0.1} \tag{3.21}$$

where: μ_l $[Pa \cdot s]$ dynamic viscosity of the liquid phase;
μ_g $[Pa \cdot s]$ dynamic viscosity of the vapor phase.
following the experimental correlation:

$$\phi_l = 1 + 3X_{tt}^{-0.83} \tag{3.22}$$

The additive constant equal to 1 in the right hand side of the equation is to conform to the lower limit of the two-phase multiplier. The average absolute deviation of the correlation with respect to the experimental results is of the order of 6.3%.

3.5 Shannak

Experiments of two-phase flow frictional pressure drop were conducted on horizontal and vertical smooth and rough pipes. The correlation [8] is based on refrigerant and air-water flows under the following conditions:

Tube diameter	$[mm]$	$[3.2; 152.4]$
System pressure	$[bar]$	$[5; 14]$
Mass flux	$[kg/m^2s]$	$[200; 1500]$

Table 3.3: Shannak correlation experimental conditions done on smooth and rough tubes.

The model includes a new definition of the Reynolds number and the friction factor for the two-phase flow, the frictional pressure drop is obtained from

$$\Delta p_{tp} = f_{tp} \frac{L}{d} \frac{G^2}{2\rho_{tp}} \tag{3.23}$$

where: ρ_{tp} $[kg/m^3]$ density of the two-phase flow;
L $[m]$ tube length;
d $[m]$ characteristic tube diameter;
The two-phase density is computed through a weighted mean of the single phase densities with respect to the mean vapor title, so that

$${\rho_{tp}}^{-1} = \frac{x}{\rho_g} + \frac{1-x}{\rho_l}. \tag{3.24}$$

The two-phase friction factor is function of the flow properties, so a new definition of two-phase Reynolds number was given in order to evaluate properly the effects of these properties on the frictional pressure drop.

The Reynolds number can be given as the ratio between the sum of inertia force of each phase and the sun of viscous force of each phase:

$$Re_{tp} = \frac{F_{I,l} + F_{I,g}}{F_{V,l} + F_{V,g}} \tag{3.25}$$

It can be re-arranged to get a direct relationship with the flow properties:

$$Re_{tp} = \frac{Gd[x^2 + (1-x)^2(\rho_g/\rho_l)]}{\mu_g x + \mu_l(1-x)(\rho_g/\rho_l)} \tag{3.26}$$

A new definition of a two-phase friction factor is obtained, applying the Chen correlation to the new proposed definition of Reynolds number.

$$f_{tp}^{-1/2} = -2log\left[\frac{\epsilon/d}{3.7065} - \frac{5.0452}{Re_{tp}} log\left(\frac{1}{2.8257}\left(\frac{\epsilon}{d}\right)^{1.1098} + \frac{5.8506}{Re_{tp}^{0.8981}}\right)\right] \tag{3.27}$$

where ϵ/d is the relative roughness of the selected tube. The relative roughness is one of the parameters that affects the pressure drop, its effect is more significant at higher vapor quality and higher mass flux.

This correlation exhibits a standard deviation of 25% from the Friedel databank, leading to an uncertainty on the analyzed pressure drop of 5.8%.

3.6 Domanski et al.

A pressure drop correlation [9] for evaporation and condensation in smooth and microfin tubes for refrigerants was developed using the NIST database analysis. A copper tube with an outside diameter of 9.52mm, root diameter of 8.92mm and helix angle β of 18° was chosen as microfin test section. The tube is enhanced by 60 fins, that affect the hydraulic diameter so that it results 5.5mm.

The pressure drop correlation exhibits the following shape:

$$\Delta p = \left[\frac{f_N L(v_{out} - v_{in})}{d_h} + (v_{out} - v_{in})\right] G^2 \tag{3.28}$$

where:

v_{out}	$[m^3/kg]$	outlet specific volume of refrigerant;
v_{in}	$[m^3/kg]$	inlet specific volume of refrigerant;
d_h	$[m]$	hydraulic diameter;
L	$[m]$	tube length;
f_N		two-phase friction factor based on NIST database.

Specific volumes of the two-phase fluid are weighted on vapor qualities at the inlet and the outlet of the test section, and the correlation for the two-phase friction factor is obtained empirically.

$$v_{out} = x v_{g,out} + (1-x) v_{l,out} \tag{3.29}$$

$$v_{in} = x v_{g,in} + (1-x) v_{l,in} \tag{3.30}$$

$$f_N = 0.00506 Re_{lo}^{-0.0951} K_f^{0.1554} \tag{3.31}$$

$$K_f = x(i_{sv} - i_{sl})/Lg \tag{3.32}$$

where:

i_{sv}	$[m^3/kg]$	refrigerant saturated vapor enthalpy;
i_{sl}	$[m^3/kg]$	refrigerant saturated liquid enthalpy.

The developed correlation predicted the evaporative pressure drop for refrigerants in smooth and microfin tubes with average absolute residual respectively of 28% and 14.9%. The condensation pressure drop data were predicted with an average absolute residual of 19.6% for both the tubes.

3.7 Kedzierski et al.

The developed correlation [10] is based on refrigerant condensation inside horizontal smooth and microfin tubes. In particular, the basic correlation coefficients have been modified in order to take into account microfin tube only, so that would be the reference equation for the accounted cases of experiments. Experimental conditions of the database are:

Tube inside diameter	$[mm]$	$[7; 8]$
Total condenser length	$[m]$	$[0.54; 4]$
Saturation temperature	$[°C]$	$[40; 50]$
Mass flux	$[kg/m^2s]$	$[100; 400]$

Table 3.4: Kedzierski correlation experimental conditions conducted on microfin tubes.

The pressure drop due to friction is given by the product of the liquid-only pressure drop and a two-phase multiplier, according to eq. 3.6, with the two-phase multiplier being:

$$\phi_l^2 = 1.376 + \frac{7.242}{X_{tt}^{1.655}} \tag{3.33}$$

The liquid friction factor for finned tube follows the equation:

$$f_l = 0.046 Re_l^{-0.2} \left(\frac{d_i}{d_e}\right) \left(\frac{A}{A_n}\right)^{0.5} (\sec\beta)^{0.75} \tag{3.34}$$

where: d_i $[m]$ equivalent inner diameter taking the fins into account;
d_e $[m]$ fin-root diameter;
A $[m^2]$ nominal flow area based on fin-root diameter;
A_n $[m^2]$ actual cross-sectional flow area.

Actually, the area ratio can be computed as given:

$$\frac{A}{A_n} = 1 - \frac{4ent}{\pi D_i^2 cos\beta} \tag{3.35}$$

where: e $[m]$ fin height;
n fin number;
t $[m]$ fin thickness.

The terms $sec\beta$ and $cos\beta$ account the swirling effect induced by the fins inside the helical microfin tube. The results indicated that this modified correlation predicted the data within an average error of 1% and an average mean deviation of 6.8%.

3.8 Haraguchi et al.

Condensation experiments on horizontal smooth and microfin tubes have been performed, with two-phase refrigerant flow under the following conditions:

The correlation [11] is based on the vapor phase multiplier (ϕ_g) and the Martinelli parameter, which is computed following eq. 3.21. Geometrical parameters of the microfin tube and the enhancement factor provided by the fins are accounted by the equivalent diameter present in the correlation.

Mass flux	$[kg/m^2s]$	[90;400]
Heat flux	$[kW/m^2]$	[3;33]

Table 3.5: Haraguchi correlation experimental conditions done on microfin tubes.

$$d_e = \sqrt{4A_c/\pi} \tag{3.36}$$

where A_c takes into account cross sectional area variation due to the presence of fins.

The friction factor and the vapor-phase multiplier for the two-phase friction pressure drop are computed as follows:

$$\phi_g = 1.1 + 1.3\{X_{tt}G/[gd_e\rho_g(\rho_l - \rho_g)]^{0.5}\}^{0.35} \tag{3.37}$$

$$f_{e,g} = 0.046Re_{e,g}^{-0.2} \tag{3.38}$$

where:

$$Re_{e,g} = Gd_ex/\mu_g \tag{3.39}$$

From the previous results it is possible to compute directly the two-phase frictional pressure gradient, re-arranging the eq. 3.5 and substituting the obtained results:

$$\left(\frac{\Delta p}{\Delta L}\right)_{tp} = 2\phi_g^2 f_{e,g}(Gx)^2/(\rho_g d_e) \tag{3.40}$$

This empirical correlation is based on the turbulent liquid film theory and Nusselt's theory, where the effect of vapor shear stress and of gravity force are taken into account. This equation correlates the experimental results within an error of 26.3% and a mean absolute standard deviation of 21%. Mean square error is computed as:

$$err_N = \sqrt{\sum_{i=1}^{N} \frac{(y(i)_{pred} - y(i)_{exp})^2}{N-1}} \tag{3.41}$$

3.9 Goto et al.

The experiments that this correlation is based on were performed for conventional groove tubes with the characteristics reported in tab. 3.9.

Tube type		Spiral	Herringbone
d_{ext}	$[mm]$	8.01	8.00
d_{int}	$[mm]$	7.30	7.24
Fins number		55	60

Table 3.6: Microfin tubes characteristics for Goto correlation.

The ranges of of refrigerant mass flux was from 200 and 340 kg/m^2s for both condensation and evaporation tests on R410A and HCF22. The correlation [12] exploits the vapor-phase friction factor and the respective multiplier for the frictional pressure drop.

$$\phi_g = 1 + 1.64 X_{tt}^{0.79} \tag{3.42}$$

- if $Re \leq 2000$

$$f_{e,g} = 16/Re_g \tag{3.43}$$

- if $2000 < Re \leq 2600$

$$f_{e,g} = 0.000147 Re_g^{0.53} \tag{3.44}$$

- if $2600 < Re \leq 6500$

$$f_{e,g} = 0.046 Re_g^{-0.2} \tag{3.45}$$

- if $6500 Re \leq 12700$

$$f_{e,g} = 0.00123 Re_g^{0.21} \tag{3.46}$$

- if $Re > 12700$

$$f_{e,g} = 0.0092 \tag{3.47}$$

where Re_g is evaluated in the same way of Haraguchi correlation, following eq. 3.39. The frictional two-phase pressure drop can be obtained re-arranging eq. 3.5, as previously indicated in Haraguchi correlation treatment.

Mean relative and absolute standard deviations are respectively 9.1% and 20.2%, while the mean square error is 23.6%.

Chapter 4

Heat transfer coefficient empirical correlations

4.1 Murata et al.

The authors proposed a correlation [13], in the form recommended by Chen, for boiling two-phase flow in the following conditions:

Tube diameter	$[mm]$	10.3
Saturation Pressure	$[MPa]$	0.2
Mass flux	$[kg/m^2s]$	[200;300]
Heat flux	$[kW/m^2]$	[10;30]

Table 4.1: Murata correlation experimental conditions.

Analyzed heat exchangers set is comprehensive of horizontal smooth and spirally grooved copper tubes. The empirical correlation is computed as follows:

$$h_{tp} = h_l E + h_{pb} S \tag{4.1}$$

$$h_l = 0.036 Re_l^{0.8} Pr_l^{0.4} \frac{k_l}{d_i} \tag{4.2}$$

$$h_{pb} = 48 \left(\frac{p_c^{0.2} p_{rm}}{M_m^{0.1} T_c^{0.9}} \right) q^{0.8} \tag{4.3}$$

$$p_{rm} = \frac{\left(\frac{p}{p_c} \right)^{0.23}}{\left(1 - 0.99 \frac{p}{p_c} \right)^{0.9}} \tag{4.4}$$

$$E = \left(1 + \frac{2}{X_{tt}} \right) (1 - x)^{0.8} \tag{4.5}$$

$$X_{tt} = \left(\frac{\mu_1}{\mu_2} \right)^{0.1} \left(\frac{1 - x}{x} \right)^{0.9} \left(\frac{\rho_2}{\rho_1} \right)^{0.5} \tag{4.6}$$

$$S = \frac{k_l}{Eh_l\delta}\left[1 - \exp\left(-\frac{Eh_l\delta}{k_l}\right)\right] \tag{4.7}$$

$$\delta = 0.08\sqrt{\frac{\sigma}{g}(\rho_l - \rho_v)} \tag{4.8}$$

where:

h_{pb}	$[W/m^2K]$	pool boiling heat transfer coefficient;
p_c	$[Pa]$	critical pressure;
p_{rm}	$[Pa]$	modified reduced pressure;
T_c	$[K]$	critical temperature;
E		enhancement factor;
S		suppression factor.

Dataset used to compute the correlation has been predicted within the 20% of the measured values.

4.2 Yun et al.

The authors [14] developed a model to take into account the effects of microfins on the heat exchange. They characterized the tube geometry using two quantity:

1. the fin height;

2. the ratio between the fin height and the the liquid film thickness.

Typical geometries of accounted tubes are:

Tube diameter	$[mm]$	[8.82;14.66]
Fin numbers		[50;70]
Helix angle	[°]	[16;30]
Fin height	$[mm]$	[0.12;0.38]

Table 4.2: Tubes characteristics chosen for Yun correlation.

The database includes only evaporation experiments, where the applied conditions cover the ranges:

Saturation Temperature	$[°C]$	[-15;70]
Mass flux	$[kg/m^2s]$	[50;637]
Heat flux	$[kW/m^2]$	[5;39.5]

Table 4.3: Yun correlation experimental conditions.

The correlation is computed as

$$h_{tp} = h_l \left[0.009622 Bo^{0.1106} \left(\frac{p_{sat} d_i}{\sigma} \right)^{0.3814} + 7.685 \frac{1}{X_{tt}^{0.51}} \left(\frac{Ge_f}{\mu_l} \right)^{-0.736} \right] Re_l^{0.2045} Pr_l^{0.7452} \left(\frac{\delta}{e_f} \right)^{-0.1302} \tag{4.9}$$

$$h_l = 0.023 Re_l^{0.8} Pr_l^{0.4} \frac{k_l}{d_i} \tag{4.10}$$

$$\delta = \frac{(1-\epsilon) d_i}{4} \tag{4.11}$$

$$\epsilon = \frac{\frac{x}{\rho_l}}{[1 + 0.12(1-x)] \left(\frac{x}{\rho_v} + \frac{1-x}{\rho_l} \right) + \frac{1.18(1-x)[g\sigma(\rho_l - \rho_v)]^{0.25}}{\sqrt{\rho_l} \dot{m}}} \tag{4.12}$$

$$X_{tt} = \left(\frac{\mu_1}{\mu_2} \right)^{0.1} \left(\frac{1-x}{x} \right)^{0.9} \left(\frac{\rho_2}{\rho_1} \right)^{0.5} \tag{4.13}$$

A mean and an average deviation f the present correlation are 20.5% and -11.7% respectively. Approximately 90% of the experimental data are correlated within a range of 30% of the measured values.

4.3 Han Chen et al.

The authors [15] analyzed the boiling heat transfer characteristics of refrigerant mixtures in a horizontal microfin tube of 7 mm outlet diameter. The experimental mass flux ranges between $[100; 250] kg/m^2 s$, while the heat flux and the saturation temperature have ranges respectively of $[11.76; 52.94] kW/m^2$ and $[-5; 8]°C$.

The basic form of the correlation is the Chen's boiling heat transfer model, which takes into account the nucleate boiling and the convective heat transfer. A modification due to the presence of fins is applied to the original correlation shape, so that

$$h_{tp} = F h_l + S h_{nb} \tag{4.14}$$

where h_l can be computed as

$$h_l = 0.023 Re_l^{0.8} Pr_l^{0.4} \frac{k_l}{d_i} \tag{4.15}$$

$$Re_l = \frac{G(1-x) d_i}{\mu_l} \tag{4.16}$$

$$Pr_l = \frac{Cp_l \mu_l}{k_l} \tag{4.17}$$

E_{rb} is a correction factor due to the microfin structure.

$$E_{rb} = \left\{ 1 + \left[2.64 Re_l^{0.036} Pr_l^{-0.024} \left(\frac{e}{d_i} \right)^{0.212} \left(\frac{l_f}{d_i} \right)^{-0.21} \left(\frac{\beta}{90} \right)^{0} .29 \right]^7 \right\}^{1/7} \tag{4.18}$$

where: l_f $[m]$ fin axial gap;
e $[m]$ fin height;

While the nucleate boiling heat transfer coefficient is computed as:

$$h_{nb} = 55 P_{re}^{0.12} (-log P_{re})^{-0.55} M^{-0.5} q^{0.67} \tag{4.19}$$

where: M $[kg/kmol]$ molar mass;
q $[kW/m^2]$ heat flux;
P_{re} reduced pressure;

The empirical coefficients are defined follows.

$$F = 1 + 7196.741 Bo^{1.16} + 1.5135 X_{tt}^{-0.86} \tag{4.20}$$

$$S = 1/(1 + 2.703 F^{1.94} Re_{lo}^{1.17}) \tag{4.21}$$

The correlated heat transfer coefficients agreed with the experimental data within the deviation of $[-15; 20]\%$.

4.4 Rollmann Spindler

Authors [16] performed experiments on horizontal microfin tubes, during flow boiling of refrigerant R407C and R410A. The measurements were conducted at saturation temperatures between -30 and +10 $°C$. The heat flux has been set varying in the range of $[1; 20] kW/m^2$. The mass flux was varied between $[25; 300] kg/m^2 s$ and the vapor quality was between 0.1 and 1.

The microfin tube was made of copper with the following characteristics.

Tube diameter at fin root	$[mm]$	8.95
Fin numbers		55
Helix angle	$[°]$	15
Fin height	$[mm]$	0.24
Tube length	$[m]$	1.0

Table 4.4: Rollmann and Spindler tube characteristics.

The correlation does not take into account any specific behavior of two-phase flow boiling in channel tubes, so the derivation of final equation is just an accurate interpolation of data referring to the Nusselt number. Hence, the final equation describes the trend of Nusselt number as function of mean quality, Boiling number, Reynolds number and Prandtl number. The analysis is divided in five steps:

1. Compute the relationship between Nusselt number and the mean vapor quality by means of a polynomial equation;
2. Include the effects of heat flux and saturated enthalpy considering Boiling number, by means of a logarithmic equation;
3. Include the effects of inertia and viscous forces by considering Reynolds number, by means of a polynomial equation;
4. Include the effects of saturation temperature by considering Prandtl number, by means of a polynomial equation;
5. Consider the reciprocal influence of each of the mentioned quantity and introduce adjustments on the empirical values.

Proceeding with the mentioned analysis the final output is:

$$Nu(x, Bo, Re, Pr) = C_4 \left(\frac{C_1}{Pr^2} + C_2 \right) Re^{2/3} [ln(Bo) + C_3] x^{\left(\frac{C_1}{Pr^2} + C_2\right)} \tag{4.22}$$

The Nusselt number is referred to diameter of the tube at the fin root and the thermal conductivity of the liquid phase in operating condition. The correlation has been developed through an analytical procedure, so it is subjected to mathematical restrictions.

A minimal positive variation of mean quality is required, otherwise $Nu \leq 0$, so this correlation is only applicable to boiling experiments. Even Prandtl number has a minimum value that ensure positive sign of Nusselt number.

Limits of applicable range are here reported:

Δx	minimum	0.024
Pr_l	minimum	2.283

Table 4.5: Rollmann and Spindler applicable limits.

The mean deviation is 9.81%, within the range of 30% there are 94.18% of the measured values.

4.5 Cavallini Rossetto

The authors [17] conduced experiments on R1234ze, R1234yf and R134a flow boiling inside microfin tubes. The tubes parameters are:

The experimental conditions that the authors applied are reported in tab. 4.7.

The correlation for the heat transfer coefficient takes into account three different physical phenomena that affect thermal properties of heat exchange:

- Nucleate boiling;
- Convection;
- Capillarity (present only in case of very low mass flow rate).

Tube diameter at fin tip	$[mm]$	[2.4;3.4]
Fin numbers		40
Helix angle	$[°]$	[7;18]
Apex angle	$[°]$	43
Fin height	$[mm]$	0.12
Tube length	$[m]$	0.3

Table 4.6: Cavallini tube characteristics.

Saturation Temperature	$[°C]$	30
Mass flux	$[kg/m^2s]$	[190;940]
Heat flux	$[kW/m^2]$	[10;50]
Quality variation		[0.07;0.3]

Table 4.7: Cavallini Rossetto correlation experimental conditions.

The related heat transfer coefficients are computed separately, they are summed up in order to compute the two-phase heat transfer coefficient.

$$h_{tp} = h_{nb} + h_{cv} + h_{cap} \tag{4.23}$$

$$h_{nb} = h_{Cooper} S F_1(d) \tag{4.24}$$

$$h_{Cooper} = 55 p_{red}^{0.12} [-log(p_{red})]^{-0.55} M^{-0.5} q^{0.67} \tag{4.25}$$

$$S = A_1 X_{tt}^B \tag{4.26}$$

where:

- $A_1 = 1.36$ and $B = 0.36$ for $G > 100 kg/m^2 s$;
- $A_1 = 1.36 sin(\beta)$ and $B = 0.36(G/100)^4$ for $G \leq 100 kg/m^2 s$;
- $F_1(d) = (d_0/d)^{0.38}$ and $d_0 = 0.01m$.

$$h_{cv} = (k_l/d) Nu_{cv,smooth} Rx^{2.14} (BondFr_v)^t F_2(d) F_3(G) \tag{4.27}$$

where:

- $t = -0.15$ for $G < 500 kg/m^2 s$; $t = -0.21$ for $G \geq 500 kg/m^2 s$
- $Nu_{cv,smooth} = Nu_{lo} \Phi$
- $\Phi = [(1 - x) + 2.63 x (\rho_l/\rho_v)^{0.5}]^{0.8}$
- $Nu_{lo} = 0.023 Re_{lo}^{0.8} Pr_l^{1/3}$
- $Bond = g \rho_l h_{fin} \pi d / (8 \sigma n_g)$
- $F_2(d) = (d_0/d)^{0.59}$ and $d_0 = 0.01m$
- $F_3(G) = (G_0/G)^Z$ and $G_0 = 100 kg/m^2 s$

- $Z = 0.36$ for $G > 100 kg/m^2 s$; $Z = -3$ for $G \leq 100 kg/m^2 s$

$$h_{cap} = 0.332 k_l / h_{fin} [G h_{lv} sin(\beta)/q]^{0.4326} F_G \tag{4.28}$$

where:

- $F_G = 0$ for $G > 100 kg/m^2 s$
- $F_G = 1 - (G/G_0)^3$ for $50 kg/m^2 s < G \leq 100 kg/m^2 s$
- $F_G = 1 - 1.75(G/G_0)$ for $G \leq 50 kg/m^2 s$

Good agreement has been obtained for R134a, indeed mean absolute deviation was 14.5% and mean standard deviation was -9.9%. Such a result shows that its prediction accuracy is not affected by reduced pressure.

4.6 Kumar Mohseni

Experimental heat transfer during condensation of pure R134a inside microfin tube has been studied by the authors [18]. The data are acquired and analyzed for different tube inclination angles. Since this thesis focuses only on horizontal flow, this condition is the only one taken into account.

Saturation Temperature	$[°C]$	[26;32]
Mass flux	$[kg/m^2 s]$	[54;107]
Heat flux	$[kW/m^2]$	[8.7;20.3]
Average vapor quality		[0.2;0.8]

Table 4.8: Kumar Mohseni correlation experimental conditions.

Outside tube diameter	$[mm]$	9.52
Inside tube diameter	$[mm]$	8.92
Fin numbers		55
Helix angle	[°]	15
Apex angle	[°]	25
Fin height	$[mm]$	0.25
Fin pitch	$[mm]$	0.48

Table 4.9: Kumar Mohseni tube characteristics.

The operating parameters are reported in tab. 4.8, while tab. 4.9 describes the geometry of the microfin tube selected for the experiments.

The following correlation has been developed to predict heat transfer coefficient at different vapor qualities, mass velocities and tube inclinations.

$$Nu = 1.09 Re_l^{0.45} F_\alpha^{0.3} \sqrt{\frac{Pr_l}{X_{tt}}} \tag{4.29}$$

where the dimensionless numbers are computed conventionally considering liquid phase properties, and the Lockhart-Martinelli parameter is obtained by:

$$X_{tt} = \left(\frac{1-x}{x}\right)^{0.9} \left(\frac{\rho_v}{\rho_l}\right)^{0.5} \left(\frac{\mu_l}{\mu_v}\right)^{0.1}. \tag{4.30}$$

F_α considers the effects of inclination of the tube, its formulation is affected by the average quality.

$$F_\alpha = \frac{[1 + (1-x)^{0.2} cos(\alpha - 10°)]}{x^{0.4}} \tag{4.31}$$

For this thesis purposes, α is fixed at 0°.

The above correlation predicted analyzed data for all inclination of finned tube on an error band of 10%.

4.7 Oh Son

The condensation heat transfer coefficients of R22, R134a and R410a in a single tube were investigated. The test section was a horizontal copper tube of 1.77mm inner diameter. The experiments were conducted at a saturation temperature of $40°C$ and mass flux ranging between $[340; 1150] kg/m^2 s$. Prediction of this correlation [19] is considered valid for

- $0.5 < Pr < 2000$
- $3000 < Re < 5 \times 10^6$

as required from Gnielinski equation. Nusselt number is so computed:

$$Nu_{Gn} = \frac{(f/8)(Re - 1000)Pr}{1 + 12.7(f/8)^{1/2}(Pr^{2/3} - 1)} \tag{4.32}$$

The friction factor is calculated using the expression:

$$f = (0.79 ln(Re) - 1.64)^{-2} \tag{4.33}$$

The Nusselt number is referred to the inner diameter and the liquid thermal conductivity.

The maximum deviation from experimental data that the correlation provided was ±13.5%.

4.8 Cavallini et al.

The presented correlation [20] has been developed on the base of condensation experiments in horizontal microfin tubes of refrigerants and pure fluids. The tests conditions and tube geometry are reported in the following tables.

The heat transfer coefficient is computed as the combination of two terms: the heat transfer coefficient for the ΔT independent zone (α_A) and the heat transfer coefficient for the ΔT dependent zone (α_D).

$$\alpha = [\alpha_A^3 + \alpha_D^3]^{1/3} \tag{4.34}$$

Saturation Temperature	$[°C]$	[30;60]
Mass flux	$[kg/m^2s]$	[100;800]
Reduced pressure		[0.24;0.51]
Average vapor quality		[0.2;0.85]

Table 4.10: Cavallini correlation, condensation experimental conditions.

Fin tip diameter	$[mm]$	7.69
Fin numbers		60
Helix angle	$[°]$	13
Apex angle	$[°]$	43
Fin height	$[mm]$	0.23

Table 4.11: Cavallini enhanced tube characteristics.

The forced convective condensation term α_A is obtained as the product of the convective heat transfer coefficient for the smooth tube by a function of geometry enhancement factor.

$$\alpha_A = AC\alpha_{lo}\left[1 + 1.128x^{0.817}\left(\frac{\rho_l}{\rho_g}\right)^{0.3685}\left(\frac{\mu_l}{\mu_g}\right)^{0.2363}\left(1-\frac{\mu_g}{\mu_l}\right)^{2.144} Pr_l^{-0.1}\right] \tag{4.35}$$

$$\alpha_{lo} = 0.023\frac{k_l}{d}Re_{lo}^{0.8}Pr_l^{0.4} \tag{4.36}$$

$$A = 1 + 1.119Fr^{-0.3821}(Rx-1)^{0.3586} \tag{4.37}$$

$$Rx = \left\{\frac{2e_{fin}n_g[1-sin(\gamma/2)]}{\pi dcos(\gamma/2)} + 1\right\}\frac{1}{cos\beta} \tag{4.38}$$

where

- $C = 1$ if $(n_{opt}/n_g) \geq 0.8$
- $C = (n_{opt}/n_g)^{1.904}$ if $(n_{opt}/n_g) < 0.8$

and

$$n_{opt} = 4064.4d + 23.257 \tag{4.39}$$

All the reported equation refer to d as the fin tip diameter.
The heat transfer coefficient for the ΔT dependent zone depends on the transition gas velocity.

$$\alpha_D = C[2.4x^{0.1206}(Rx-1)^{1.466}C_1^{0.6875} + 1]\alpha_{DS} + C(1-x^{0.087})Rx\alpha_{lo} \tag{4.40}$$

$$\alpha_{DS} = \frac{0.725}{1 + 0.741\left[\frac{1-x}{x}\right]^{0.3321}}\left[\frac{k_l^3\rho_l(\rho_l-\rho_g)gh_{lg}}{\mu_l d\Delta T}\right]^{0.25} \tag{4.41}$$

where

- $C_1 = 1$ if $J_G \geq J_G^*$
- $C_1 = (J_G/J_G^*)$ if $J_G < J_G^*$

and the transition gas velocity is defined as:

$$J_G^* = 0.6 \left\{ \left[\frac{7.5}{4.3 X_{tt}^{1.111}} \right]^{-3} + 2.5^{-3} \right\}^{-1/3} \tag{4.42}$$

	High pressure	**Medium low pressure**
$e_R[\%]$	-3.8	-8.0
$e_{AB}[\%]$	9.1	12
$\sigma_N[\%]$	11	13

Table 4.12: Predictive performances of Cavallini experimental correlation for condensation tests.

Present model is based on databank considering high pressure experiments and low and medium pressure experiments conducted by Cavallini in the previous year, Eckels and Kedzierski. The heat transfer coefficients predicted in case of high pressure tests presented lower deviation from experimental data, with respect to the values obtained for medium and low pressure. The values of average deviation (e_R), mean absolute deviation (e_AB) and standard deviation (σ_N)are reported in tab. 4.12.

4.9 Kedzierski Goncalves

The author proposed a correlation [21] for convective condensation inside microfin tube of pure refrigerants. The analysis is limited to heat transfer coefficient and pressure drop for horizontal flows. In this section the heat transfer correlation is presented. For pressure drop analysis and relative correlation development, see section 3.7.

The test section was a copper microfin tube with the following geometrical parameters:

Test section lenght	$[m]$	3.34
Fin root diameter	$[mm]$	8.91
Tube wall thickness	$[mm]$	0.30
Hydraulic diameter	$[mm]$	5.45
Fin numbers		60
Helix angle	$[^\circ]$	18
Fin height	$[mm]$	0.2

Table 4.13: Kedzierski microfin tube characteristics.

The convective condensation Nusselt numbers were correlated following the hypothesis that the fluid properties that govern nucleate pool boiling can be well represented by a product of the reduced pressure, the acentric factor and other dimensionless variables to various powers. The above reduced pressure terms and several other locally evaluated terms were used to correlate the measured local Nu for all condensing flow conditions and refrigerants in authors' study. Simplifications led to:

Saturation Temperature	$[°C]$	[20;50]
Mass flux	$[kg/m^2s]$	[57;552]
Average vapor quality		[0.06;1.0]
Heat flux	$[kW/m^2]$	[0.72;39]

Table 4.14: Kedzierski correlation, condensation experimental conditions.

$$Nu = 4.94Re^{0.235}Pr_l^{0.308}p_{red}^{-1.16x^2}(-log_{10}(p_{red}))^{-0.887x^2}Sv^{2.708x} \tag{4.43}$$

where S_v is defined ad the non-dimensional refrigerant specific volume:

$$S_v = \frac{v_g - v_l}{xv_g + (1-x)v_l} \tag{4.44}$$

The Nusselt is referred to the hydraulic diameter. The databank used for the analysis was predicted with different accuracy depending on the analyzed data.

	Deviation [%]
Mori and Nakayama (1983)	±20
Chiang (1993)	-20
Khanpara et al. (1986)	-30
Chamra and Webb (1995)	±40

Table 4.15: Predictive performances of Kedzierski Goncalves correlation for condensation.

Chapter 5

Experimental apparatus

5.1 Plant characteristics

The experimental apparatus, which scheme is depicted in fig. 5.1, is composed by three main circuits:

1. refrigerant circuit;
2. demineralized water circuit;
3. cooling water circuit.

These loops are designed to interact each other, exchanging thermal power, in order to provide the desired test condition. Every part is equipped with instruments and controls to set and monitor the thermodynamic properties of the fluids and components' operating conditions. All the measurements are performed on a *test section*, that consists in a concentric heat exchanger. The refrigerant circuit is endowed with a *visualization apparatus*, which allows a visual identification of the flow pattern. The characteristics of these components will be further discussed in the following sections. The interaction between the parts of the plant have two main purposes:

1. to set and keep the operating conditions of a particular component of the plant, task performed by the **water and glycol circuit**;
2. to set and keep the operating condition for measurement execution, task performed by the **demineralized water circuit**.

The description of the facility components aims to give the following information:

- purpose;
- design;
- instrumentation;
- interaction with the other parts of the plant.

In this chapter will be discussed also the experiment protocols and the effect of instruments error on the measurements.

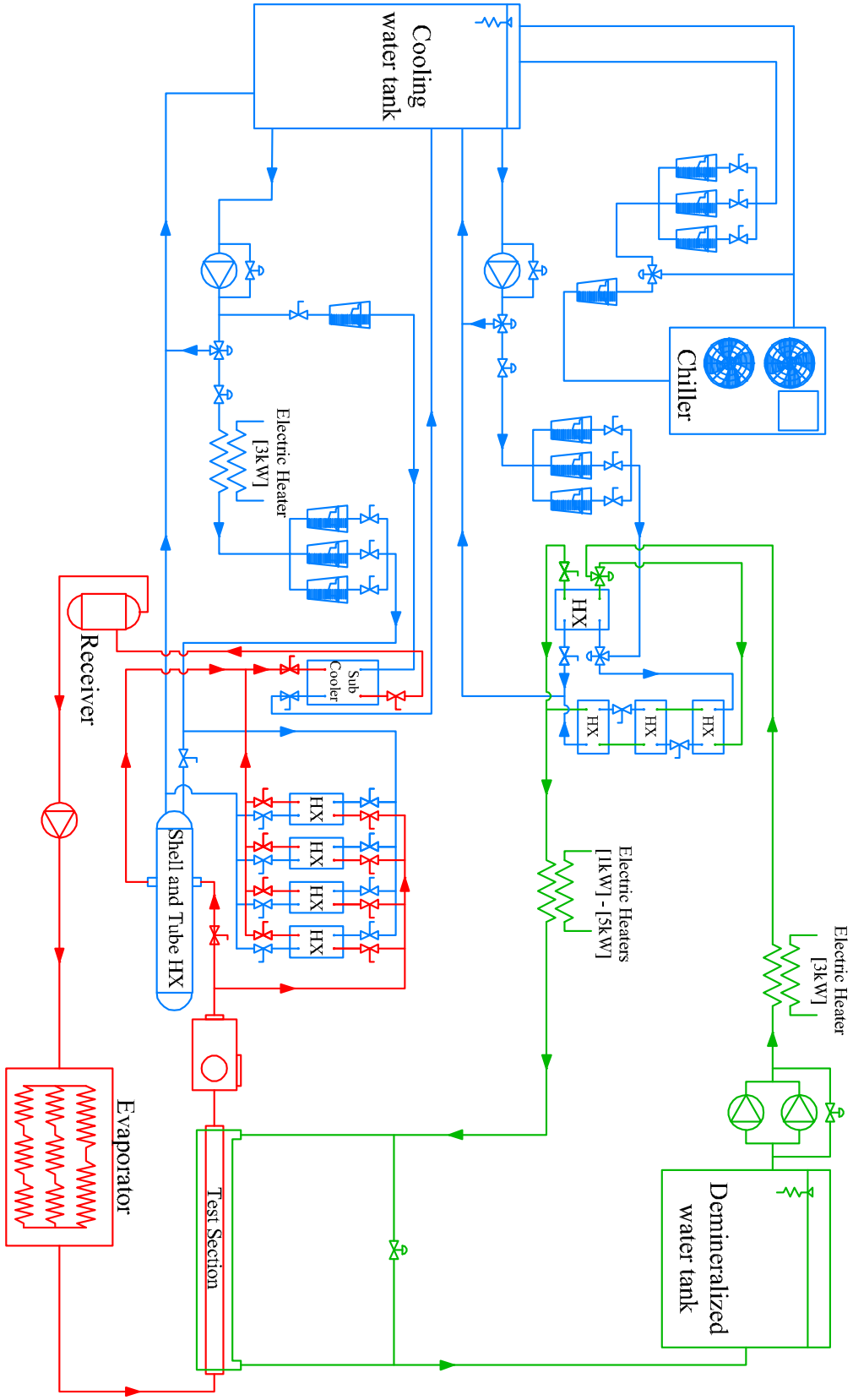

Figure 5.1: Scheme of the experimental facility and circuits interactions.

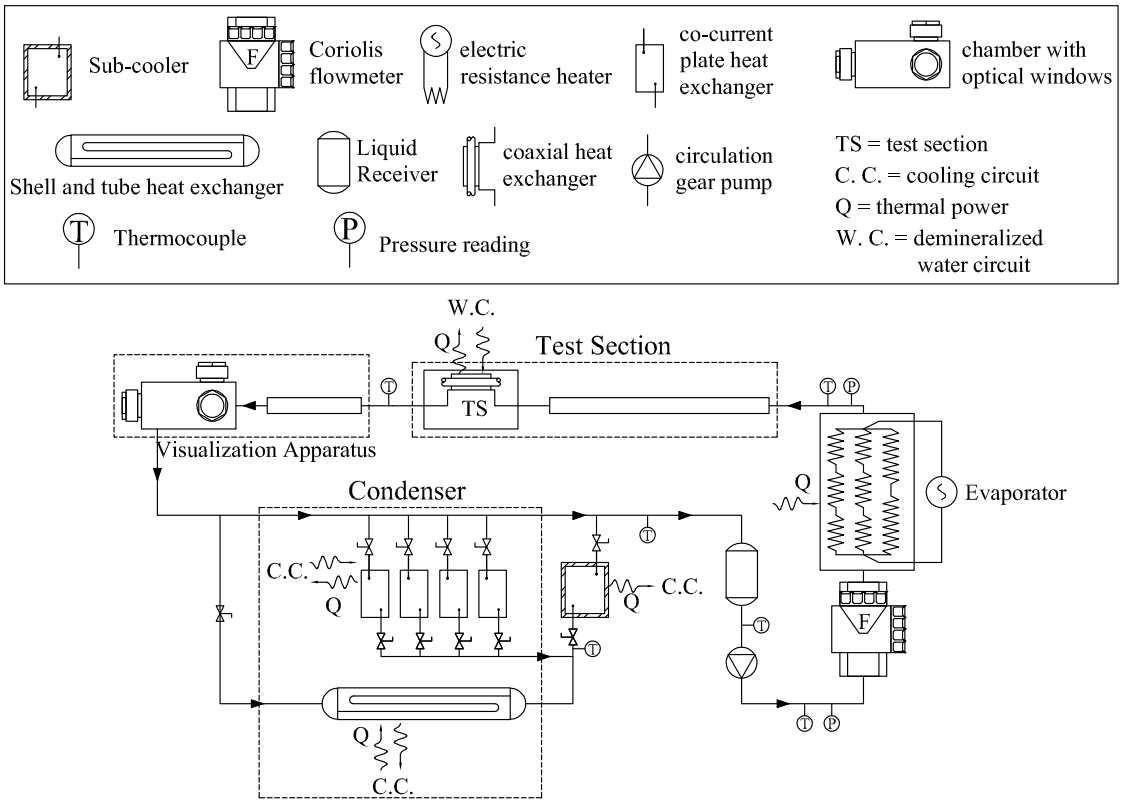

Figure 5.2: Refrigerant loop.

5.2 Refrigerant circuit

5.2.1 Purpose

The tasks of the refrigerant circuit are:

1. to bring a specified liquid vapor mixture at the inlet of the test section;
2. to drain the refrigerant from the visualization apparatus to the condenser.

5.2.2 Design

The component of the refrigerant circuit (fig. 5.2) are:

1. the test section;
2. the visualization apparatus;
3. the condenser, composed by a parallel of four plate heat exchangers and one shell and tube heat exchanger

- the shell and tube heat exchanger: it is a condenser designed for refrigerants (refrigerant side volume 14 dm^3; water side volume 5.2 dm^3). It provides the condensation of the refrigerant outlet from the test section through the heat exchange with the cooling circuit and it can be exploited as liquid storage. The refrigerant inlet is located close to the highest point of the rear header of the condenser, while the outlet is at the bottom of the frontal header. In order to set an efficient heat exchange and to reduce pressure drop, it is recommended to work with a water velocity in the range of 1.2 m/s 2.8 m/s;
- the plate heat exchangers: they are disposed in parallel so that it is possible to exploit different combinations of them, this ensures an high flexibility of the system.

4. the sub-cooler: it is a plate counter current heat exchanger which ensures the outlet stream to be fully liquid. This avoids cavitation problems in the pump;

5. the liquid receiver: a container used to manage eventual excess of liquid in the system;

6. the gear pump, it is equipped with an inverter such that it is possible to control the speed of the pump with an uncertainty of 0.01% with respect to the maximum power. Its range of applicability is limited by volume flow rate between values of $[4; 400]l/h$. It provides the correct mass flow rate in the test section;

7. the Coriolis flow-meter: this instrument gives as output the mass flow rate and the density of the fluid at the inlet of evaporator;

8. the evaporator: it is composed by eight electric resistances, each of 50 Ω. The configuration of the resistances is aimed to obtain a total power of 9 kW distributed with a decreasing pattern of power so to improve phase equilibrium. The evaporator aims to provide the power needed to set the desired quality of the refrigerant at the inlet of the test section. The evaporator control system takes as input a reference time interval (from 1 to 4 seconds) and the desired percentage of the maximum power. The needed power is so provided by the integral average of the maximum power;

9. the thermal insulator, the evaporator case is completely filled with rubber foam, so the thermal losses are negligible with respect to the provided ones. To reach a value of thermal loss close to 1.0 W/m, both the calming sections and the test section are insulated by means of a rubber foam tube 10 cm thick. For both condensation and evaporation, the enthalpic flow in the worst case is 1571 W (corresponding to the lowest applied mass flow rate of 25 kg/h and the minimum inlet quality of 0.1) so the thermal loss allowed leads to a deviation with respect to the desired inlet quality of 0.004. It is negligible considering that the deviation due to regime fluctuations is an order of magnitude greater. Hence, this portion of the loop can be considered adiabatic with respect to the ambient, indeed the thermal loss corresponds to the 0.3% of the inlet thermal power. All the other loop's components are insulated with a rubber foam 2 cm thick.

5.2.3 Instrumentation

Refrigerant temperature is measured upstream and downstream of the test section, at the outlet of the condenser and downstream the Coriolis flow-meter. The measurement is acted by means

of thermocouples inserted in 60 mm long, 3-4 mm o.d., stainless steel L-shaped wells located on the duct axis. The pressure of the fluid is measured by three absolute pressure gauges located upstream and downstream the evaporator. Every electric resistance of the evaporator is endowed with a thermocouple due to safety reasons.

5.2.4 Interaction with the other parts of the facility

The refrigerant circuit has a thermal power exchange with:

- the water loop, in the test section, to set the heat flux or the quality change from which to obtain the desired measurements on the refrigerant. The test section behaves like a counter current concentric tube heat exchanger;

- the cooling circuit, in the condenser and the sub-cooler. Shell and tube heat exchanger or plate ones can be both exploited to get the condensation of the refrigerant and in the sub-cooler is extracted the thermal power to guarantee a fully liquid stream at the inlet of the pump.

5.3 Demineralized water circuit

5.3.1 Purpose

The water circuit is designed to perform a quality variation of the refrigerant two-phase flow inside the test section. To respond to this particular task, mass flow rate and temperature difference of the water must be fixed. The inlet temperature of the test section is set through an iterative procedure so to have $\Delta T = 2K$ and the PID controllers on electrical heaters select the necessary thermal power that has to be provided to the demineralized water.

5.3.2 Design

The parts of the circuits (fig. 5.3) are:

1. the counter current concentric heat exchanger on the test section;

2. the demineralized water tank, it is a 200 l tank thermal insulated through an elastomer layer 2 cm thick;

3. the pumps, they are connected in parallel. Both of them are centrifugal pumps with a directly connected shaft. The smaller one has a power of 0.55 kW and it works with a mass flow rate in the range of $[1; 4.8]m^3/s$; the more powerful has a power of 4 kW and it works with a mass flow rate in the range of $[2.4; 9.6]m^3/s$;

4. an electric resistance of 3 kW, to warm up the water upstream the heat exchange with the cooling circuit and to prevent the water from freezing due to the low temperature that the mix of water and glycol can reach.

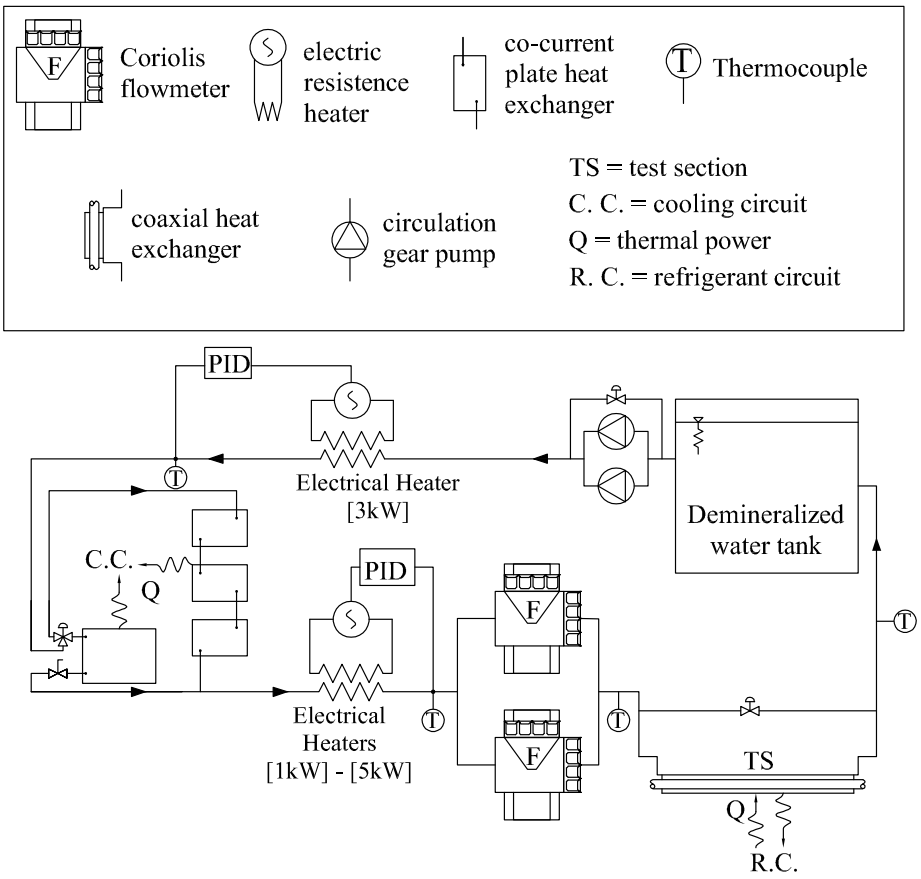

Figure 5.3: Water loop.

5. the plate heat exchangers, three of them are connected in series and they present the same contact surface and shape. The fourth one is connected in parallel and it has a contact surface greater than the sum of series ones, so it is used when the desired heat flux on the test section is low;

6. two electric resistances of 1 and 5 kW downstream the heat exchange with the cooling circuit in order to set the desired temperature at the inlet of the test section;

7. the thermal insulator, it is a rubber foam tube 2 cm thick.

5.3.3 Instrumentation

On the water circuit there are two kinds of measurement devices:

- K-type thermocouples: they are six in number, grouped in two thermal probes located at the inlet and at the outlet of test section and are used to measure the bulk temperature of the water stream. Each probe consists of three thermocouples cemented in three fine wells

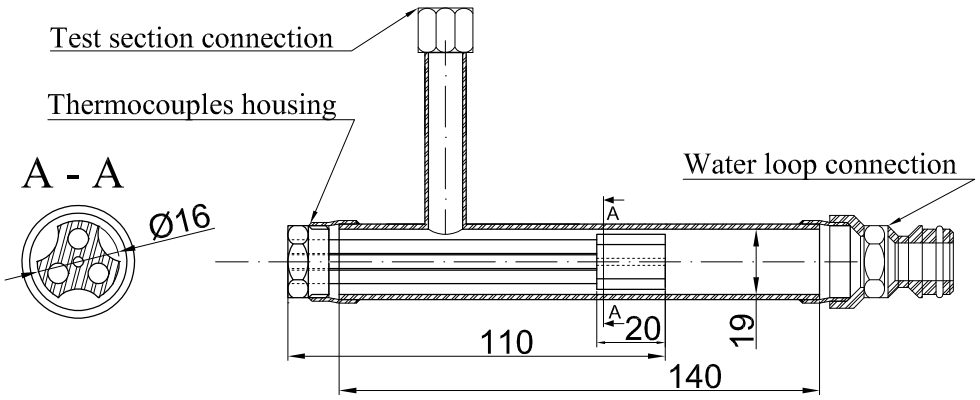

Figure 5.4: Temperature probe placed in the water loop

drilled in a brass cylinder with an outer diameter of 16 mm and a height of 20 mm depicted in fig. 5.4. Such a cylinder reduces the area of stream cross-section, thus promoting flow mixing and hence equalization of the liquid temperature. Dimensions of thermocouples' housing and connections to the test sections are designed such that the reading of the thermocouples is not affected by the flow regime, which varies due to the shape of the components;

- the Coriolis flow-meter, they are connected in parallel. The one that provides the lower uncertainty ($\pm 0.15\%$ of the reading) can be used for mass flow rates in the range of $[0; 400]; kg/h$, for values of mass flow rate higher than 400 kg/h it is necessary to exploit the flow-meter with a range of $[0; 6500]; kg/h$ that provides the higher uncertainty ($\pm 0.3\%$ of the reading).

5.3.4 Interaction with the other parts of the facility

The water loop has thermal power exchange with:

- the refrigerant circuit, in the test section, to produce the quality variation defined for the experiment;

- the cooling circuit, in the plate heat exchangers, to reduce the temperature of the water. It is not always required; performing some experiments that interaction does not take place.

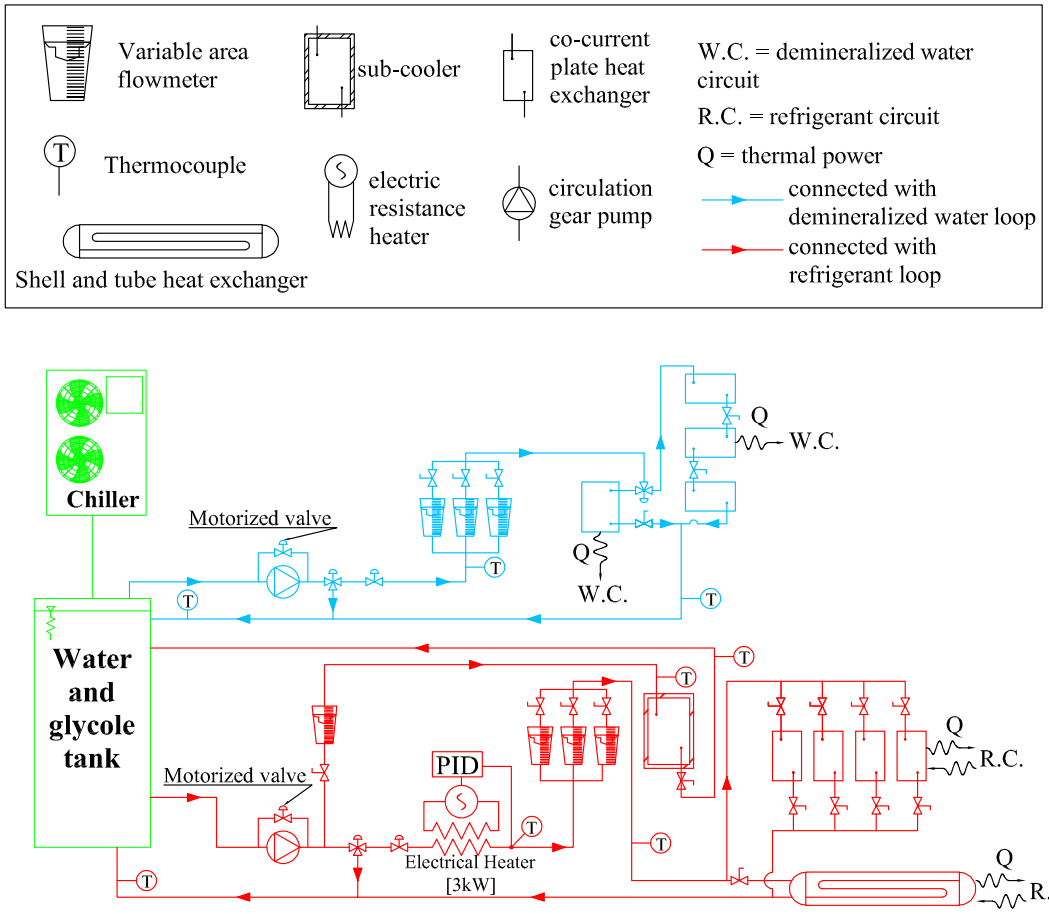

Figure 5.5: Water and glycol circuit.

5.4 Water and glycol circuit

5.4.1 Purpose

The cooling loop is a service part of the plant. It is not directly involved in measurement and it does not have a straight connection with the test section. It has the task to fix the temperature of:

- the condenser: to set the right pressure such that in the test section there is the proper temperature for the measurement;
- the liquid refrigerant: before it enters the circulation pump, to avoid cavitation;
- the water flowing to the test section: to set the the thermal power exchanged in the test section.

5.4.2 Design

The coolant flowing in the circuit is a mixture of water (70%) and glycol (30%) and its freezing temperature is 253.15 K ($-20°C$).

It is divided in two sub-circuits (fig. 5.5):

- a circuit aimed to exchange thermal power with the demineralized water circuit, composed by:

  1. one centrifugal circulation pump endowed with a bypass valve;
  2. a parallel of three variable area flow-meters;
  3. the plate heat exchangers used to chill the water, see section 5.3;
  4. the tank: it has a volume of 0.75 m^3 and is thermally insulated with a 2 cm thick elastomer layer;

- a circuit aimed to exchange thermal power with the refrigerant circuit, composed by:

  1. one centrifugal circulation pump endowed with a bypass valve;
  2. a 3 kW electric heater;
  3. a parallel of four variable area flow-meters;
  4. the shell and tube heat exchanger to condense the refrigerant out-flowing from the test section (see sections 5.2;
  5. the sub-cooler;
  6. the thermal insulator, it is a plastic foam tube 2 cm thick.
  7. the chiller: it is an industrial machine produced by Carrier, model 30RA021C9HZ nominal power is 21kW, set to cool the mixture to 261.15 K ($-12°C$). It works in a discontinuous way, a sensor activates the chiller when the temperature of the mixture in the tank is above 264.15 K ($-9°C$) and stops it when a temperature of 261.15 K ($-12°C$) is reached;

5.4.3 Instrumentation

There are two type of measurements instrument, namely, variable area flow-meters and thermocouples. The former are manually regulated with a valve to set volumetric flow rate. They are seven:

- one is connected directly to the sub-cooler;
- three are before the branches with plates heat exchangers on the refrigerant circuit;
- three are before the branches with plates heat exchangers on the water circuit.

5.4.4 Interaction with the other parts of the facility

The cooling circuit exchanges thermal power with both the other loops, see sections 5.2 and 5.3). The interaction with refrigerant circuit is mainly characterized by extraction of thermal power to induce the refrigerant to condense; but in the transient occurring at the start of the facility, heat exchangers can be used also as evaporators in order to extract liquid refrigerant trapped in heat exchangers themselves.

5.5 Test section

The test section is the part of the refrigerant loop where measurements take place.

5.5.1 Purpose

The tasks of the test section are:

1. the flow regime development;
2. to provide or remove the thermal power required for evaporation or condensation of the refrigerant;
3. to perform temperature and pressure drop measurement.

Two types of tubes has been used as the inner component of the subsection: one *smooth* and one *microfin*. The choice aims to compare the behavior of the refrigerant (in terms of heat transfer coefficient and pressure drop) in the two cases. The characteristic of the tubes are the following ones:

Tube		**Smooth**	**Microfin**
inner diameter (fin root)	$[mm]$	8.92	8.96
outer diameter	$[mm]$	9.52	9.52
wet perimeter $[S_p]$	$[mm]$	28.0	44.9
cross section area $[A_c]$	$[mm^2]$	62.5	62.2
hydraulic diameter $[D_h]$	$[mm]$	8.92	5.28
exchanging area ratio		1.00	1.68
fin number $[N]$			60
height	$[mm]$		0.2
apex angle	$[°]$		40
helix angle $[\alpha]$	$[°]$		18

Table 5.1: Smooth and microfin tube characteristics

In the present analysis, the hydraulic diameter (D_h) was used to correlate the pressure drop data. Kedzierski and Goncalves [21] recommend that the hydraulic diameter for micro-fin tubes be calculated as:

$$D_h = \frac{4A_c cos(\alpha)}{NS_p} \tag{5.1}$$

In fig. 5.6 it is depicted a comparison between the two sections, in order to highlight the effect of the fins on the tube geometry.

5.5.2 Design

The test section (fig. 5.7) is made of:

1. a calming section: it is a copper smooth tube (9.52 mm outer diameter, 8.92 mm inner diameter) aimed to reach the thermal equilibrium between liquid and vapor refrigerant and the development of the flow pattern. There are two references about the minimum length required for the development of the flow pattern in adiabatic tubes:

   Simpson [22] proposed:

   $$\frac{L}{D} \geq 128 \qquad \Rightarrow \qquad L \geq 1.14m \tag{5.2}$$

   Weisman [23] proposed:

   $$\frac{L}{D} \geq 60 \qquad \Rightarrow \qquad L \geq 0.54m \tag{5.3}$$

   where: L $[m]$ tube length;
   D $[m]$ tube inner diameter.

   The calming section length is 4.7 m, this value is larger than minimum length and it has been chosen to respect all the mechanical constrains of the facility.To reduce temperature difference between liquid and vapor, the flow passes in both channels of a plate heat exchanger placed between the evaporator outlet and the calming section inlet;

2. a subsection (fig. 5.7 and fig. 5.8) is a concentric tube heat exchanger. The refrigerant flows in the inner tube, it is microfin, made of copper, 1.3 m long (tab. 5.5.1); while demineralized water flows in the outer tube (a plexiglas tube 20 mm outer diameter, 14 mm inner diameter, its length is such that the distance between demineralized water inlet and outlet is 1.07 m). The inner tube, the outer tube and the demineralized water loop are connected by a two housing element (fig. 5.8) endowed with four threaded holes (one for every arm of the cross), placed at both ends of the outer tube, suitably designed to:

   (a) fasten, through compression between two O-rings inserted on the edge of the hole, the outer tube;

   (b) fasten, with a straight fitting, the inner tube;

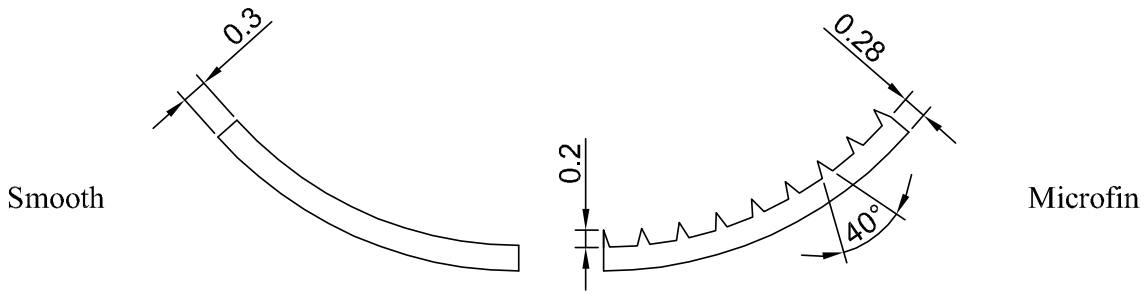

Figure 5.6: Tubes geometry.

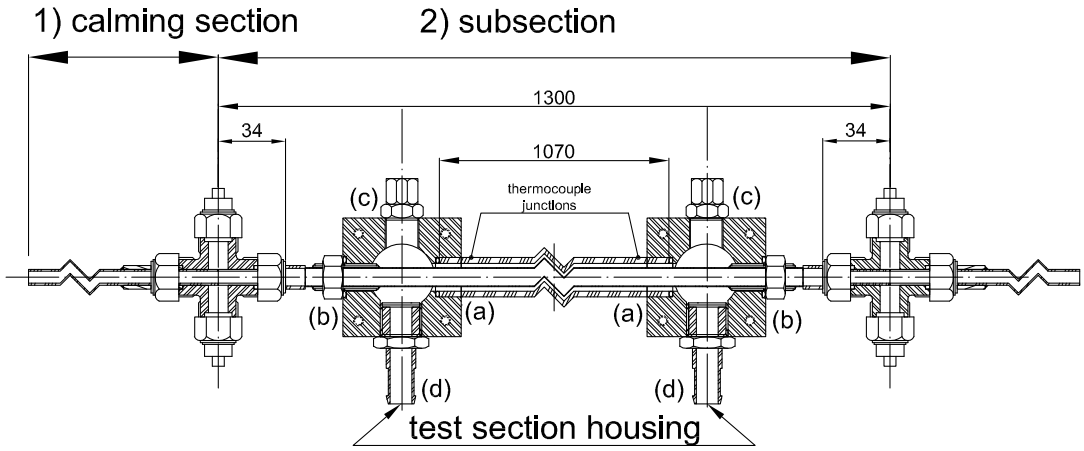

Figure 5.7: Test section.

(c) insert thermocouples in the external annulus of the subsection and glue them in the grooved machined in the external wall of the inner tube; to avoid thermocouples damaging they are placed in heat shrink tubing filled up with silicone. All the tubing are inserted in a straight fitting and then fixed to the housing by means of a silicone plug that also avoids water leakages;

(d) connect water side and demineralized water loop: water junctions has been designed to be identical both for the inlet and the outlet of water flow.

The distance between the demineralized water inlet and outlet is assumed as the active heat transfer length for the subsection. Calming section is insulated by placing a 1 cm thick foam plastic annulus over the copper tube and 10 cm thick glass-wool annulus over the foam plastic annulus. The test section insulation consists of a 10 cm thick rubber foam annulus.

The subsection is connected to the loop, without any change in the duct internal diameter, via two 4-way cross fittings, to make easier the change of the pressure transducer connection passing from evaporation to condensation and viceversa. Two pressure taps are drilled in each junction; the gap between the inner surface of the fitting and the outer surface of the tube serves as a pressure annular-chamber; pressure taps are connected via a manifold to pressure transducers.

5.5.3 Instrumentation

In the test section the following measurements are performed:

- temperature:
  - the test section is equipped with six K-type thermocouples to measure wall temperatures, which are placed at 140 mm from either ends in groups of three. They are disposed one on the upper part of the inner tube surface, one on the bottom part and one at the same height of the tube axis, such a configuration is useful to observe the

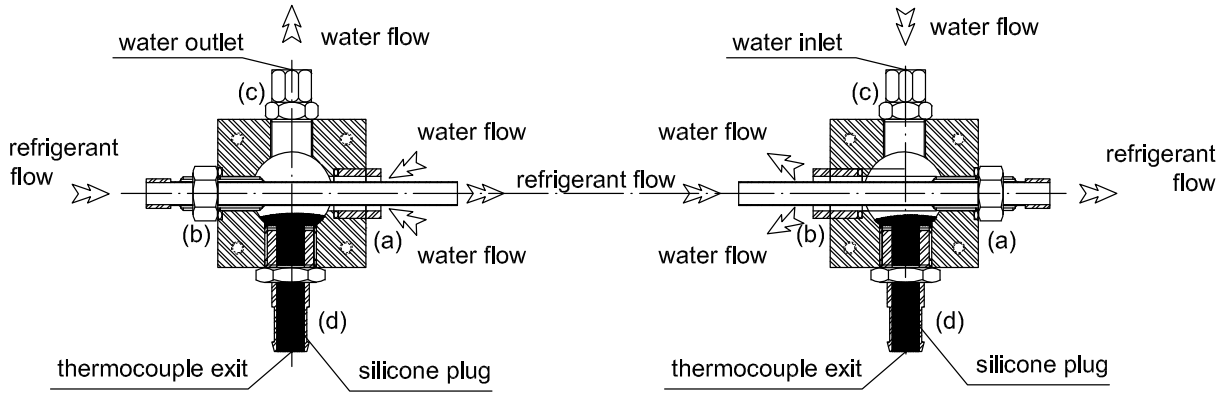

Figure 5.8: Subsection: connections.

different behavior of the wall temperature depending on the flow regime. Thermocouple wires are 0.15 mm diameter, and they are cemented in longitudinal grooves (50 mm long, 0.5 mm large and 0.2 mm deep) machined in the outside wall of the tube (fig. 5.9);

– the inlet and the outlet of the subsection are equipped with K-type thermocouples inserted in 60 mm long, 3 mm o.d., stainless steel L-shaped wells located on the duct axis to measure refrigerant temperature (fig. 5.9);

- pressure: the refrigerant inlet pressure is measured with an absolute strain-gauge transducer, whereas pressure drop along the test section is measured with two inductive differential pressure transducers.

5.5.4 Interaction with the other parts of the facility

The test section interacts thermally only with the demineralized water circuit. The experiments require condensation or evaporation of a specified amount of the refrigerant flow entering in the test section, the removal or supplying of latent heat is performed by demineralized water in the subsection.

5.6 Visualization apparatus

5.6.1 Purpose

The visualization apparatus is a part of the refrigerant loop and it has two main purposes:

- to eliminate the perturbation due to the temperature and pressure probes at the end of the test section;
- to allow visual inspections of the flow regime of the refrigerant at the end of the test section.

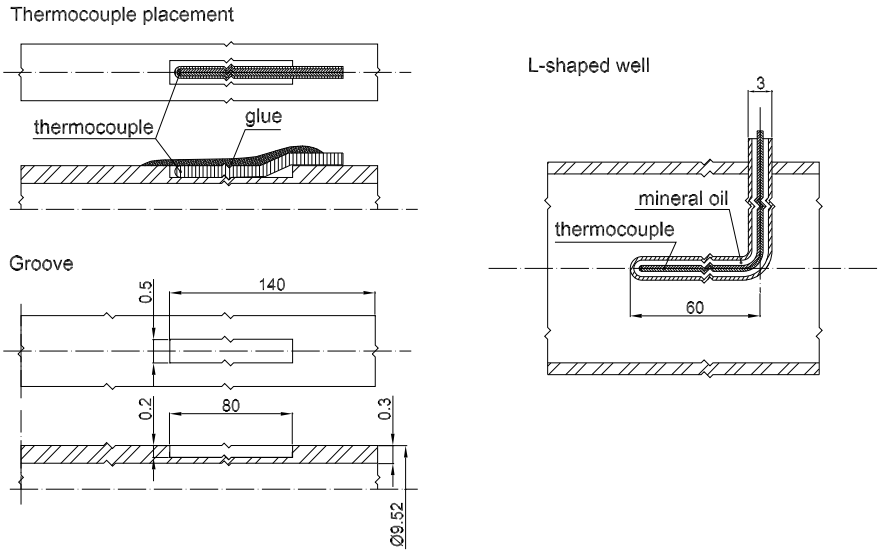

Figure 5.9: Groove for thermocouple placement.

5.6.2 Design

The visualization apparatus is made of two components:

- the calming section: it is an adiabatic conduit 0,5 m long made by the same tube used to realize the inner part of a subsection. It is placed after the test section to eliminate the perturbation of the flow due to the pressure taps and to the L-shaped wells. It is connected to the chamber with a straight fitting. The ending part of the calming section is inserted in the chamber and it is cut along a vertical plane inclined of 45° with respect to the tube axis. The calming sections is insulated by a 1 cm thick, foam plastic annulus on the copper tube, 10 cm thick, rubber foam annulus on the foam plastic annulus.

- the chamber (fig. 5.10) where the refrigerant flows into: it is a steel box with three glass windows 1 cm thick, one for recording videos with a camera, and two for illumination. To ensure seal the round windows are fixed by a properly designed threaded nut, two nitrile rubber rings avoid leakage and the breaking of the glass window after the tightening. The lower part is inclined to drain the liquid toward the exit duct, it brings liquid and vapor to the condenser.

5.6.3 Instrumentation

No instruments are installed in the test section. On the outside, near the visualization window, which is aside the calming section, is placed an high speed camera to record the flow regime at the end of the calming section. Near the illumination windows, which is above the calming section, is placed a led spotlight (100 W).

5.6.4 Interaction with the other parts of the facility

The visualization apparatus does not interact thermally with the other parts of the plant.

5.7 Instrumentation

Four types of measurements are performed on the facility:

1. temperature;
2. pressure;
3. flow rate;
4. video recording.

5.7.1 Temperature

Temperature measurements are performed with:

- thermocouples, they are of two kinds:
  1. K-type (Nickel/Chromium-Nickel), the *Laboratorio tarature termometriche* of the Department of Energy of the Politecnico di Milano calibrated them and certified the uncertainty of 0.1K, they are used to measure:
     - the wall temperature of the test section;
     - the refrigerant temperature at the inlet and the outlet of the test section;
     - the refrigerant temperature at the inlet and outlet of the sub-cooler;
     - the water temperature at the inlet and the outlet of the subsection. To measure the adiabatic mixing temperature three thermocouples connected in series are inserted in different points of a copper block placed in the water flow. The signal coming from the probe is related to the sum of the temperatures measured by the thermocouples, the result of its division by three represent the adiabatic mixing temperature. To reduce the error linked with the axial conduction thermocouple wires were inserted in three stainless steel tubes 11 cm long welded to the copper block. A brass plug lets the tubes to exit from the duct and avoid water leakage.
  2. J-type (Iron/Constantan), calibrated by the manufacturer who gives an uncertainty of 0.1K, they are used to measure the temperature of the evaporator heating elements.

  All the reference junctions are placed in a single Dewar flask filled with melting ice obtained from demineralized water.

5.7.2 Pressure

Pressure measurements are performed by pressure gauges placed at:

- the inlet of the test section and connected to the data acquisition system;

- the outlet of the test section and connected to the data acquisition system;
- at the inlet of the part of refrigerant loop that is dedicated to condensation, here the transducer is only an indicator of the existing condition;
- at the inlet of the evaporator, here the transducers are only indicators of the existing condition;

They are of two kinds:

- **absolute**, connected to a pressure tap located at the inlet of the first subsection, 16 bar full scale and a linear voltage output in the range [0;20]mV. The probe was calibrated by the builder and it has a linearity deviation of 0.2% of the full scale.
- **differential**, connected to pressure taps placed at: the inlet of the subsection and at the outlet of the subsection. There are two of them:
  1. with 2.07bar full scale and a linear current output in the range $[4; 20]mA$, a resistance of 267 Ohm turns the current output in voltage output.
  2. with 6.9bar full scale and a linear current output in the range $[4; 20]mA$.

manufacturer		**Baker Hughes**	**Stellar Tech.**	
model		**PTX5072-TA-A1-CA**	**DT1950-25PB**	**DT1950-50PB**
reference		**Absolute**	**Differential**	
pressure range	$[bar]$	$[0; 16]$	$[-1.04; +1.04]$	$[-3.45; +3.45]$
uncertainty		$\pm 0.2\% fullscale$	$\pm 0.1\% fullscale$	
output	$[mA]$	$[4; 20]2wires$		

Table 5.2: Pressure transducers.

The system does not have an automatic pressure control system, so the pressure has to be set by varying the temperature of the refrigerant. By selecting the correct temperature and mass flow rate of the cooling fluid and the appropriate heat exchange surface between the two streams, it is possible to set the needed pressure for all the desired condition that has been taken into account.

5.7.3 Flow rate

There are two kinds of flow-meter installed:

- volumetric flow-meter: **variable area**, the measurement comes from the position of a float. In the coolant loop there are seven flow-meters; the volumetric flow rate is indicated by a scale, which is placed aside the glass tube where the float moves. The flow-meters, that indicate the volume flow rate reaching plate heat exchangers on the water circuit and refrigerant circuit, are disposed in order to cover the entire range of volume flow rates between $[0; 4000]; l/h$, each one with a certified uncertainty of $\pm 2\%$ of the full scale. The flow-meter assigned to the sub-cooler duct has a scale of $[0; 250]; l/h$, with a certified uncertainty of $\pm 2\%$ of the full scale;

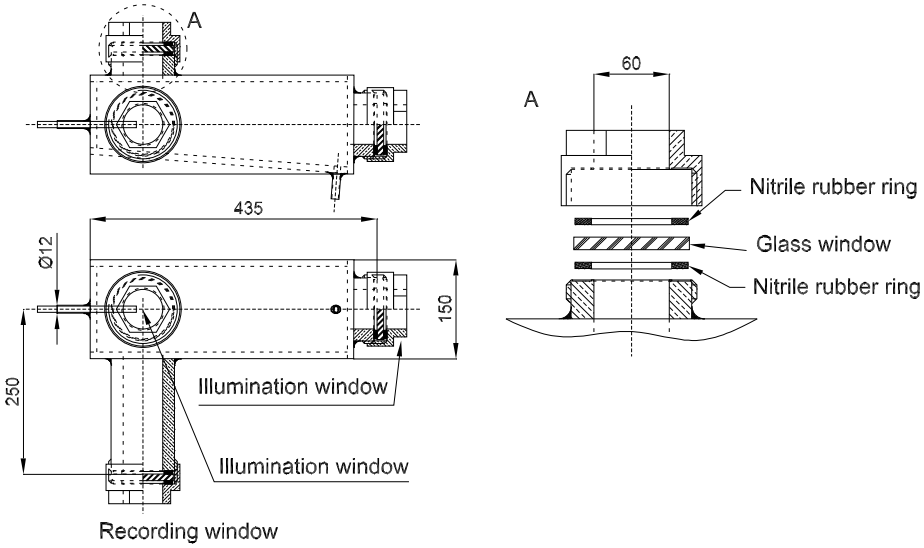

Figure 5.10: Camber of the visualization apparatus

- mass flow-meter: **Coriolis**, its working principle is based on the effects of the Coriolis force, performs mass flow rate and density measures. They are three in number (their characteristics are in tab. 5.3 and tab. 5.4) and placed on:

  1. the refrigerant loop at the inlet of the evaporator;
  2. the water loop at the inlet of the test section.

manufacturer		**Hendress+Hauser**
model		**Promass 80F**
range of full scale values	$[kg/h]$	$[0; 400]$
range of full scale values	$[kg/min]$	$[0; 6.67]$
full scale uncertainty		$\pm 0.15\%$
ambient temperature range	$[°C]$	$[-20; +60]$

Table 5.3: Coriolis mass flow-meters.

manufacturer		**Krohne**
model		**Optimass 1300C**
range of full scale values	$[kg/h]$	$[0; 6500]$
range of full scale values	$[kg/min]$	$[0; 108.3]$
full scale uncertainty		$\pm 0.3\%$
ambient temperature range	$[°C]$	$[-40; +55]$

Table 5.4: Coriolis mass flow-meters.

5.8 Data acquisition and processing

Through the program *LabVIEW2014* the output of the measurement devices are stored in arrays. A *MatLab* code is exploited in order to compute:

1. the specific enthalpy of refrigerant at the evaporator inlet conditions;
2. the inlet quality x_{in} in the test section;
3. the thermal power exchanged in the test section;
4. the outlet quality x_{out} in the test section;
5. the outlet temperature and, consequently, the mean logarithmic temperature in the test section;
6. the mean heat transfer coefficient of the test section.

The program, through instruments calibration curves, converts voltage signals in physical quantities(pressure, temperature, etc.). Measurements are displayed on the screen, so that it is possible to verify the correct working condition of the facility and start the data recording.

The vapor quality x_{in} at the inlet of the test section is calculated with:

- the following assumptions:
  1. steady state;
  2. kinetic energy change negligible compared to the enthalpy change;
  3. potential energy change negligible compared to the enthalpy change;
  4. thermal losses negligible compared to the enthalpy flux;
  5. constant specific heat capacity in the considered range of temperatures.
- energy balance between the inlet of the evaporator and the inlet of subsection

$$\dot{Q}_{evap} = \dot{Q}_{sub-sl} + \dot{Q}_{sl-in} \tag{5.4}$$

This equation can be elaborated as:

$$\dot{Q}_{evap} = G[C_p \Delta T_{sub-sl} + x_{in}(h_{sv} - h_{sl})] \tag{5.5}$$

where:

G	$[kg/s]$	refrigerant mass flow rate;
ΔT_{sub-sl}	$[K]$	difference between T_{sub} ad T_{sat};
T_{sub}	$[K]$	temperature at the inlet of evaporator;
T_{sat}	$[K]$	saturation temperature of the refrigerant;
C_p	$[J/kg/K]$	refrigerant specific heat capacity;
x_{in}		inlet vapor quality;
h_{sl}	$[J/kg]$	saturated liquid refrigerant enthalpy;
h_{sv}	$[J/kg]$	saturated vapor refrigerant enthalpy;
$\dot{Q}_{evap}$	$[W]$	power provided from the evaporator;
$\dot{Q}_{sub-sl}$	$[W]$	power needed to get *sl* starting from *sub-c.* fluid;
$\dot{Q}_{sl-in}$	$[W]$	power needed to get x_{in} starting from *sl* fluid;

The specific heat capacity of the fluid is computed considering the average temperature between sub-cooled and saturated conditions. Values of saturated enthalpy refer to the inlet temperature of the subsection. Solving eq. 5.5 for the inlet quality:

$$x_{in} = \frac{C_p \Delta T_{sub-sl} - \frac{\dot{Q_{evap}}}{G}}{h_{sl} - h_{sv}} \tag{5.6}$$

The thermal power exchanged in the test section with demineralized water is evaluated with an energy balance on the two sides of the concentric heat exchanger, assuming:

1. steady state;
2. negligible enthalpy variation due to the pressure drop;
3. the only thermal power exchange is the one between refrigerant and water,
4. linear variation of the refrigerant temperature between inlet and outlet only due to the pressure drop along the test section.

$$Th.Power = \begin{cases} \dot{Q} = \dot{m}_w c_w (T_{w,in} - T_{w,out}) \\ \dot{Q} = G(h_{out} - h_{in}) \end{cases} \tag{5.7}$$

where:	$\dot{Q}$	$[W]$	thermal power exchanged;
	$\dot{m}_w$	$[m^3/s]$	demineralized water mass flow rate;
	c_w	$[J/kg/K]$	demineralized water specific heat;
	$T_{w,out}$	$[K]$	outlet demineralized water temperature;
	$T_{w,in}$	$[K]$	inlet demineralized water temperature.
	h_{out}	$[J/kg]$	outlet refrigerant enthalpy;
	h_{in}	$[J/kg]$	inlet refrigerant enthalpy;

Solving system of eq. 5.7 for the outlet enthalpy, the outlet quality results:

$$Outlet.Condition = \begin{cases} h_{out} = \frac{\dot{m}_w c_w (T_{w,in} - T_{w,out})}{G} - h_{in} \\ x_{out} = \frac{h_{out} - h_{sl}}{h_{sv} - h_{sl}} \end{cases} \tag{5.8}$$

Values of saturated enthalpy refer to the outlet temperature of the subsection. The mean heat transfer coefficient is calculated with:

$$h = \frac{\dot{Q}}{S \Delta T_{mean-log}} \tag{5.9}$$

where:	h	$[W/m^2/K]$	mean heat transfer coefficient;
	$\dot{Q}$	[W]	thermal power exchanged;
	S	$[m^2]$	exchanging surface, referred to the inner diameter;
	$\Delta T_{mean-log}$	$[K]$	mean logarithmic temperature difference in the subsection;

The process of analysis is required only for the computation of the mean heat transfer coefficient, since the pressure drop are directly measured by the differential pressure transducers.

5.9 Uncertainty analysis

The experiment aims to measure:

- pressure drop;
- mean heat transfer coefficient.

These quantities are affected by uncertainty because they are determined (directly or indirectly) by instruments characterized by non zero uncertainty. It is important to evaluate the uncertainties of these quantities to establish measurement.

Pressure drop is straight determined with strain gauges, the uncertainty of the measurement is the one of the instrument. Mean heat transfer coefficient is determined indirectly, its value is deduced by other measured quantities. In his case the uncertainty has to be evaluated using the uncertainty propagation algorithm.

The problem of computing the uncertainty of a quantity y, function of n independent variables: x_1, x_2, ...,x_n, can be set in the following way:

$$y = f(x_1, x_2, ..., x_i, ..., x_n) \tag{5.10}$$

where: y dependent quantity;
x_i i-th independent variables (measured quantity);
n number of independent variables.

Every measured quantity has an uncertainty $\pm U_{x_i}$ (i=1,2,...,n). These uncertainties cause an uncertainty $\pm U_y$ in the computed result y.

$$y \pm U_y = f(x_1 \pm U_{x_1}, x_2 \pm U_{x_2}, ..., x_i \pm U_{x_i}, ..., x_n \pm U_{x_n}) \tag{5.11}$$

Expanding the function f in Taylor series:

$$y + \delta y = f(x_1, x_2, ..., x_i, ..., x_n) + \sum_{i=1}^{n} \frac{\partial f}{\partial x_i} \delta x_i + E \tag{5.12}$$

where: E higher order terms.

Substituting:

$$\delta x_i = \pm U_{x_i} \tag{5.13}$$
$$\delta y = \pm U_y \tag{5.14}$$

The previous equation become:

$$\begin{aligned} &f(x_1 \pm U_{x_1}, x_2 \pm U_{x_2}, ..., x_i \pm U_{x_i}, ..., x_n \pm U_{x_n}) = \\ &f(x_1, x_2, ..., x_i, ..., x_n) + \sum_{i=1}^{n} \pm U_{x_i} \frac{\partial f}{\partial x_i} + E \end{aligned} \tag{5.15}$$

In actual practice the uncertainties are small quantities, thus higher order terms are negligible.

The uncertainty U_{x_i} are random values. It follows the uncertainty U_y is the sum of random variables U_{x_i}. The standard deviation of U_y is the square root of the sum of the U_{x_i} variances. The uncertainty U_y can be expressed as:

$$U_y = \sqrt{\sum_{i=1}^{n} \left(U_{x_i} \frac{\partial f}{\partial x_i} \right)^2} \tag{5.16}$$

The relative uncertainty, of the generic quantity f, is defined as:

$$u_f = \frac{U_f}{f} \tag{5.17}$$

5.9.1 Thermodynamic quality uncertainty

Applying eq. 5.16 to the expression of inlet quality (see eq. 5.6), the uncertainty results:

$$\begin{aligned} U_{x_{in}} = \Bigg\{ & \left(\frac{\partial x_{in}}{\partial \dot{Q}_{evap}} \dot{Q}_{evap} u_{\dot{Q}_{evap}} \right)^2 + \left(\frac{\partial x_{in}}{\partial G} G u_G \right)^2 \\ & + \left(\frac{\partial x_{in}}{\partial C_p} C_p u_{C_p} \right)^2 + \left(\frac{\partial x_{in}}{\partial h_{sv}} h_{sv} u_{h_{sv}} \right)^2 \\ & + \left(\frac{\partial x_{in}}{\partial h_{sl}} h_{sl} u_{h_{sl}} \right)^2 + \left(\frac{\partial x_{in}}{\partial \Delta T_{sub-sl}} \Delta T_{sub-sl} u_{\Delta T_{sub-sl}} \right)^2 \Bigg\}^{1/2} \end{aligned} \tag{5.18}$$

the expressions of the derivatives are:

$$\frac{\partial x_{in}}{\partial \dot{Q}_{evap}} = \frac{1}{G(h_{sv} - h_{sl})} \tag{5.19}$$

$$\frac{\partial x_{in}}{\partial G} = -\frac{\dot{Q}_{evap}}{G^2(h_{sv} - h_{sl})} \tag{5.20}$$

$$\frac{\partial x_{in}}{\partial C_p} = -\frac{\Delta T_{sub-sl}}{h_{sv} - h_{sl}} \tag{5.21}$$

$$\frac{\partial x_{in}}{\partial h_{sv}} = \frac{C_p \Delta T_{sub-sl} - \frac{\dot{Q}_{evap}}{G}}{(h_{sv} - h_{sl})^2} \tag{5.22}$$

$$\frac{\partial x_{in}}{\partial h_{sl}} = \frac{\frac{\dot{Q}_{evap}}{G} - C_p \Delta T_{sub-sl}}{(h_{sv} - h_{sl})^2} \tag{5.23}$$

$$\frac{\partial x_{in}}{\partial \Delta T_{sub-sl}} = -\frac{C_p}{h_{sv} - h_{sl}} \tag{5.24}$$

The uncertainty depends on:

- power of the evaporator;
- refrigerant mass flow rate;

		evaporation	condensation
T_0	$[°C]$	5	35

Table 5.5: T_0 for boiling and condensation.

- subcooled and saturation temperature;
- saturated liquid and vapor enthalpy;
- relative uncertainty of measurement of:
  - saturated liquid specific enthalpy;
  - saturated vapor specific enthalpy;
  - ΔT between subcooled and saturation condition

In this calculation it is assumed that the specific heat capacity of the refrigerant is not affected by the temperature of the subcooled liquid. Actually these two quantities are connected since the reference temperature for C_p is the average temperature between subcooled and saturated liquid, but the variation of heat capacity in the accounted temperature range can be considered negligible for uncertainty analysis.

The enthalpy values are calculated on the base of temperature and pressure measured by transducers and the refrigerant thermodynamic tables. It is assumed negligible the thermodynamic tables uncertainty so that enthalpy uncertainty depends only by temperature and pressure measures. To evaluate the uncertainty of saturated liquid and vapor specific enthalpy a single intensive property is enough to determine the enthalpy. Enthalpy variations caused by slight variation of temperature are evaluated with a Taylor expansion around T_0:

$$Sat.Condition.Enthalpy = \begin{cases} h_{sl} = h_{sl}(T) & \Rightarrow \quad dh_{sl} = \frac{\partial h_{sl}}{\partial T}\big|_{T_0} dT \\ h_{sv} = h_{sv}(T) & \Rightarrow \quad dh_{sv} = \frac{\partial h_{sv}}{\partial T}\big|_{T_0} dT \end{cases} \tag{5.25}$$

where: h_{sl} $[J/kg]$ saturated liquid specific enthalpy;
h_{sl} $[J/kg]$ saturated vapor specific enthalpy;
T_0 $[K]$ reference temperature.

In tab. 5.5 are indicated the reference temperature used to evaluate enthalpy uncertainty. The uncertainty expressions, given by certifications or manuals, are:

- Thermocouples (both for type K and J) [Absolute]:

$$U_T = 0.1K \tag{5.26}$$

- Mass Flow-meter (PROMASS 80F)[Relative]:

$$u_{\dot{m}_l} = \left(\pm 0.15 \pm \frac{0.100}{G} 100 \right) \frac{1}{100} \tag{5.27}$$

- Evaporator[Absolute]:

$$U_{\dot{Q}_{evap}} = 0.1W \tag{5.28}$$

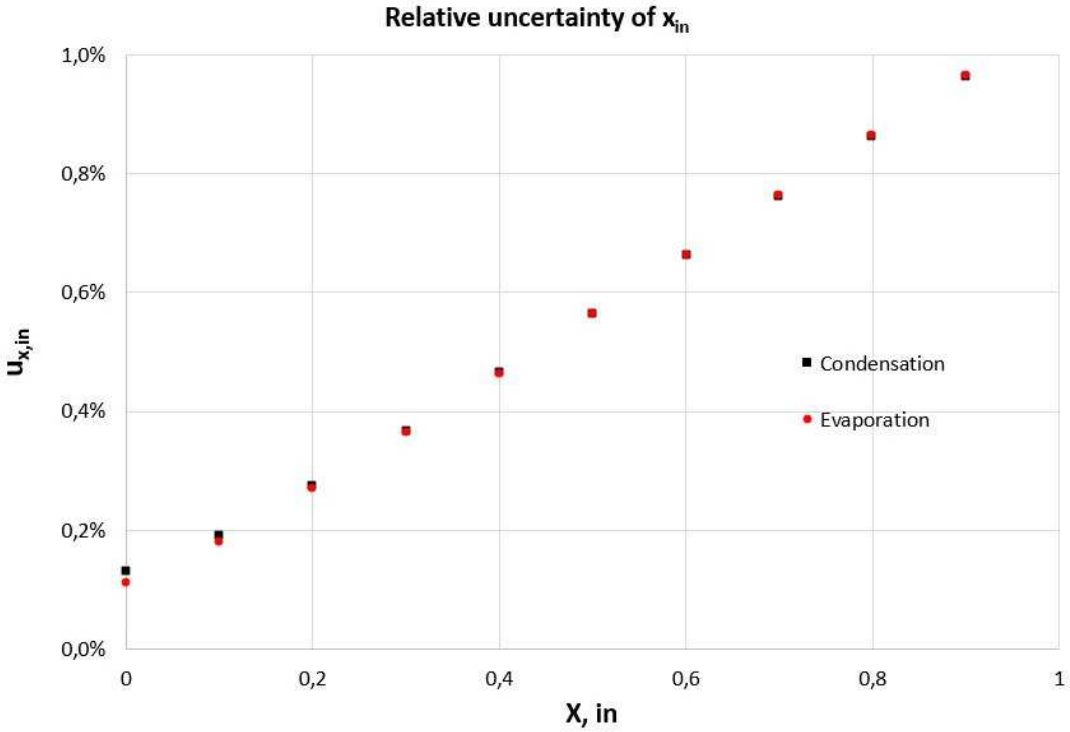

Figure 5.11: Relative uncertainty of x_{in}, with respect the inlet quality.

In equation eq. 5.27 the mass flow rate must be expressed in $[kg/h]$.

In fig. 5.11 is presented the trend of inlet quality uncertainty with respect to the quality itself, both for evaporation and condensation conditions. The chart shows a linear relationship between the two values, where the maximum uncertainty is reached for high quality values and it is minor than 1%. The analysis has been performed with typical values of temperatures shown during the tests and established temperatures of saturation in evaporation and condensation conditions:

- $T_{sat,evap} = 5[°C]$
- $T_{sat,cond} = 35[°C]$
- $T_{subcooled,evap} = -2[°C]$
- $T_{subcooled,cond} = 30[°C]$

All the other quantities are computed starting by these values. The mass flow rate of refrigerant accounted in the analysis is $25[kg/h]$, the inlet quality uncertainty is not affected by this parameter since the relative uncertainty is accounted.

5.9.2 Heat transfer coefficient uncertainty

The uncertainty is calculated starting by the definition (eq. 5.9), it follows that the relative uncertainty is:

$$u_h = \sqrt{u_{\dot{Q}}^2 + u_S^2 + u_{\Delta T_{mean-log}}^2} = \sqrt{\left(\frac{U_{\dot{Q}}}{\dot{Q}}\right)^2 + \left(\frac{U_S}{S}\right)^2 + \left(\frac{U_{\Delta T_{mean-log}}}{\Delta T_{mean-log}}\right)^2} \tag{5.29}$$

where: u_i relative uncertainty of the i-th quantity;
$U_{\dot{Q}}$ $[W]$ thermal power absolute uncertainty;
U_S $[m^2]$ surface absolute uncertainty;
$U_{\Delta T_{mean-log}}$ $[K]$ mean-log temperature difference absolute uncertainty;

The heat exchange surface corresponds to the outlet surface of the test section, which is simply computed as:

$$S = \pi d_{out} L. \tag{5.30}$$

The absolute uncertainty of the exchange surface derives from the same formulation discussed previously.

$$U_S = \sqrt{\left(\frac{\partial S}{\partial d_{out}} U_{d_{out}}\right)^2 + \left(\frac{\partial S}{\partial L} U_L\right)^2} \tag{5.31}$$

where:

$$\frac{\partial S}{\partial d_{out}} = \pi L \tag{5.32}$$

$$\frac{\partial S}{\partial L} = \pi d_{out} \tag{5.33}$$

and $U_L = 10mm$ tube length absolute uncertainty;
$U_{d_{out}} = 0.1mm$ diameter absolute uncertainty.

The obtained value of absolute uncertainty of the heat exchange surface is $4.6 \times 10^{-4}[m^2]$, which corresponds to 1.4% of the total area.

The analysis of $\Delta T_{mean,log}$ is performed in an analogous way, taken into account typical values of demineralized water temperature both in condensation and in boiling experiments. It is useful so focus on the effect of mean logarithmic temperature difference on the heat transfer coefficient uncertainty. This study is performed for the range of $\Delta T_{mean,log}$ exhibited during the experiments.

$$\begin{aligned} {U_{\Delta T_{mean,log}}}^2 = \Bigg\{ &\left(\frac{\partial \Delta T_{mean,log}}{\partial T_{r,in}} U_{T_{r,in}}\right)^2 + \left(\frac{\partial \Delta T_{mean,log}}{\partial T_{r,out}} U_{T_{r,out}}\right)^2 \\ &+ \left(\frac{\partial \Delta T_{mean,log}}{\partial T_{w,in}} U_{T_{w,in}}\right)^2 + \left(\frac{\partial \Delta T_{mean,log}}{\partial T_{w,out}} U_{T_{w,out}}\right)^2 \end{aligned} \tag{5.34}$$

Computing partial derivatives for each temperatures, as if all the other parameters were constant, the absolute uncertainty for typical $\Delta T_{mean,log}$ exhibited in evaporation conditions is 0.1K, that leads to a relative uncertainty of 1.5%.

The thermal power exchanged is expressed by eq. 5.7. Assuming negligible, compared to the other, the relative uncertainties of the demineralized water specific heat. It is evaluated at the mean temperature between inlet and outlet, the relative uncertainty of the thermal power exchanged is:

$$u_{\dot{Q}} = \sqrt{u_{\dot{m}_w}^2 + u_{\Delta T_w}^2} = \sqrt{\left(\frac{U_{\dot{m}_w}}{\dot{m}_w}\right)^2 + \left(\frac{U_{\Delta T_w}}{\Delta T_w}\right)^2} \tag{5.35}$$

where: u_i relative uncertainty of the i-th quantity;
$U_{\dot{m}_w}$ $[kg/s]$ water mass flow rate absolute uncertainty;
$U_{\Delta T_w}$ $[K]$ temperature difference absolute uncertainty.

The mass flow-meter installed on the demineralized water loop has the same relative uncertainty of the one installed on refrigerant circuit:

$$u_{\dot{m}_l} = \left(\pm 0.15 \pm \frac{0.100}{G} 100 \right) \frac{1}{100} \tag{5.36}$$

It follows the relative uncertainty of the heat transfer coefficient depends on:

1. the demineralized water temperature difference between outlet and inlet ΔT_w;
2. the temperature difference between the wall and the refrigerant ΔT.

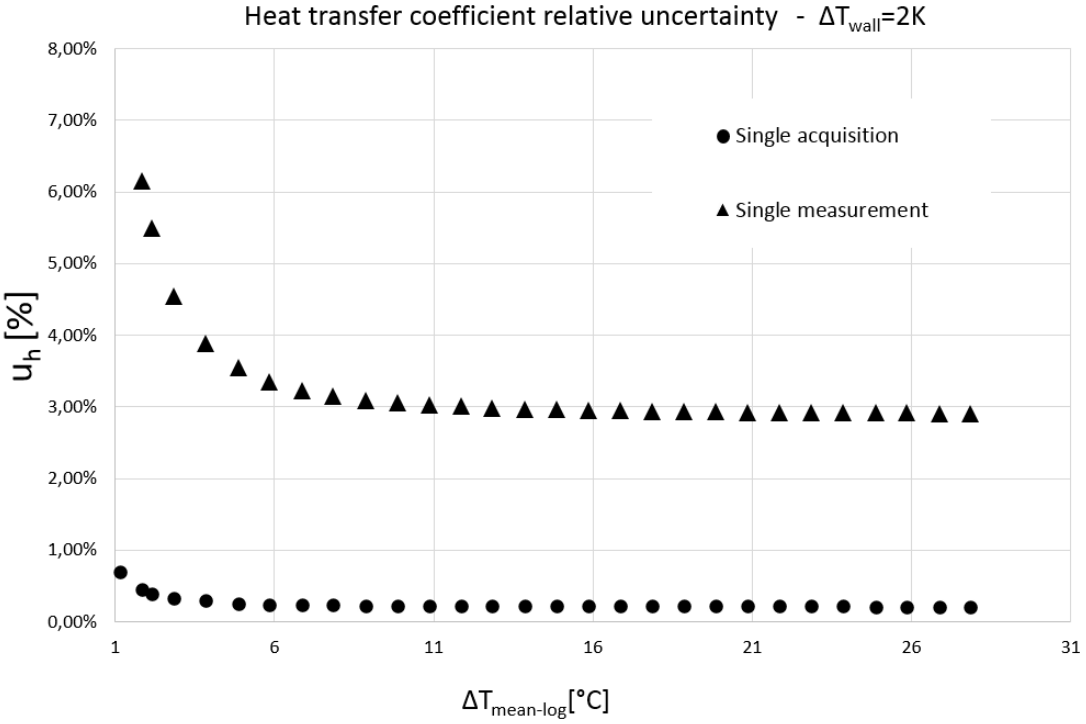

Figure 5.12: Relative uncertainty of h, with respect the mean logarithmic temperature difference.

The fig. 5.12 shows the trend of heat transfer coefficient uncertainty with respect to the $\Delta T_{mean-log}$ between the inlet and outlet of the test section. It must be considered that the analysis has been performed taking into account a $\Delta T_{wall} = 2K$ and the accounted range includes both the cases of evaporation and condensation. It has been considered as *measurement* the result of instrument reading at a fixed time, *acquisition* is the output of the averaged measurements that have been collected per each test. It results evident the effect of test repetition on the relative uncertainty.

The chart shows two different curves:

- The curve indicated with triangular marker relates to one single measurement. Any data needed to computed the heat transfer coefficient is measured only once, no repetition on the experiment is performed;

- The curve indicated with circular marker relates to a complete test. It implies the acquisition of 180 measurements, as indicated in 5.10

The difference between the two result is due to the propagation of the error in case of repeated measurements, in particular

$$u_{acquisition} = \frac{u_{measurement}}{\sqrt{N}} \tag{5.37}$$

where N is the number of conducted measurements.

The uncertainty of the heat transfer coefficient exhibits an asymptotic behavior, at increasing $\Delta T_{mean-log}$, to the value of 0.2%. It is possible to notice that for all the applicable range the uncertainty has a lower value with respect to the acceptable one, fixed at 5%. This precision level is guaranteed by the high number of acquisitions that are analyzed for each test. For temperature difference grater than $2K$ the the uncertainty is affected only slightly by variation of ΔT_{wall}, but since it is in the acceptable range, it is not necessary to change this inlet parameter.

The uncertainty is affected also by thermal power exchanged and the surface of the heat transfer, nevertheless these parameters influence marginally the heat transfer coefficient uncertainty. The geometrical parameters of the test section are fixed, and the exchanged thermal power varies only due to the different transition enthalpy related to the saturation pressure of the system. Hence, it is not necessary to perform an analysis taking into account variability range of exchanged thermal power.

5.10 Facility management

5.10.1 Start up

The following sequence of operations are required to set up the facility for the experiment:

1. **Thermocouples reference setting:** activation of the ice machine and to prepare the ice to fill the Dewar flask. This operation lasts about an hour and a half. Until the end of this operation is not possible to start the data acquisition because the reference junctions are not in known and steady conditions. It follows the readings of the thermocouples are wrong.

2. **Coolant loop setting:** activation of the chiller in the coolant loop. The control system of the chiller is designed to keep constant the coolant temperature inside the tank. Approximately half an hour is required to reach the right operating condition.

3. **Refrigerant loop setting:** opening of the valves to allow the refrigerant to flow, placed on the:

    - duct connecting the evaporator to the calming section of the test section. When the heating components are working in the evaporator the pressure of the refrigerant loop increases, pushing the fluid against the valve's wall. Keeping it closed during working condition, prevents the refrigerant to flow inside the loop and can cause high mechanical stresses on the neighboring components;
    - heat exchangers used as condensers. It is not required them to be all open (actually it depends on the required working conditions), the system is designed so that it can operate with all or just one heat exchanger open;

Once the loop is completely open, the pump has to be activated starting the inverter and setting the speed of the gear pump, with this operation the refrigerant start to flow in the loop (rotation speed can be neither too low because that bring to overheating of the engine, nor too high because it cause cavitation).

4. **Demineralized water loop opening:** opening of the valves placed on the:

   - duct connecting the water tank with the pumps;
   - plate heat exchanger to enable the heat transfer with the water and glycol circuit;
   - duct connecting the plate heat exchangers and the subsection. On the water circuit a by-pass valve is installed to prevent the interaction between water and refrigerant loop, during experiments the by-pass duct must be completely closed.

   It is required the activation of the resistance to set the demineralized water tank temperature: some degree above the refrigerant temperature in the test section during evaporation, some degree below the refrigerant temperature in the test section during condensation. The pump has to be activated, through a switch, before the coolant exchanges heat with the water, this could lead the water to freeze damaging the loop's components;

5. **Coolant loop opening:** opening of the ball valves placed on the:

   - duct headed to the cooling systems of the liquid refrigerant and the water, entering the flow-meter (to assure a single phase flow) and the gear pump;
   - plate heat exchangers, both on the refrigerant circuit and on the water circuit.

6. **Evaporator setting:** this process is divided in two steps: the evaporator and the single heating components' switch must be opened; the desired power transferred to the refrigerant has to be set.

7. **Activation of the computer HP-Z420**;

8. **Starting of the acquisitions**.

5.10.2 Regulation

During the experiment the main parameters to be checked are:

- the refrigerant mass flow rate, it depends on the the speed of the gear pump. Acceptable values of mass flow rates do not differ from the set one more than $\pm 0.5 kg/h$;

- the pressure of the refrigerant loop, it must be set such that the saturation temperature of the fluid is $5°C$ evaporation or $35°C$ condensation. There are different methods to control the pressure:

  1. to vary the volume flow rate of the coolant reaching the heat exchangers. The temperature of the fluid inside the condenser changes, this would lead to a variation of the pressure of the entire loop. It is very effective on the accounted parameter, so that a small variation of coolant flow rate causes a considerable pressure variation;

2. to vary the temperature of the coolant at the condenser inlet. The loop shows the same behavior described in the previous method, but the effect on the pressure is minor;
3. to open or close one or more plate heat exchangers. This operation aims to add or subtract a consistent volume to the loop, such that the pressure is influenced.

The acceptability pressure range is respected until the saturation temperature of the fluid at the actual pressure does not differ from the desired one more than $\pm 0.1K$;

- water temperature difference between the inlet and the outlet of the subsection. The experiments are performed setting a fixed heat flux in the test section, in order to observe this constraint the mass flow rate of the demineralized water and the temperature difference must be constant(see section 5.8), a ΔT of $2K$ has been set for all the conducted experiments. The water mass flow rate is set manually through a valve, the temperature difference is controlled by varying the inlet temperature of the water. The temperature difference is considered acceptable in the range of $\pm 0.1K$ from the desired value;

- the temperature on the water at the inlet of the test section, it is controlled by means of a PID controller which enables the control of the temperature with an uncertainty of $\pm 0.1K$. This precision level is required to respect the constrain on the temperature difference previously indicated;

- the power provided to the fluid from the evaporator, the PID controller allows a very precise control of the power. The fluctuations of the evaporator power are due to the grid power variation so the facility has not the control of the parameter, but generally the stability of the electric grid is sufficient to provide a stable value of the power.

The regulation of the facility aims to control the mentioned parameters, so that they all fall inside their applicability ranges at the same time, the time required to fix the nominal condition is about a hour. Inlet quality of the refrigerant in the test section and mass flow rate are the parameter that mostly affect the refrigerant loop stability, so they are also responsible for the duration of regulation process. In particular, high inlet quality ($[0.75; 0.9]$) and high mass flow rates (more than $100kg/h$) make it difficult to adjust the system in evaporation experiments. The facility shows a higher stability in condensation tests.
When these rules are satisfied the experiment starts.

5.10.3 Experiment execution

The procedure schedules thirteen acquisition cycles, the repetition is applied to prevent random errors to influence the results. The duration of a single cycle is three minutes, during which instruments provide 180 readings that are recorded by the program. The measurements for each cycle are the means of 180 readings, during acquisition process standard deviation of all the recorded parameter is computed. Data are acquired by computer HP-Z420 by means of program *LabVIEW2014*, which is exploited both for the monitoring of the facility and for the acquisition process. The outputs of all the instruments are voltage values, so these values must be converted in physical quantities through a multimeter. It computes the physical outputs using the interpolation curves of each instrument, in the units of measure corresponding to the quantity measured.
The results are automatically saved in an appropriate folder, named with a specific code:

- E or C depending if the recorded data refer to evaporation or condensation experiment;
- value of the applied mass flow rate;
- $[x_{in} - x_{out}]$ the values of inlet and outlet vapor quality in the test section.

The folder contains thirteen files with *.txt* extension, each one corresponding to a cycle. The output format has been chosen such that values can be read and analyzed easily by *Matlab* program.
Data elaboration begins running the appropriate *Matlab* code and entering the daily environment pressure. The program output consists in:

1. *heat transfer coefficient* $[W/m^2/K]$;
2. *pressure drop* $[kPa]$;
3. refrigerant mass flux $[kg/m^2/s]$;
4. vapor average quality;
5. exchanged power $[W]$;
6. inlet temperature of refrigerant $[°C]$;
7. outlet temperature of refrigerant $[°C]$;
8. inlet pressure of refrigerant $[bar]$;
9. temperature difference of water $[°C]$;
10. vapor quality difference;
11. water mass flow rate $[kg/h]$.

All the auxiliary properties necessary to compute these values are calculated through linear interpolation of tabulated values, specific for each physical property of the refrigerant, directly by the program; it also computes the standard deviation of each output parameter. Heat transfer coefficient and pressure drop are the objectives of the experiments, the other values are printed in the output to give a reference on the conducted test and to let a comparison between them and the nominal condition. The comparison between the actual and the nominal conditions, considering also the standard deviation, establishes the success or the failure of the experiment. Only in case of success data are stored in the archive to be further analyzed. Afterward, collected data are gathered and analyzed by means of charts on *Excel* and *Matlab* files.

Chapter 6

Heat transfer coefficient and pressure drop measurement

Measurements was conducted in order to evaluate the heat transfer coefficient and pressure drop in horizontal microfin duct both in boiling and condensation conditions. The operating conditions are defined on the base of three quantities:

- the mass flux;
- average vapor quality, it is computed as the mean between inlet and outlet quality.

$$x_m = \frac{x_{in} + x_{out}}{2} \tag{6.1}$$

  where: x_m average vapor quality in the test section;
  x_{in} vapor quality at the inlet of the test section;
  x_{out} vapor quality at the outlet of the test section.

- quality variation of refrigerant in the test section.

$$\Delta x = |x_{out} - x_{in}| \tag{6.2}$$

  where: Δx vapor quality variation in the test section. The absolute value is used to have a positive value both in condensation and evaporation.

The experiments have been performed at fixed mass flux and quality variation, by varying the mean vapor quality.

In table tab. 6.2 and tab. 6.1 are reported the ranges of the operating conditions respectively in evaporation and condensation tests.

In particular experimental mean vapor qualities chosen for the tests are reported in tab. 6.3, while the mass fluxes is reported in tab. 6.4.

The tab. 6.6 reports the total number of experiments that have been conducted in boiling and condensation condition.

The heat fluxes have been established considering $50 kg/h$ and 0.1 quality difference as reference operating conditions, these values were chosen for convenience. From this choice and the geometrical parameter of the heat exchanger, heat flux reported in tab. 6.1 and tab. 6.2 are needed to reach the operating conditions. Heat flux is different between evaporation and condensation

	Condensation		
Saturation Temperature	$[°C]$	[35]	
		Min	Max
Refrigerant Mass Flux	$[kg/m^2s]$	110	440
Heat Flux	$[kW/m^2]$	7.5	15.0
Water mass flow rate	$[kg/h]$	103	206
Average vapor quality		0.2	0.9

Table 6.1: Experimental conditions of condensation tests.

	Evaporation		
Saturation Temperature	$[°C]$	[5]	
		Min	Max
Refrigerant Mass Flux	$[kg/m^2s]$	110	380
Heat Flux	$[kW/m^2]$	8.6	17.2
Water mass flow rate	$[kg/h]$	103	206
Average vapor quality		0.15	0.9

Table 6.2: Experimental conditions of evaporation tests.

	Average vapor quality								
Evaporation	0.15	0.25	0.35	0.45	0.55	0.65	0.75	0.85	0.9
Condensation		0.2	0.3	0.4	0.5	0.6	0.7	0.8	0.9

Table 6.3: Average quality for evaporation and condensation experiments.

	Evaporation			
Mass Flow rate$[kg/h]$	25	50	75	85
Mass Flux$[kg/m^2s]$	110.0	220.0	330.0	380.0
	Condensation			
Mass Flow rate$[kg/h]$	25	50	75	100
Mass Flux$[kg/m^2s]$	110.0	220.0	330.0	440.0

Table 6.4: Mass flux for evaporation and condensation experiments.

	Condensation		**Evaporation**	
$m_r[kg/h]$	$q = 7.5kW/m^2$	$q = 15kW/m^2$	$q = 8.6kW/m^2$	$q = 17.2kW/m^2$
	Δx			
25	0.2	0.4	0.2	0.4
50	0.1	0.2	0.1	0.2
75	0.067	0.133	0.067	0.133
85	-	-	0.058	0.116
100	0.05	0.1	-	-

Table 6.5: Quality variation in both condensation and evaporation experiments, depending on refrigerant mass flow rate and heat flux.

tests because the enthalpy of phase transition in condensation condition ($T_{sat} = 35°C$) is lower than in boiling condition ($T_{sat} = 5°C$). It implies that the thermal power needed to reach the correspondent vapor quality is lower in condensation experiments, since geometrical parameter are constant the heat flux is proportional to the thermal power. As highlighted in tab. 6.5, the quality variation in the test section is inversely proportional to the mass flow rate of refrigerant. All the experiments have been performed at fixed heat flux, so depending on the mass flow rate also the quality variation changes. Experiments have been conducted for the selected heat flux and for a doubled value, so that it is possible to evaluate its influence on the analyzed data. Heat flux increment is achieved by increasing the demineralized mass flow rate in the test section.

$$q = \frac{\dot{m}_r h_{lv} \Delta x}{S} \tag{6.3}$$

$$\frac{q^{'}}{q} = \frac{\Delta x^{'}}{\Delta x} \tag{6.4}$$

To compare the performances of a microfin tube against the smooth tube the following indexes are introduced:

- enhancement factor:

$$E = \frac{h_{mf}}{h_s} \tag{6.5}$$

where: E enhancement factor;
h_{mf} $[W/m^2K]$ microfin tube heat transfer coefficient;
h_s $[W/m^2K]$ smooth tube heat transfer coefficient.

- penalization factor:

$$P = \frac{\left(\frac{\Delta p}{L}\right)_{mf}}{\left(\frac{\Delta p}{L}\right)_{s}} \tag{6.6}$$

where: P penalization factor;
$\left(\frac{\Delta p}{L}\right)_{mf}$ $[Pa/m]$ microfin tube Δp per unit length;
$\left(\frac{\Delta p}{L}\right)_{s}$ $[Pa/m]$ smooth tube Δp per unit length.

To compare microfin tubes with each other it should be appropriate to define an objective function and to maximize with respect to suitable constraints. It is common practice, when no particular constraints are defined, to use the ratio of enhancement factor to the penalization factor, which is called efficiency index:

$$I = \frac{E}{P} \tag{6.7}$$

where: I efficiency index.

	Total number of tests
Evaporation	75
Condensation	56
Total	131

Table 6.6: Mass flux for evaporation and condensation experiments.

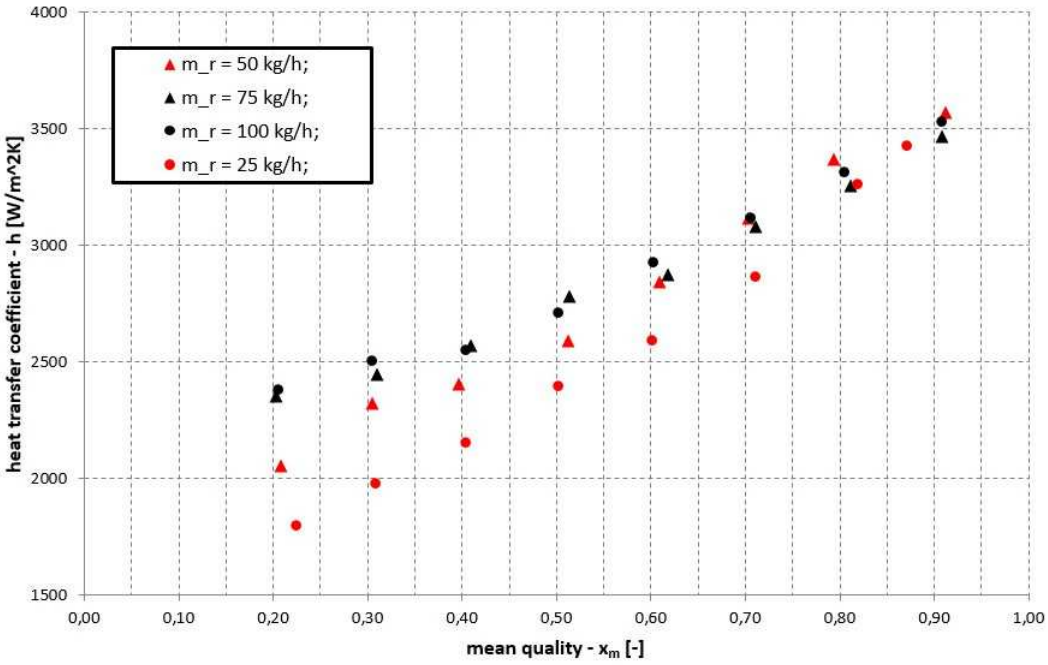

Figure 6.1: Condensation heat transfer coefficient h versus average quality ($q = 7.5kW/m^2$).

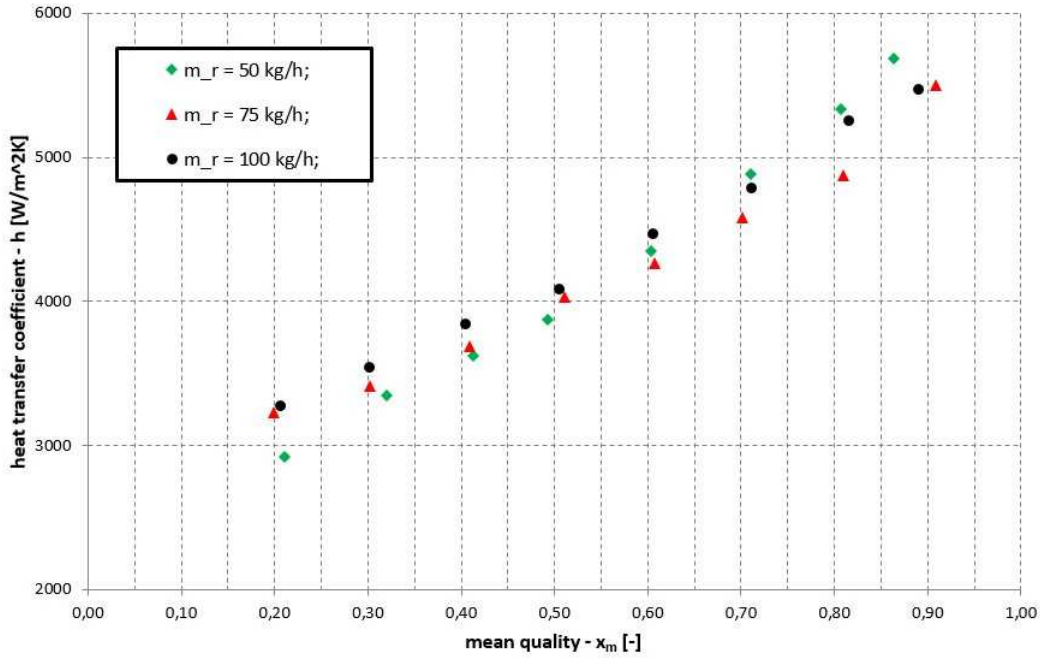

Figure 6.2: Condensation heat transfer coefficient h versus average quality ($q = 15.0kW/m^2$).

6.1 Condensation experimental results

The experimental results for heat transfer coefficient in condensation condition are reported in fig. 6.1 and fig. 6.2, the charts mark tests performed with single or doubled heat flux. The choice of heat flux was guided by the necessity to avoid too high or too low quality variation in the test section. Selected values of heat flux provides a reasonable quality variation range, that is function of the refrigerant mass flow rate. The graphic depicted in fig. 6.1 shows that the heat transfer coefficient increases with the mean vapor quality. From charts, it can be observed that the experimental curves for $\dot{m}_r = 75kg/h$ and $\dot{m}_r = 100kg/h$ exhibit a similar trend. Such a behavior suggests that, at fixed mean vapor quality and heat flux, the same flow pattern has developed for the mentioned range of mass flow rates. $\dot{m}_r = 25kg/h$ curve shows a different behavior, this indicates that a different flow pattern sequence is developed along the curve. Heat transfer coefficient values are significantly lower than those obtained for higher mass flow rate at low mean quality, while for high vapor quality the experiments shows similar heat transfer coefficients for the whole range of studied mass flow rate. At low mean vapor quality, the $\dot{m}_r = 50kg/h$ curve shows an intermediate course between $\dot{m}_r = 25kg/h$ and $\dot{m}_r = 75kg/h$. For high vapor mean quality, at fixed heat flux, the heat transfer coefficient is not influenced by mass flow rate. Both fig. 6.1 and fig. 6.2 show heat transfer coefficients in this condition that, taking into account the experimental uncertainty, can be considered equal. The curves at fixed mass flow rate for $q = 15.0kW/m^2$ nearly coincide for the whole range of vapor quality, while for $q = 7.5kW/m^2$ it can be seen a difference related to the mass flow rate. Hence, it is possible to state that at increasing heat flux, the influence of mass flow rate on heat transfer coefficient decreases.

Graphics depicted in fig. 6.3 and fig. 6.4 report the experimental pressure drop measured in condensation tests. As already observed for the heat transfer coefficient, also pressure drop exhibits a different behavior for curve conducted at $\dot{m}_r = 25kg/h$ with respect to the higher mass flow rate. It can be interpreted in terms of a different flow pattern established in the duct. At increasing mass flow rate, its influence on pressure drop decreases. All the curves present a maximum value at mean vapor quality near to $[0.7; 0.8]$, for very high vapor quality the pressure drop decreases because almost all the refrigerant flowing in the duct is in vapor phase.

Experiments performed with a doubled heat flux are reported in fig. 6.4, pressure drop measured in this condition is nearly the same to the single heat flux data. This suggests that heat flux has no influence on pressure drop.

In fig. 6.5, fig. 6.6 and fig. 6.7 a comparison between experiments with single and double heat flux is depicted. Heat transfer coefficient is increased in experiments conducted with a higher heat flux, in particular the divergence between the two cases grows up with the mean vapor quality, such a behavior is observed for all the compared mass flow rates. Pressure drop is not affected significantly, but it must be noticed that pressure drop is lower for lower heat flux case at fixed mass flux and mean quality.

6.2 Evaporation experimental results

Experiments in evaporation condition exhibit a discrepancy on the refrigerant temperature at the inlet of the test section at high mass flow rate ($[75; 100]kg/h$) . In particular, a consistent temperature difference ($[1.5; 2.0]°C$) is denoted between thermocouples readings and the saturation temperature derived from pressure gauge measurements. It can be attributed to a non-equilibrium

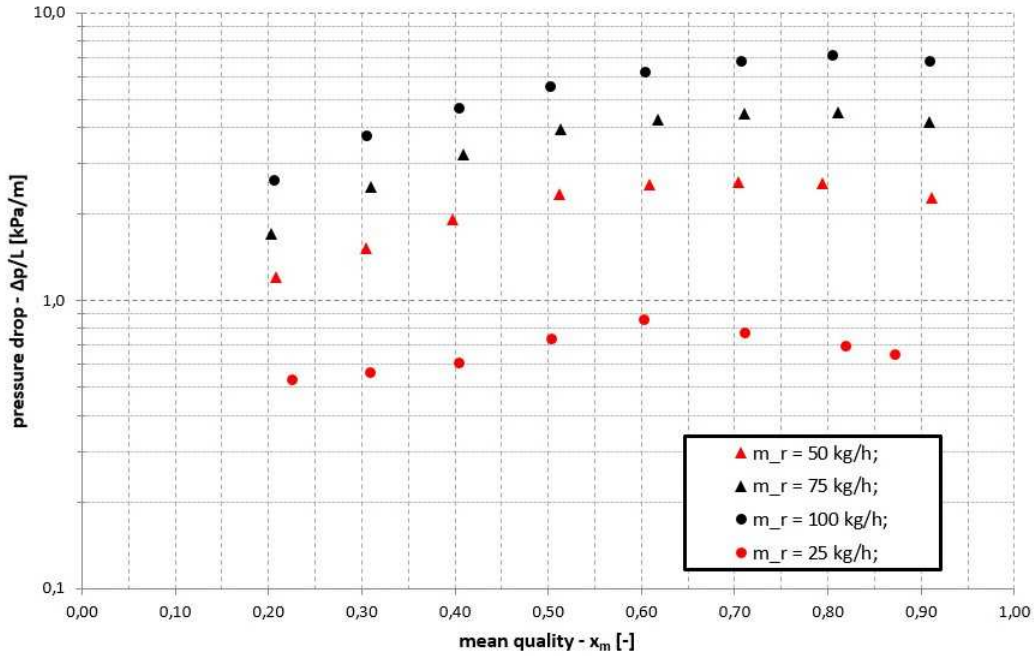

Figure 6.3: Condensation pressure drop Δp versus average quality ($q = 7.5kW/m^2$).

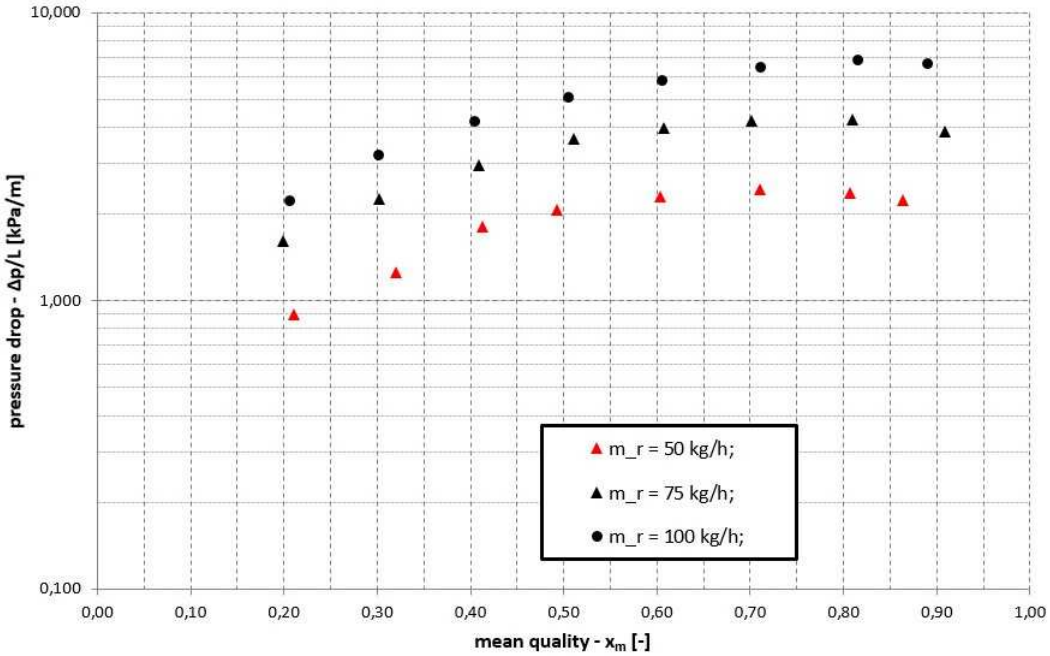

Figure 6.4: Condensation pressure drop Δp versus average quality ($q = 15.0kW/m^2$).

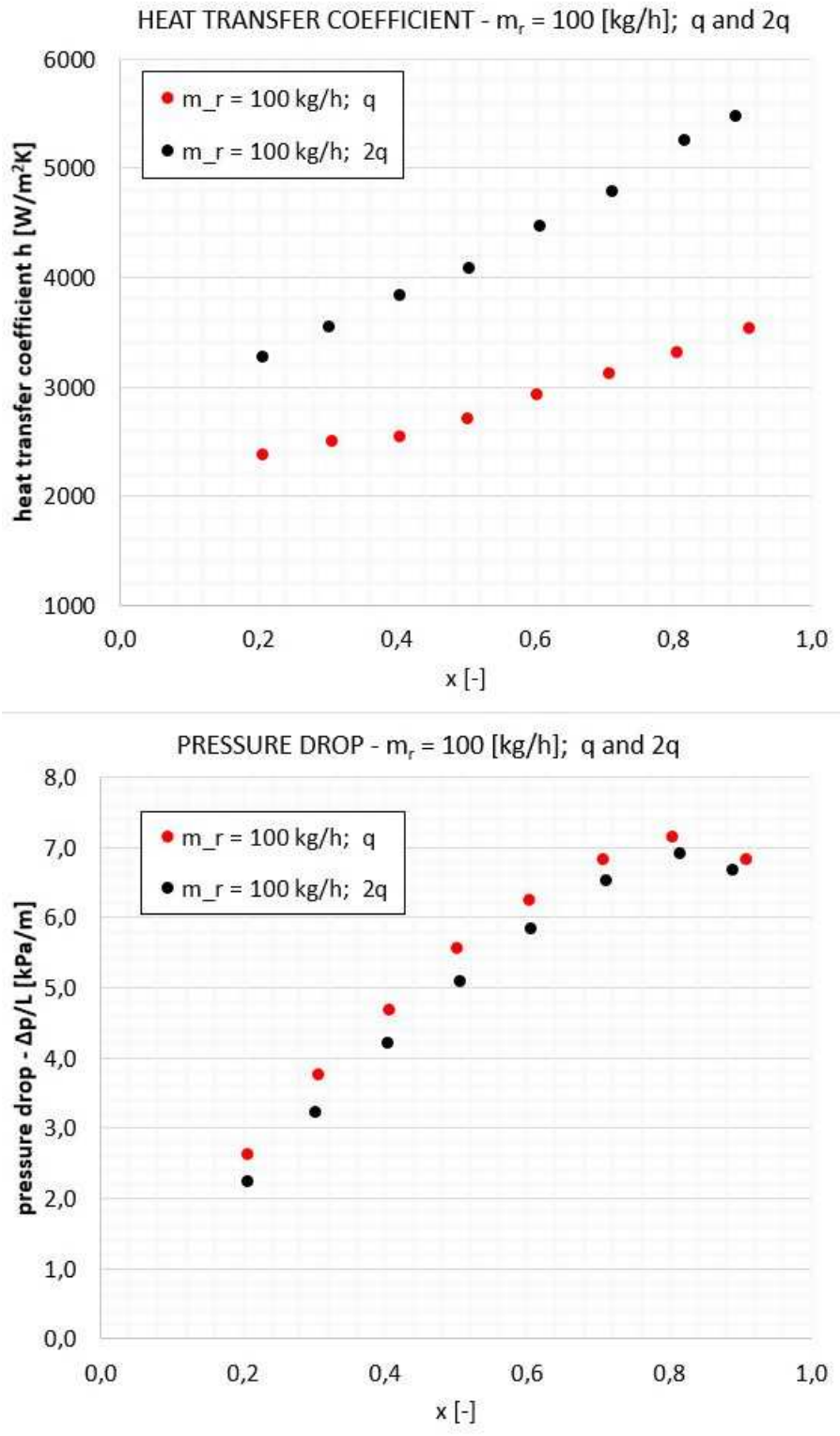

Figure 6.5: Condensation heat transfer coefficient and pressure drop versus mean vapor quality for $\dot{m}_r = 100kg/h$, comparison between experimental data with single heat flux ($q = 7.5kW/m^2$) and double heat flux ($q = 15.0kW/m^2$).

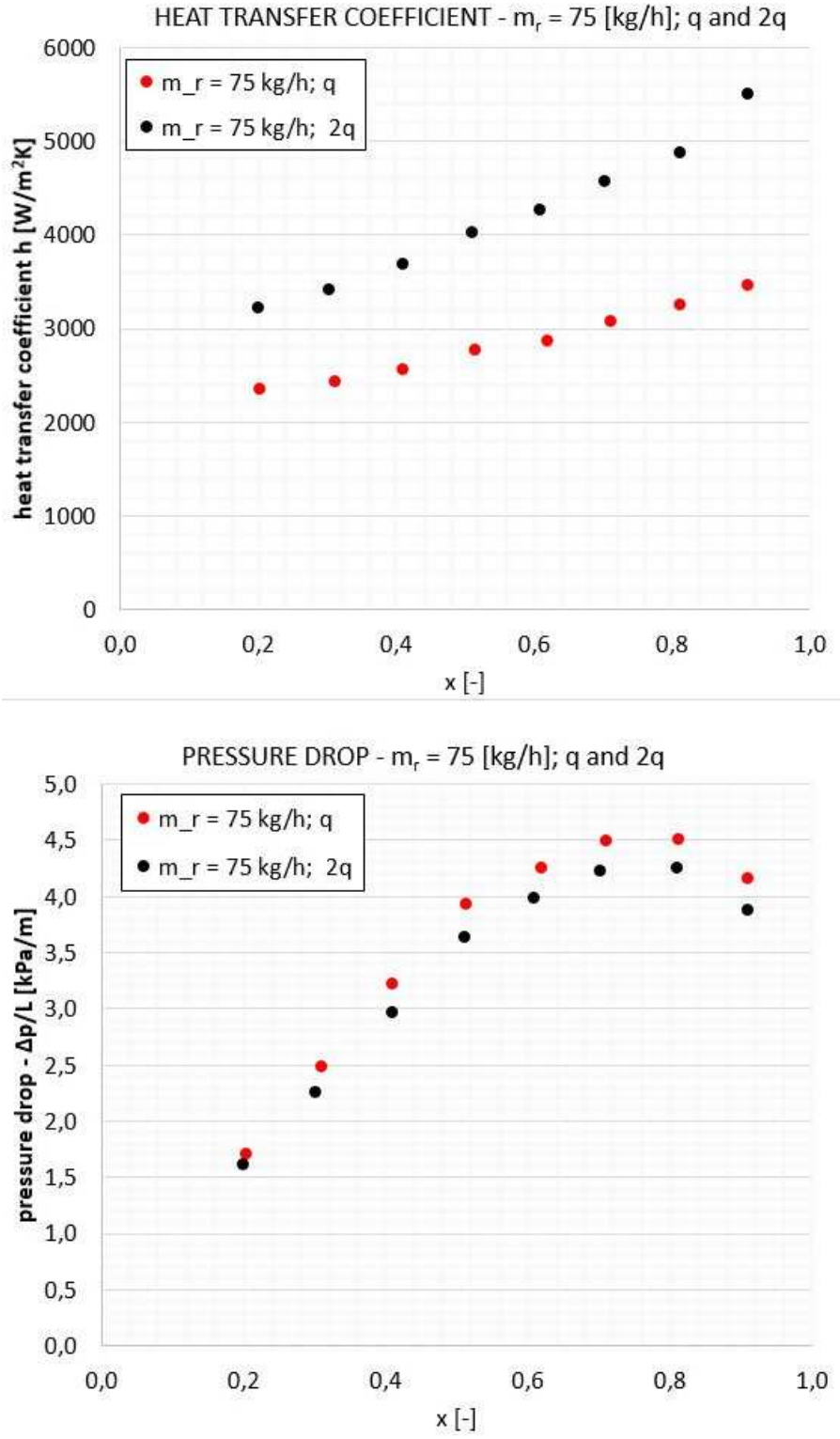

Figure 6.6: Condensation heat transfer coefficient and pressure drop versus mean vapor quality for $\dot{m}_r = 75kg/h$, comparison between experimental data with single heat flux ($q = 7.5kW/m^2$) and double heat flux ($q = 15.0kW/m^2$).

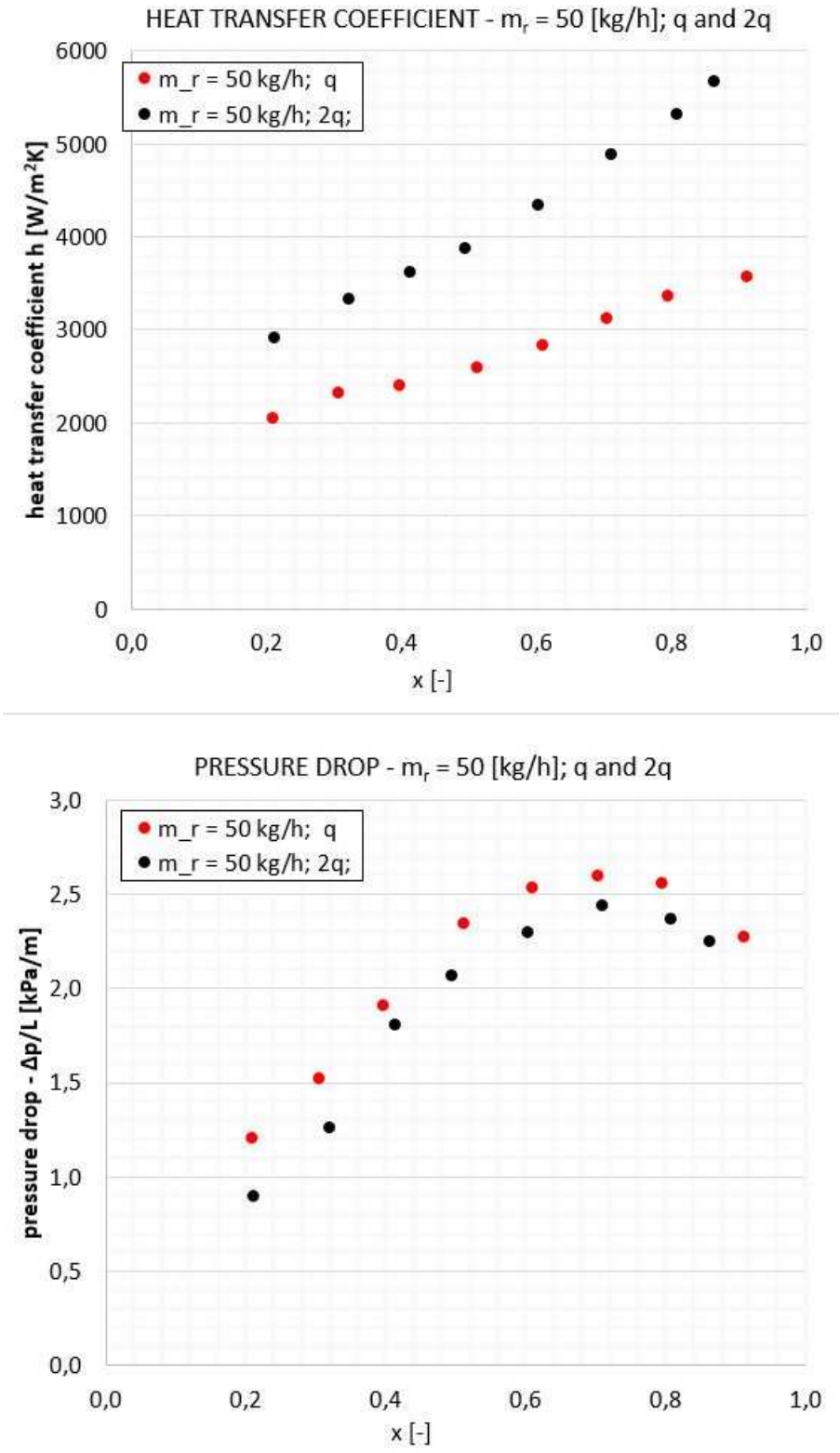

Figure 6.7: Condensation heat transfer coefficient and pressure drop versus mean vapor quality for $\dot{m}_r = 50kg/h$, comparison between experimental data with single heat flux ($q = 7.5kW/m^2$) and double heat flux ($q = 15.0kW/m^2$).

of the phases at the inlet of the test section and it makes the collected data unreliable. This problem led to the choice not to compare those experimental results with predictive correlations.

Results of evaporation tests are reported in the following section, no further analysis is performed on tests conduced at $[75; 100]kg/h$.

The experimental values of boiling heat transfer coefficients at variable mean quality are reported in fig. 6.8 and fig. 6.9. Difference in heat transfer coefficient shown in the charts consists in the selected heat flux. In fig. 6.8 tests, the heat flux has been set equal to $8.6kW/m^2$.

It is evident the different trend of heat transfer coefficient obtained for $\dot{m}_r = 25kg/h$, that is much lower than $\dot{m}_r = 50kg/h$, $\dot{m}_r = 75kg/h$ and $\dot{m}_r = 85kg/h$ at low vapor quality. For very high vapor quality heat transfer coefficient values are aligned with higher mass flow rate results. In the range of $[50; 75]kg/h$ the heat transfer coefficient can be considered equivalent between the uncertainty related to the measurements. At high vapor quality the curve for $\dot{m}_r = 85kg/h$ shows a decreasing trend, it is an unexpected results that may be related to the non-equilibrium of the phases in the duct. At high mass flow rate the velocity of the flow is increased, so that the gap between vapor and liquid phase velocities is too high for them to reach the thermal equilibrium. For this reason it has been chosen to consider the whole curve as unreliable. The same incongruity can be observed for the heat transfer coefficient at 0.9 and 0.95 vapor quality for $[50; 75]kg/h$ mass flow rate. In this case only the mentioned operating condition are excluded from the analysis.

Experiments conduced on smooth tube [see literature] exhibit an abrupt decrease of heat transfer coefficient in correspondence of dryout condition. Such a behavior cannot be observed in this analysis, it is a consequence of helical fins that provides to the fluid a rotary movement so that the liquid flows in the outer part of the duct and does not separate from the channel walls.

Comparing fig. 6.8 and fig. 6.9 the heat flux affects significantly the heat transfer coefficient, since in case of doubled heat flux the heat transfer coefficient is much higher with respect to the correspondent data provided from single heat flux experiment. Both the chart highlight that mass flow rate does not affect the experimental results in the range of $[50; 75]kg/h$ for low vapor quality. This implies that it is not necessary to increase the mass flow rate out of this range, in order to improve the heat transfer process.

Experimental pressure drop for the same evaporation tests is reported in fig. 6.10 and fig. 6.11. It is evident the increase of pressure drop along the test section with the mean vapor quality in the range of $[0.15; 0.7]$, the slopes of all the reported curves decreases moving to high vapor quality. Maximum values of pressure drop are shown for a mean quality of 0.75, higher mean vapor quality corresponds to decreased pressure drop. However, the change in the slope direction is not rapid enough for the dryout to be responsible of that behavior. The trend of pressure drop is not influenced by the increase of mass flow rates, all the curves exhibit the same shape at varying the mean vapor quality. The mass flow rate affects the absolute value of the measured pressure drop. The ratio between pressure drop for $\dot{m}_r = 50kg/h$ and for $\dot{m}_r = 25kg/h$ varies between 2 and 3. An analogous behavior can be recognized comparing $\dot{m}_r = 75kg/h$ and for $\dot{m}_r = 25kg/h$ with a pressure drop ratio correspondent to the same mean average quality in the range of $[4.5; 6.5]$. Pressure drop ratio between curves for $\dot{m}_r = 85kg/h$ and for $\dot{m}_r = 25kg/h$ ranges in $[4.5; 8]$. Such a behavior suggests a non linear dependence with the mass flow rate and a higher increase of pressure drop with the mass flux at higher vapor quality.

Similar trends are exhibited for doubled heat flux, as shown in fig. 6.11, where the maximum pressure drop is measured for $x_m = 0.75$, for all the analyzed mass flow rates. The chart shows also that values for $\dot{m}_r = 85kg/h$ and $\dot{m}_r = 75kg/h$ settle down in a narrow range, suggesting a

decreasing influence on pressure drop at increasing the mass flux.

The effect of heat flux on the heat transfer coefficient and pressure drop is reported in fig. 6.12, fig. 6.13 and fig. 6.14. It is evident that the heat flux increment affects the heat transfer coefficient, the ratio between heat transfer coefficient, at fixed mass flow rate and fixed mean vapor quality, for single or double heat flux is less than 2. This can be explained by the definition of heat transfer coefficient, that is related to the exchanged thermal power, the exchange surface and the mean logarithmic temperature difference. To increase the heat flux implies a linear increment of the exchanged power, but the increase of demineralized mass flow rate affect the mean logarithmic temperature difference. In particular for evaporation experiments the outlet temperature of the water is higher, so that also $\Delta T_{mean,log}$ has a higher value, this is the reason why there isn't a linear dependence between heat flux and heat transfer coefficient.

Pressure drop is not affected by the heat flux variation, it is shown in the charts that values of pressure drop at fixed mass flow rate and mean vapor quality are almost the same.

6.3 Evaluation of microfin enhancement

Advantages and drawbacks of using an enhanced duct are evaluated comparing the microfin tube with a smooth tube. For this analysis, experimental data from Colombo, Lucchini and Muzzio database [24] are considered. The data have been selected such that the operating conditions, the fluid and the tube geometry (diameter, thickness, orientation) were similar to those of experiments conduced on the microfin duct, tab. 6.7 reports the geometry of smooth tube used for comparison. Comparison between smooth and microfin tube is limited to the operating conditions reported in tab. 6.8, since they are the only experiments that have been conduced on both the ducts. Experiments in evaporation condition were not take into account because tests performed on microfin tube are unreliable (see section 6.2).

Inner diameter	$[mm]$	8.92
Outer diameter	$[mm]$	9.52
Wet perimeter	$[mm]$	28.0
Cross section area	$[mm^2]$	62.5

Table 6.7: Geometrical parameter of smooth tube studied in Colombo, Lucchini and Muzzio experimental investigation.

Condition	*Condensation*
Mass flow rate $[kg/h]$	50
Quality variation	0.2
Average vapor quality	[0.2;0.8]

Table 6.8: Experimental conditions of tests used to compare microfin and smooth tube.

penalization factor of microfin tube is depicted in fig. 6.15. The chart shows an increment of pressure drop for the whole curve, with a maximum penalization for mean vapor quality of 0.2. Pressure drop at low mean quality is more than doubled, while the penalization factor tends to decrease at growing the vapor quality. For a 0.8 mean quality pressure drop of microfin and smooth tube are almost the same, resulting in a penalization factor close to 1.

Increase of heat transfer coefficient in microfin tube can be observed in fig. 6.16. Microfin geometry leads to an improvement of heat transfer process, that reaches the maximum enhancement for 0.7 vapor quality. It can be observed that there is not a high variation on enhancement factor along the curve, the value of E is in the range of $[1.27; 1.53]$.

Efficiency index gives a very useful indication on the benefits related to presence of microfin, fig. 6.17 reports the values of I. For quality range $[0.2; 0.6]$ the efficiency index is lower than one, it indicates that pressure drop in microfin tube increases more than heat transfer coefficient. For high vapor quality efficiency index is greater than one, this is a favorable condition for heat transfer process. It would be favorable to obtain high values of I or, at least, higher than one, but the exhibited trend does not exclude studied duct from applications. Objectives and constrains of any industrial application must be analyzed individually, to verify if the performances of the heat exchanger are aligned with the facility aim.

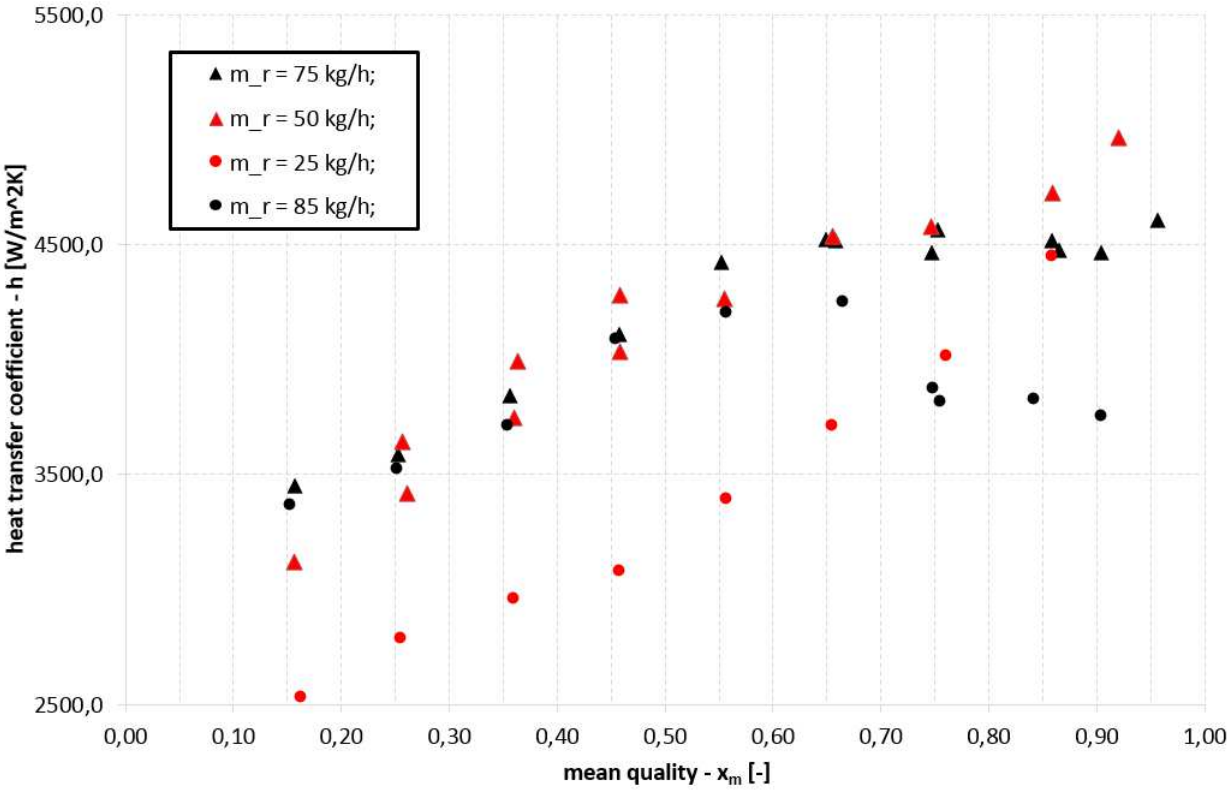

Figure 6.8: Boiling heat transfer coefficient h versus average quality ($q = 8.6kW/m^2$).

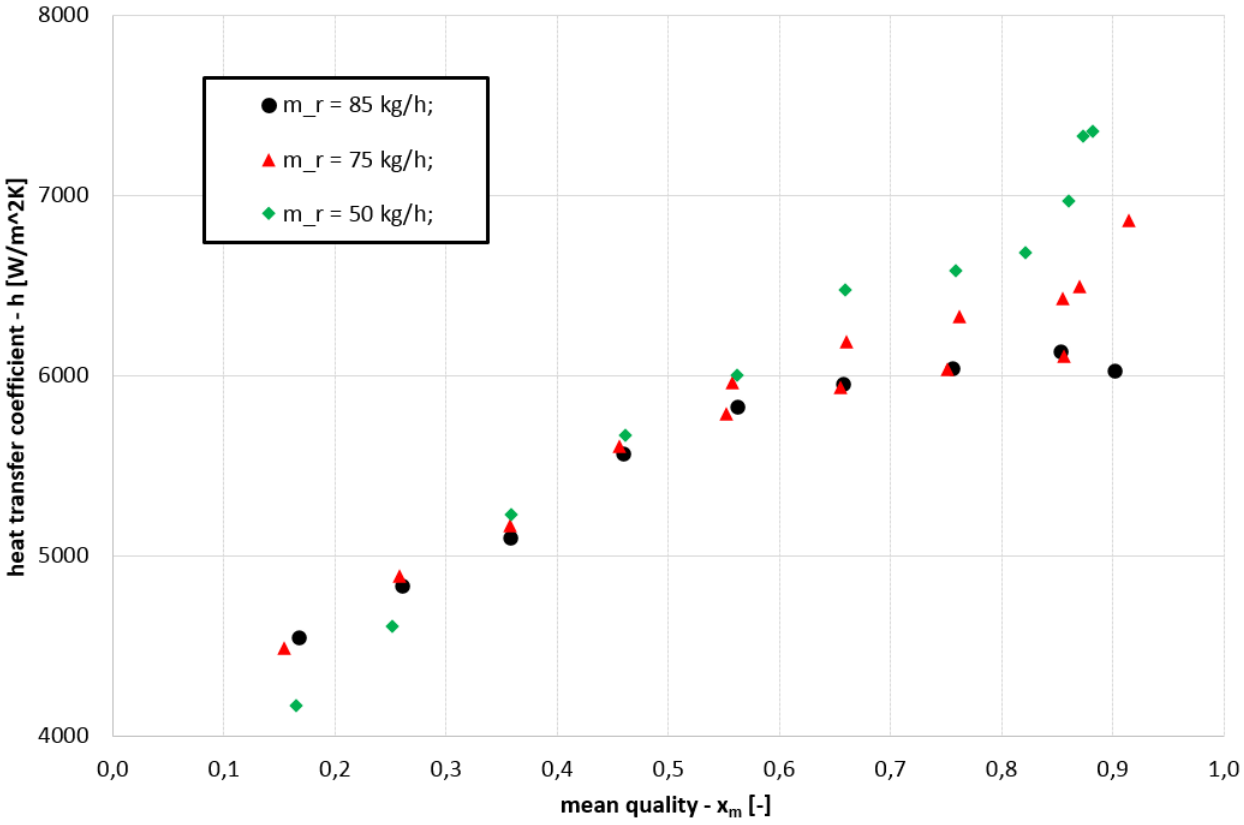

Figure 6.9: Boiling heat transfer coefficient h versus average quality ($q = 17.2kW/m^2$).

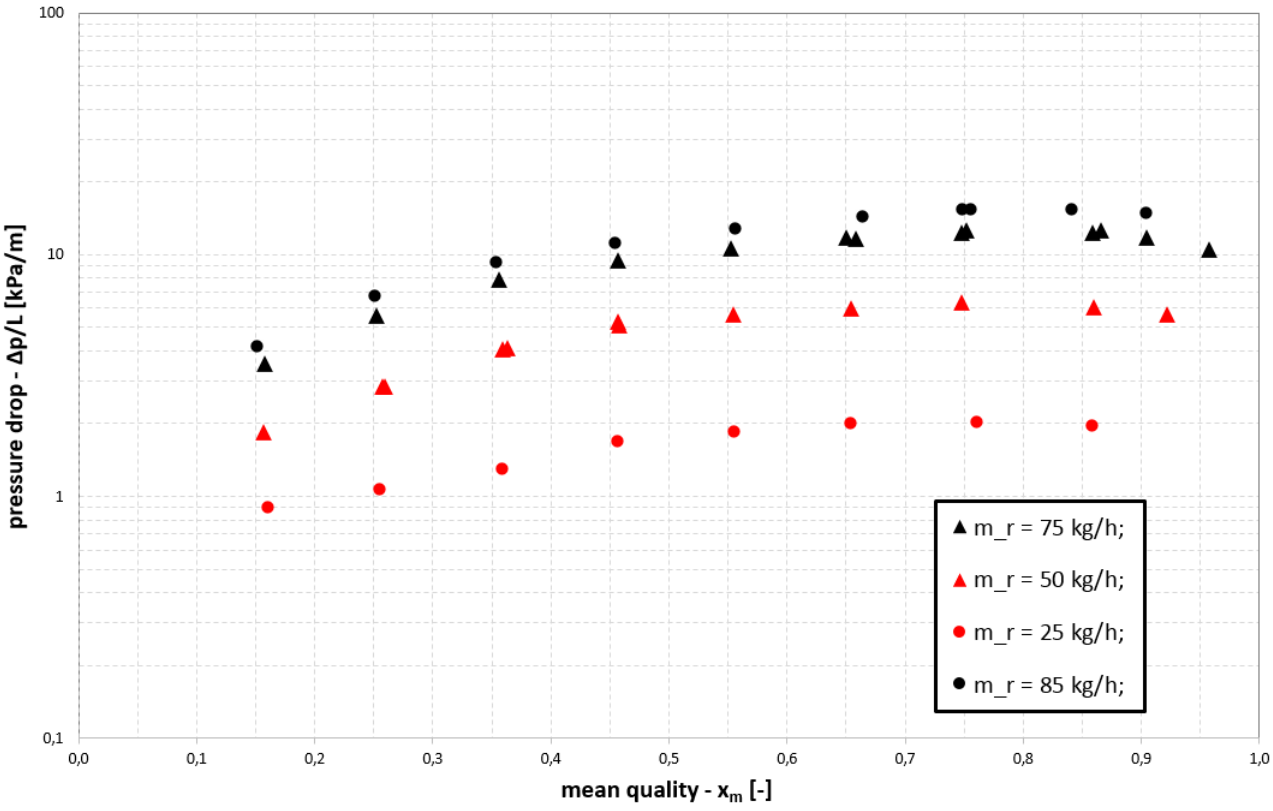

Figure 6.10: Evaporation pressure drop Δp versus average quality ($q = 8.6 kW/m^2$).

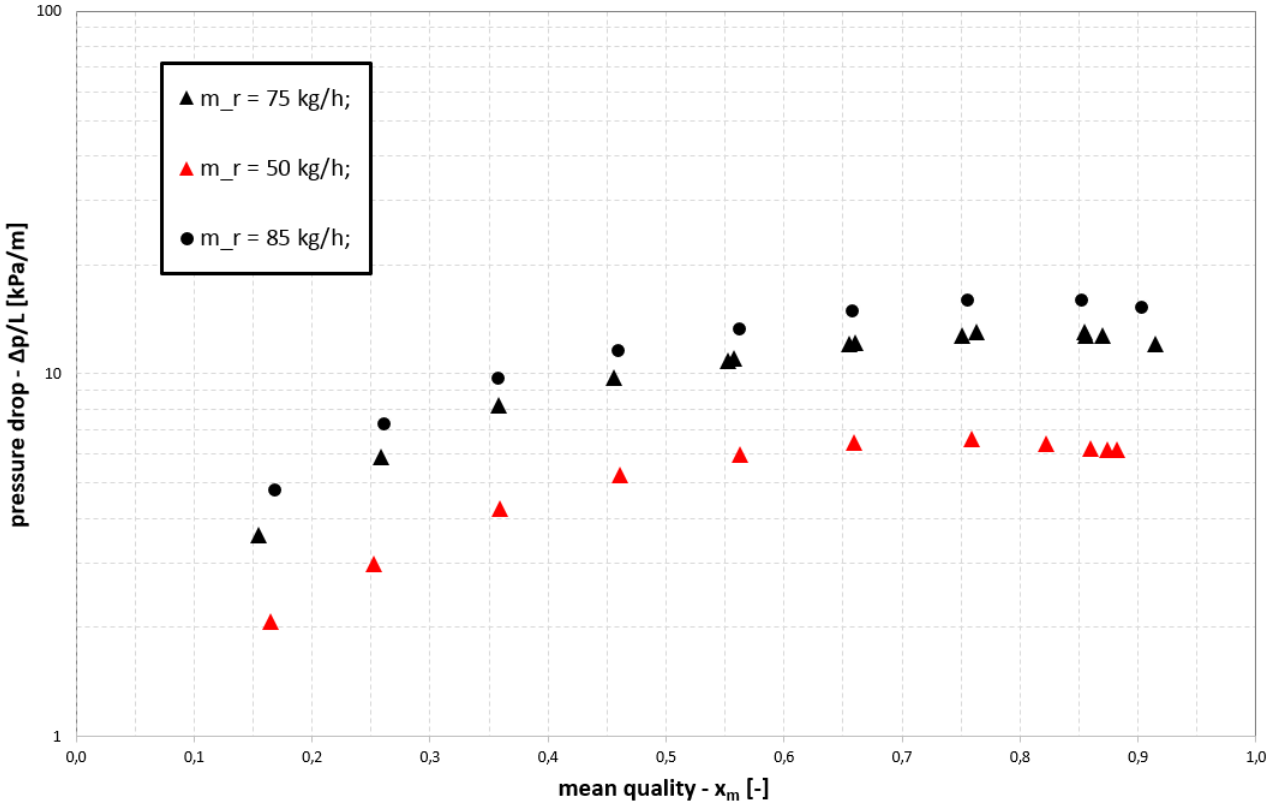

Figure 6.11: Evaporation pressure drop Δp versus average quality ($q = 17.2 kW/m^2$).

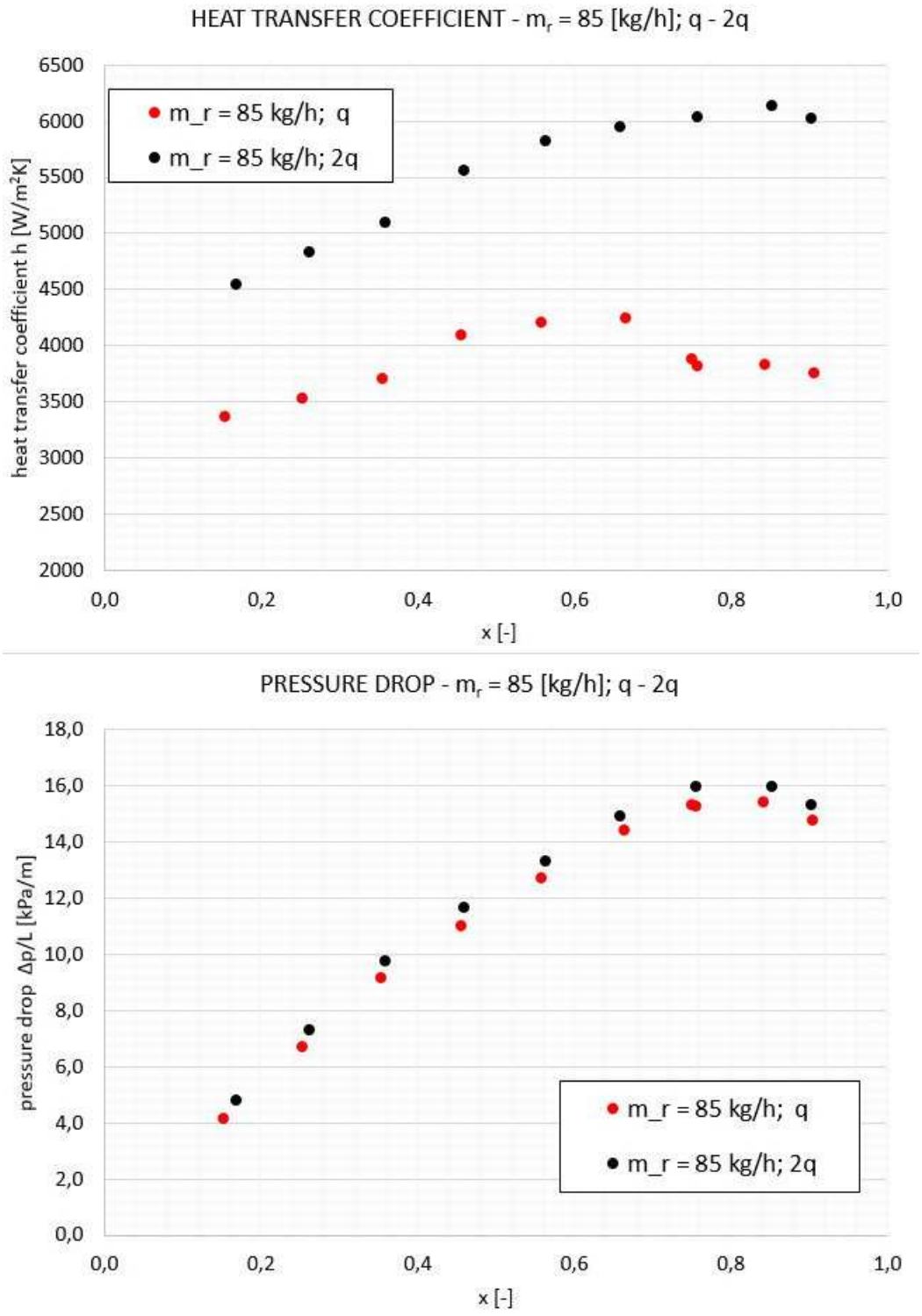

Figure 6.12: Boiling heat transfer coefficient and pressure drop versus mean vapor quality for $\dot{m}_r = 85kg/h$, comparison between experimental data with single heat flux ($q = 8.6kW/m^2$) and double heat flux ($q = 17.2kW/m^2$).

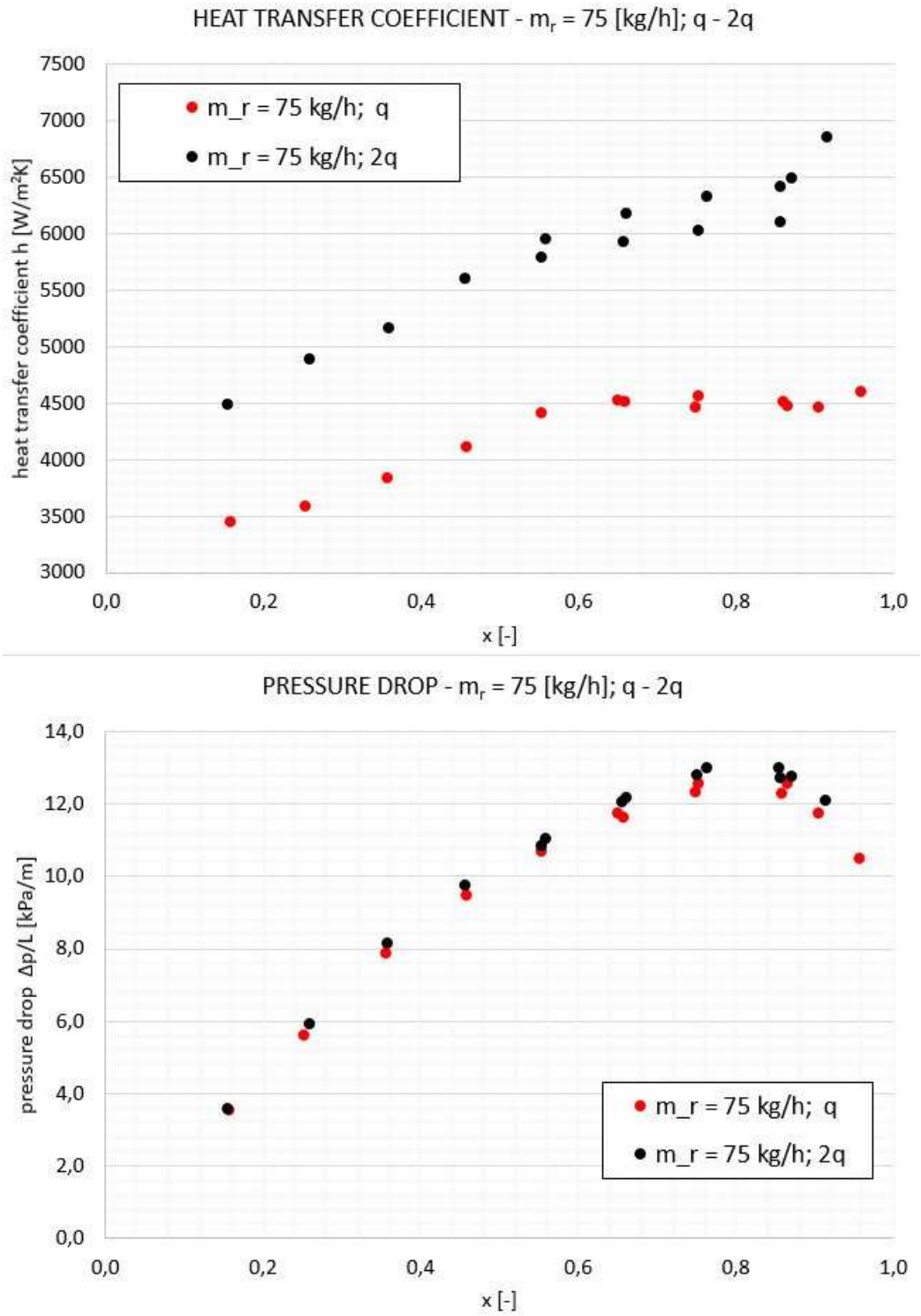

Figure 6.13: Boiling heat transfer coefficient and pressure drop versus mean vapor quality for $\dot{m}_r = 75kg/h$, comparison between experimental data with single heat flux ($q = 8.6kW/m^2$) and double heat flux ($q = 17.2kW/m^2$).

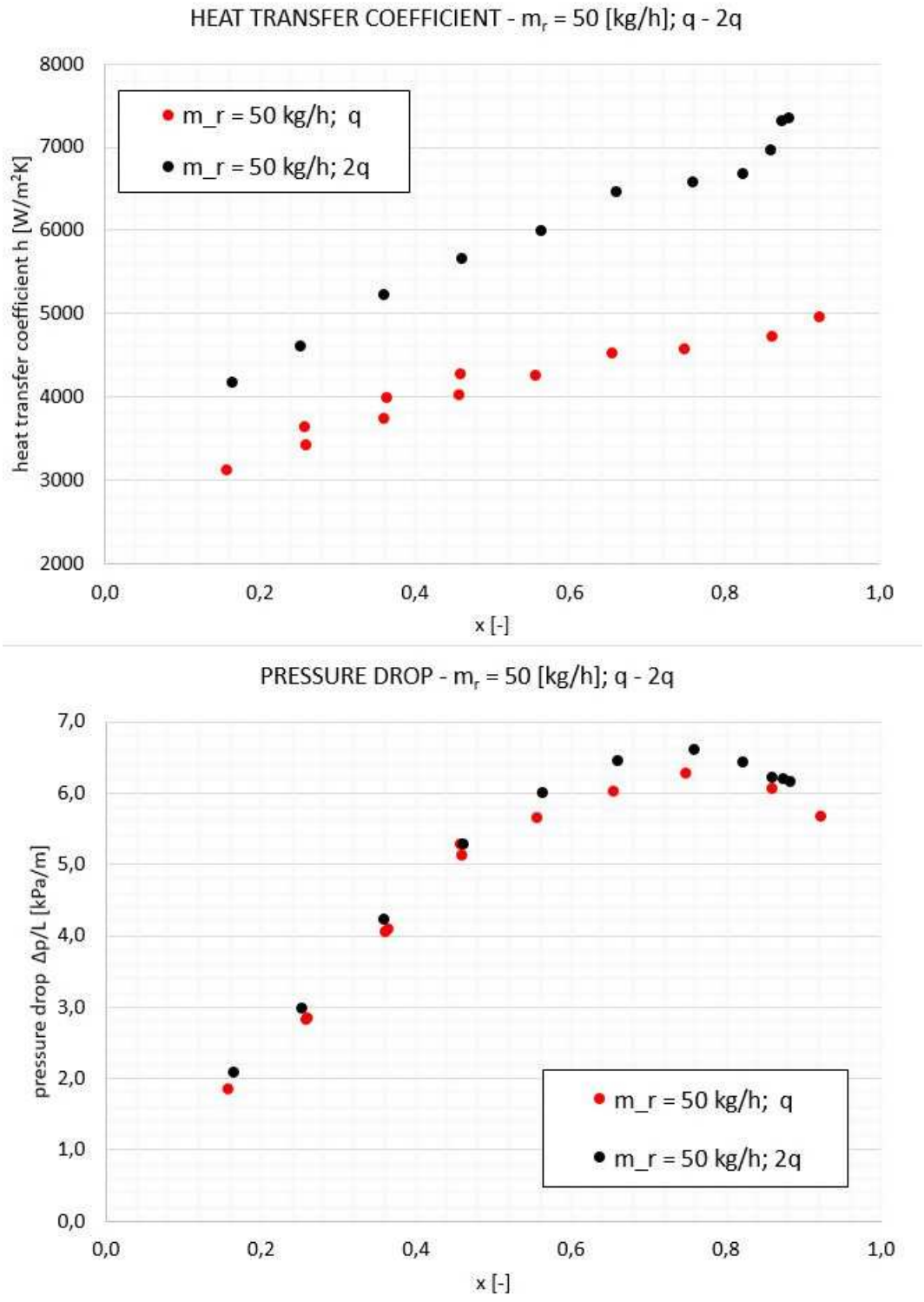

Figure 6.14: Boiling heat transfer coefficient and pressure drop versus mean vapor quality for $\dot{m}_r = 50kg/h$, comparison between experimental data with single heat flux ($q = 8.6kW/m^2$) and double heat flux ($q = 17.2kW/m^2$).

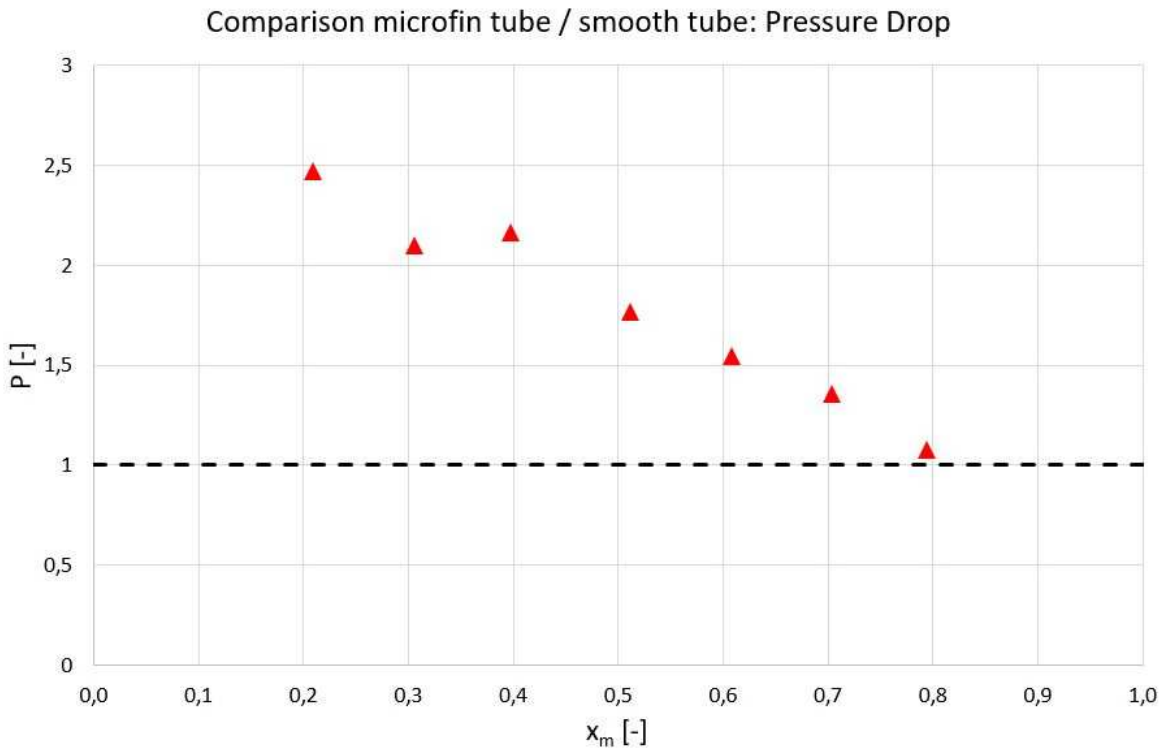

Figure 6.15: Comparison on pressure drop per unit length obtained by smooth and microfin tube, P is defined in eq. 6.6.

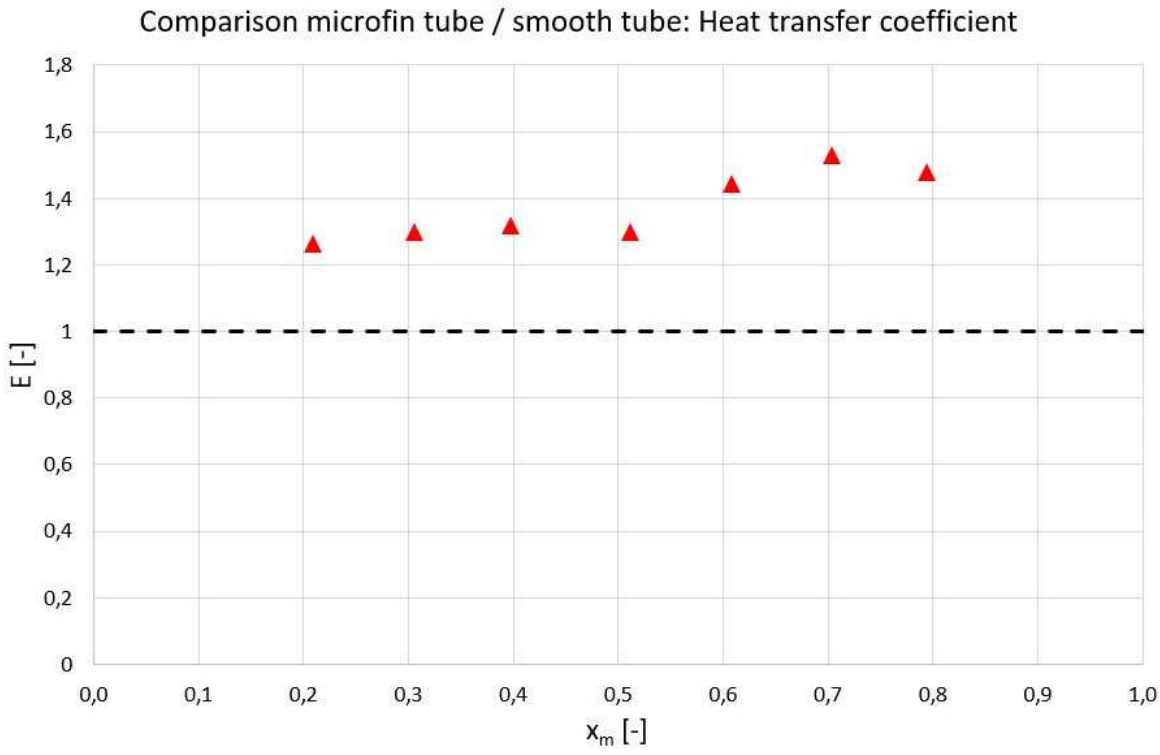

Figure 6.16: Comparison on heat transfer coefficient obtained by smooth and microfin tube, E is defined in eq. 6.5.

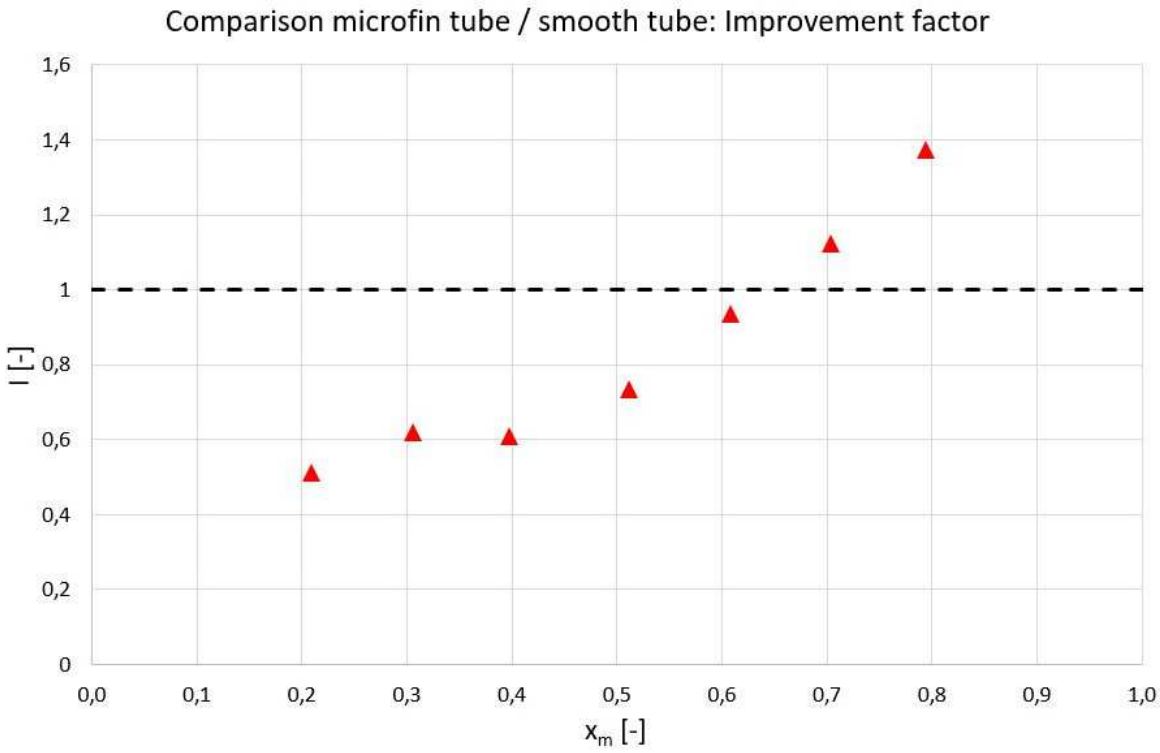

Figure 6.17: Comparison between penalization and enhancement factors, it is an index of improvement due to the presence of microfins, I is defined in eq. 6.7.

Chapter 7

Comparison between data and correlation

In this chapter the correlations presented in 3 and4 are analyzed. Predicted data are compared with the experimental results to evaluate the performances of the correlation.

The correlation capability to predict experimental data is evaluated studying:

- the mean relative standard deviation ($\sigma_{\%}$);
- the relative error ($e_{\%}$);
- the correspondence between trend of the predictions and experimental data.

Where:

$$\sigma_{\%} = \sqrt{\frac{\left(\frac{y(i)_{pred} - y(i)_{exp}}{y(i)_{exp}}\right)^2}{N-1}} \tag{7.1}$$

$$e_{\%} = \frac{y(i)_{pred} - y(i)_{exp}}{y(i)_{exp}} \tag{7.2}$$

7.1 Pressure drop in condensation condition

The analysis of pressure drop in condensation condition refers to the following correlations: Shannak [8], Muller and Steinhagen [6], Bandarra [7], Sun Mishima [5], Kedzierski [21], Domansky [9], Haraguchi [11] and Goto [12].

fig. 7.1 reports a parity plot which includes all the analyzed correlation in any tested condition.

Parity plots for evaluation of pressure drop correlation in condensation condition are reported in fig. 7.2 and fig. 7.3. It shows that the best fitting correlations was developed by Shannak, Muller and Steinhagen, Goto. They obtain a very good agreement with the experimental data mostly for high mass flow rates, while at low mass flux the deviations increase. On the contrary Haraguchi correlation has high predictive performance for low mass flow range $[25; 50] kg/h$ and at higher mass flow rate it tends to overestimate the pressure drop. Kedzierski and Sun Mishima correlations have similar predictive properties since in most the cases predicted data fit the measures with a lower deviation than $\pm 30\%$. Domansky correlation underestimates experimental data for the

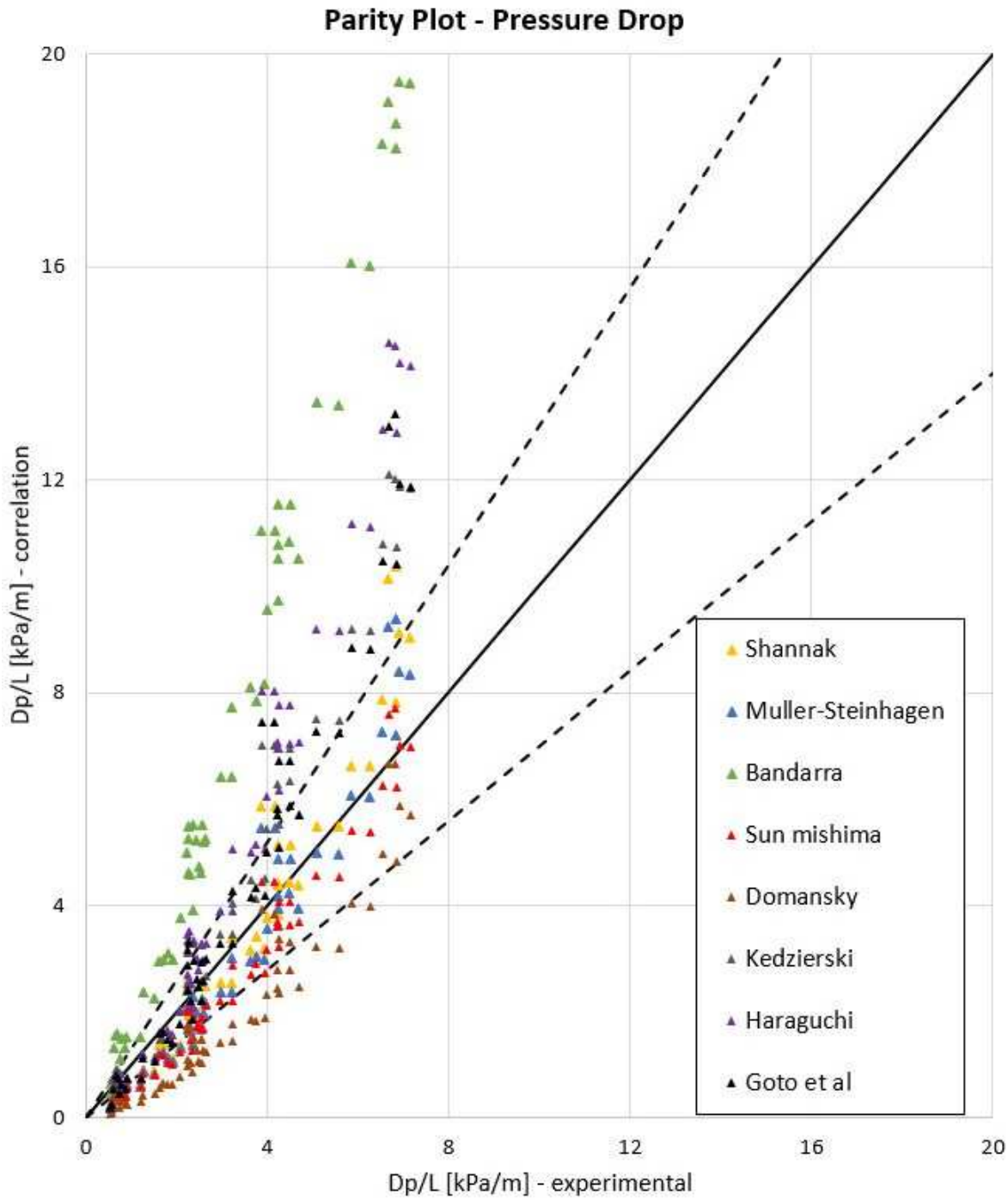

Figure 7.1: Comparison between data and correlation predictions for condensation pressure drop.

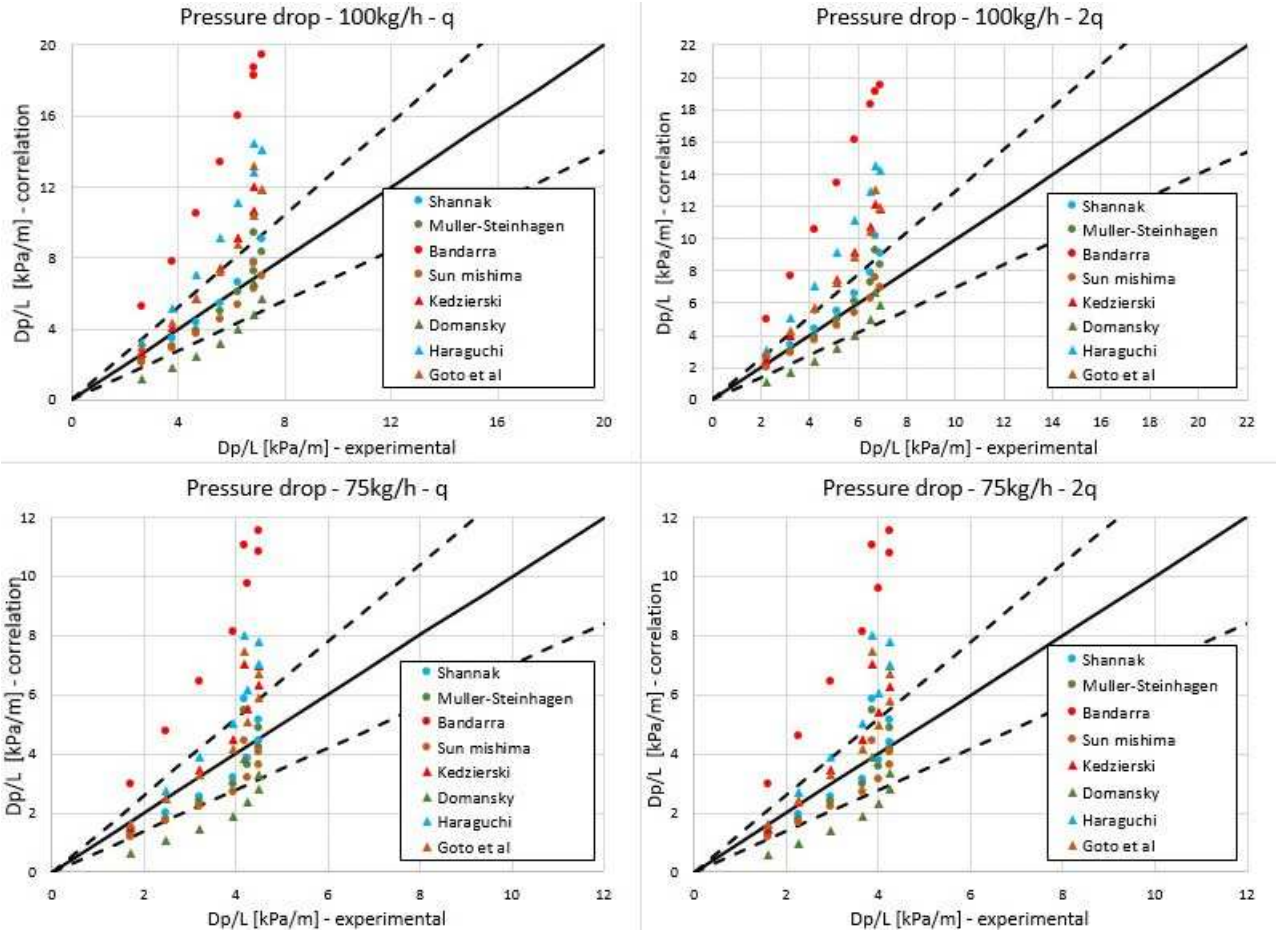

Figure 7.2: Comparison between data and correlation predictions for pressure drop at high mass flow rate $[75; 100] kg/h$.

	Heat transfer coefficient	
Correlation	$\sigma_{\%}$	$e_{\%}$
Shannak	28.5	-9.0
Muller Steinhagen	28.1	-14.4
Bandarra	125.5	117.9
Sun Mishima	29.8	-23.9
Kedzierski	50.2	-46.5
Domansky	39.5	22.3
Haraguchi	56.5	34.0
Goto	40.1	17.0

Table 7.1: Mean percentage relative deviation and error of pressure drop correlations.

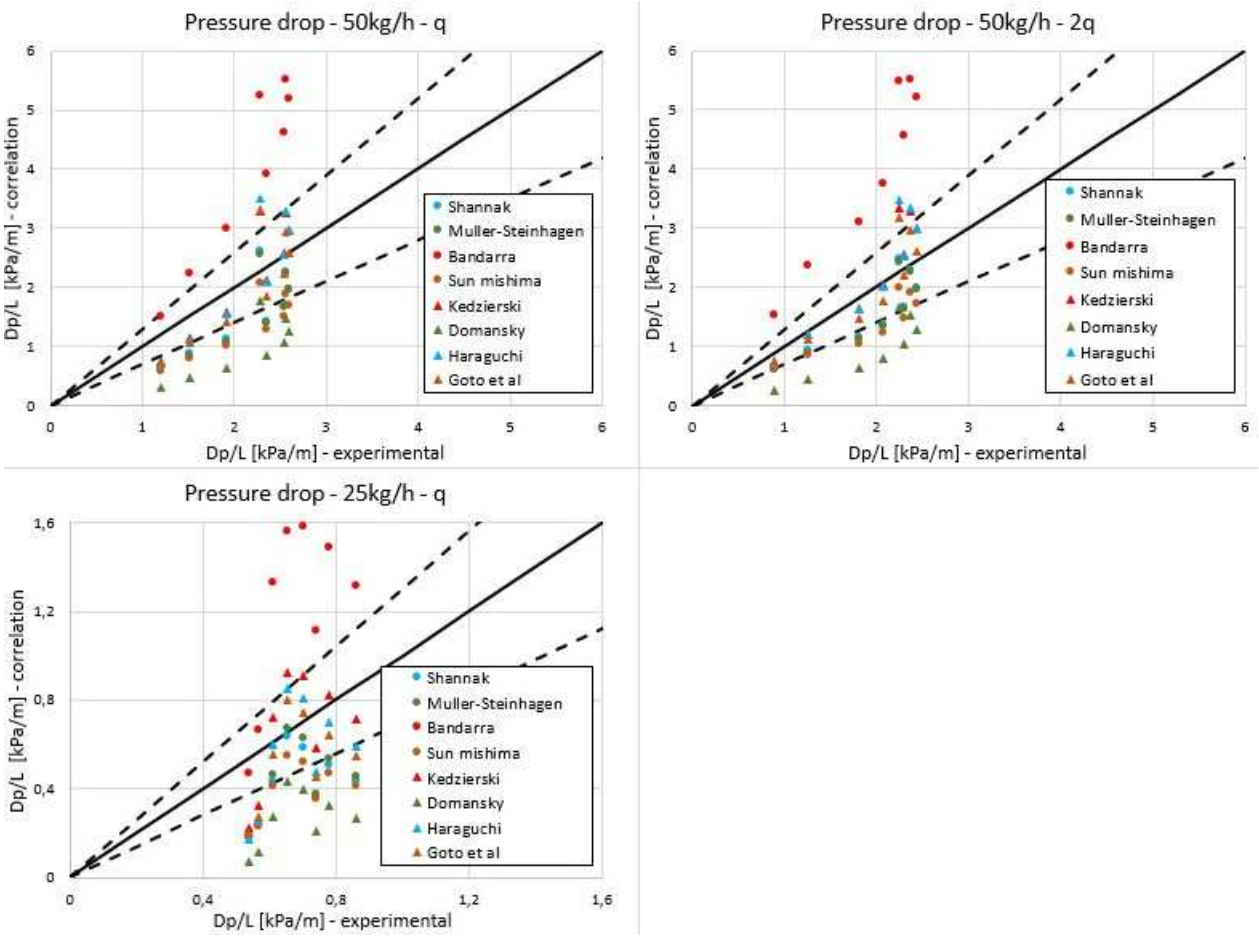

Figure 7.3: Comparison between data and correlation predictions for pressure drop at low mass flow rate $[25; 50] kg/h$.

whole range of experiments. Bandarra correlation shows the worst agreement with the measured pressure drop, since it overestimates them with standard deviation greater than 100%, as shown in tab. 7.1.

Muller Steinhagen and Shannak correlation have the best predictive performances, but the trend of pressure drop is well predicted only at low vapor quality, at increased vapor quality experimental pressure drop decreases while there is no tendency variation in the presented curves. Bandarra correlation exhibit a decrease of predictive pressure drop at high mean quality but its deviation and relative error are the greatest. Analysis of correlation's error highlights the performances of each correlation, it is evident that none of the curves' error is constant with the vapor quality (see fig. 7.6 and fig. 7.7).

From fig. 7.8 and fig. 7.9 it is possible to understand the results of correlations in the analyzed range of operating conditions.

7.2 Heat transfer coefficient in condensation condition

For the analysis of condensation heat transfer coefficient, selected correlations are the following ones: Kumar Mohseni [18], Oh Son [19], Cavallini [20] and Kedzierski [21].

fig. 7.10 provides an overview of all the correlations that has been studied to predict heat transfer coefficient in condensation condition.

As shown in fig. 7.11 and fig. 7.12, Kedzierski correlation proved to be a good predictor for double heat flux condition, while for single heat flux it tends to overestimate the heat transfer coefficient, in particular for high mass flow rate. On the contrary Kumar Mohseni developed the correlation that best fits the experimental data for single heat flux tests. Oh Son correlation has a similar trend to Kumar Mohseni but its prediction shows high accuracy only in intermediate mass flow rate range, for low mass flux the heat transfer coefficient is underestimated and, viceversa, for high mass flux it is overestimated. Cavallini correlation has the worst predictive performances for the whole range of experiments, it tends to overestimate the heat transfer coefficient mostly in case of high mean vapor quality.

At high mass flow rate the Kumar Mohseni correlation predicts experimental values with a very low deviation, the trend of measured pressure drop at increasing vapor quality is the one described by the correlation curve. For experiments conduced with double heat flux ($q = 15kW/m^2$) an offset is shown with respect to the gathered measures, while with a single heat flux ($q = 7.5kW/m^2$) this deviation is not present. At low mass flow rate experimental values are close to Kedzierski predictions, even if the trend of the curve is not well fitted with the data. This situation is better represented in fig. 7.15 and fig. 7.16.

In fig. 7.17 it is possible to find which experimental conditions is better predicted by the different correlations.

7.3 Pressure drop in evaporation condition

The following pressure drop correlations have been selected for data analysis: Shannak [8], Muller and Steinhagen [6], Bandarra [7], Sun Mishima [5], Domansky [9] and Goto [12].

The parity plot depicted in fig. 7.18 reports all the predicted pressure drop with respect to the experimental data, any tested condition is taken into account.

The same analysis is performed separately for any experimental condition (see fig. 7.19 and

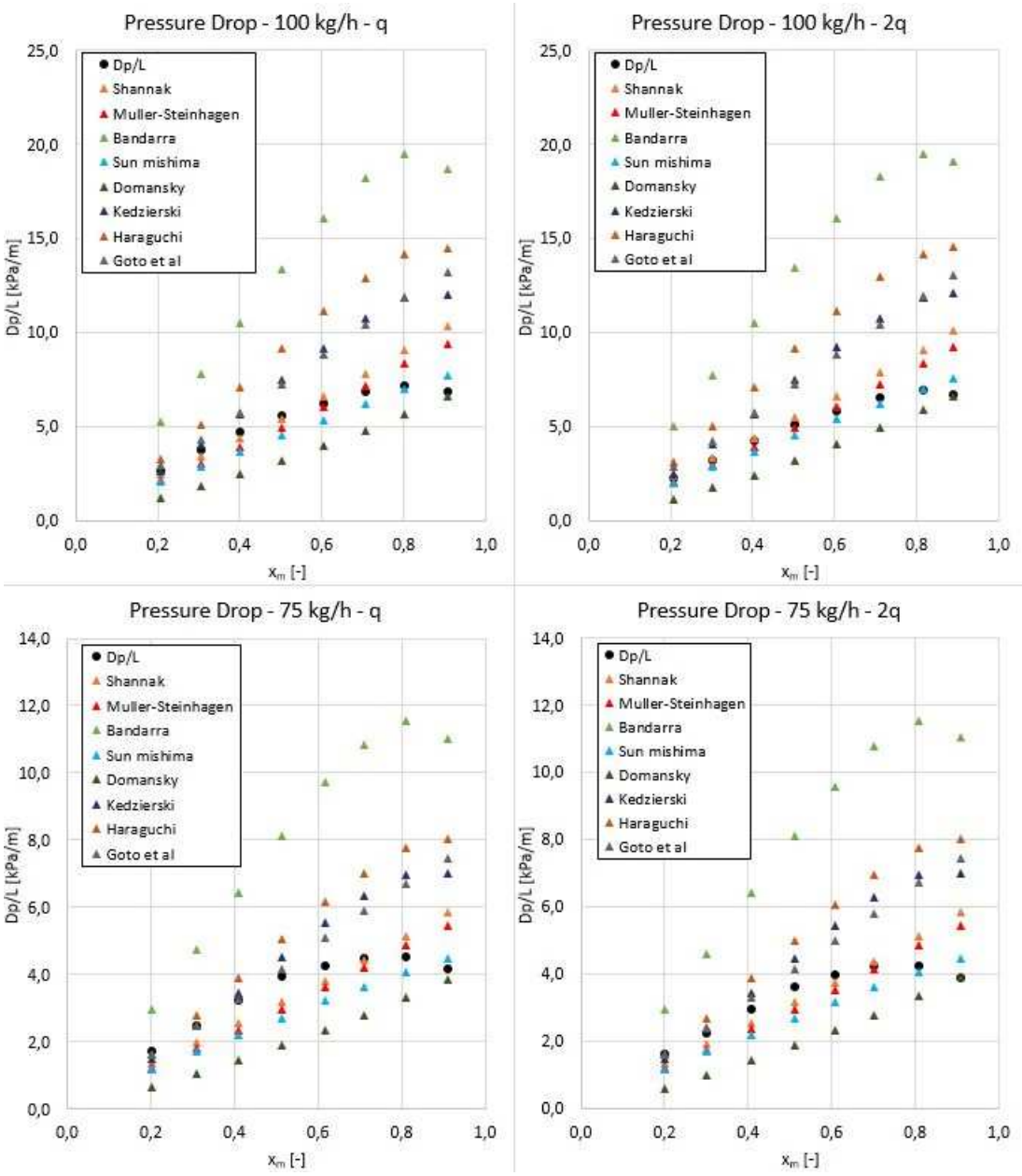

Figure 7.4: Predicted heat transfer coefficient trend with respect to the mean vapor quality at high mass flow rate $[75; 100] kg/h$.

	Heat transfer coefficient	
Correlation	$\sigma_{\%}$	$e_{\%}$
Kumar Mohseni	30.9	-25.9
Oh Son	34	-10.8
Cavallini	133.1	121.7
Kedzierski	31	12.8

Table 7.2: Mean relative deviation and error of condensation heat transfer coefficient correlations.

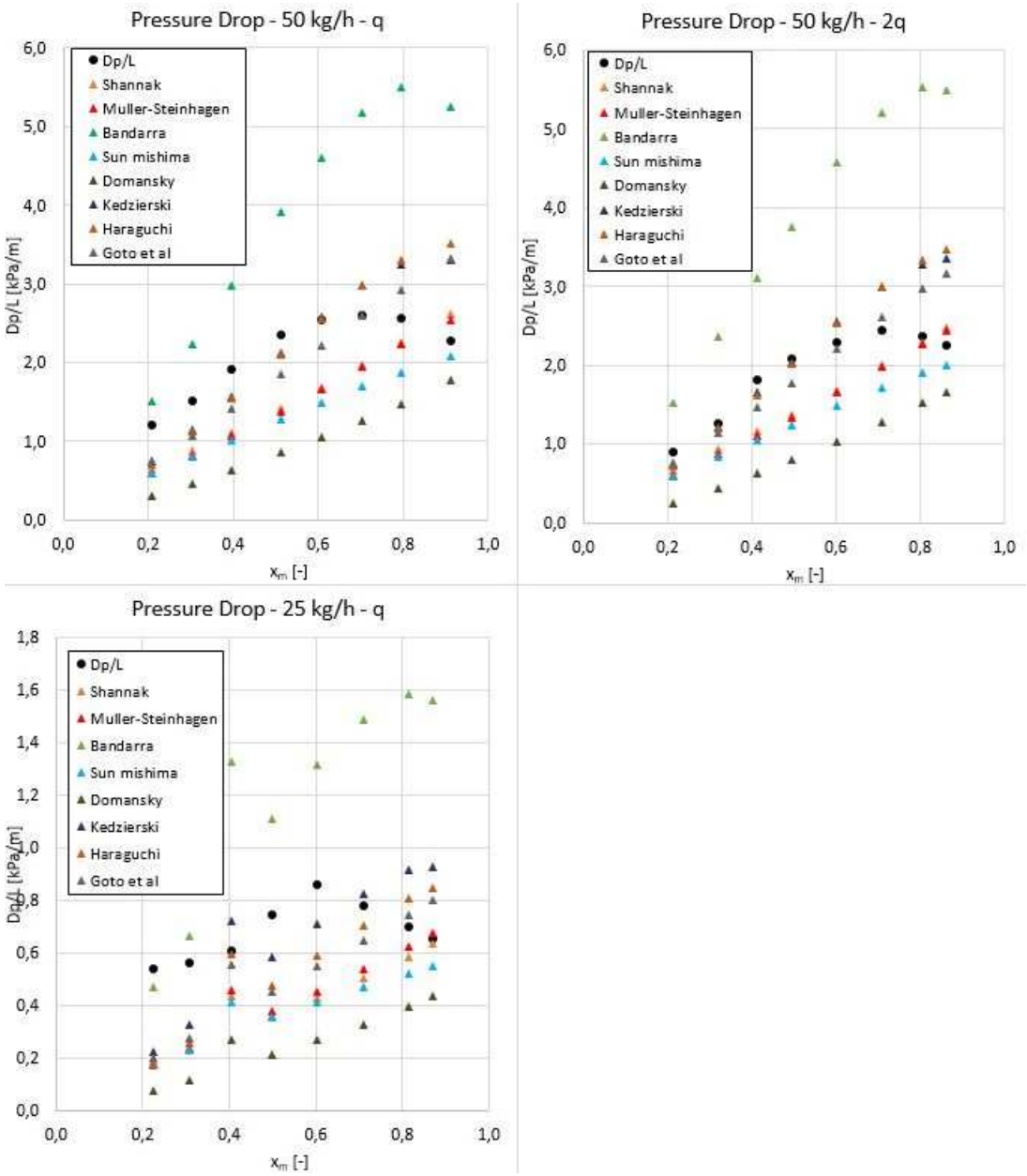

Figure 7.5: Predicted heat transfer coefficient trend with respect to the mean vapor quality at low mass flow rate $[25; 50] kg/h$.

	Pressure drop	
Correlation	$\sigma\%$	$e\%$
Shannak	29.8	-21.4
Muller Steinhagen	31.8	-25.3
Bandarra	67.8	59.4
Sun Mishima	40.5	-38.3
Domansky	42.8	-40.4
Goto	32.4	-10.2

Table 7.3: Mean percentage error and relative deviation of boiling pressure drop correlations.

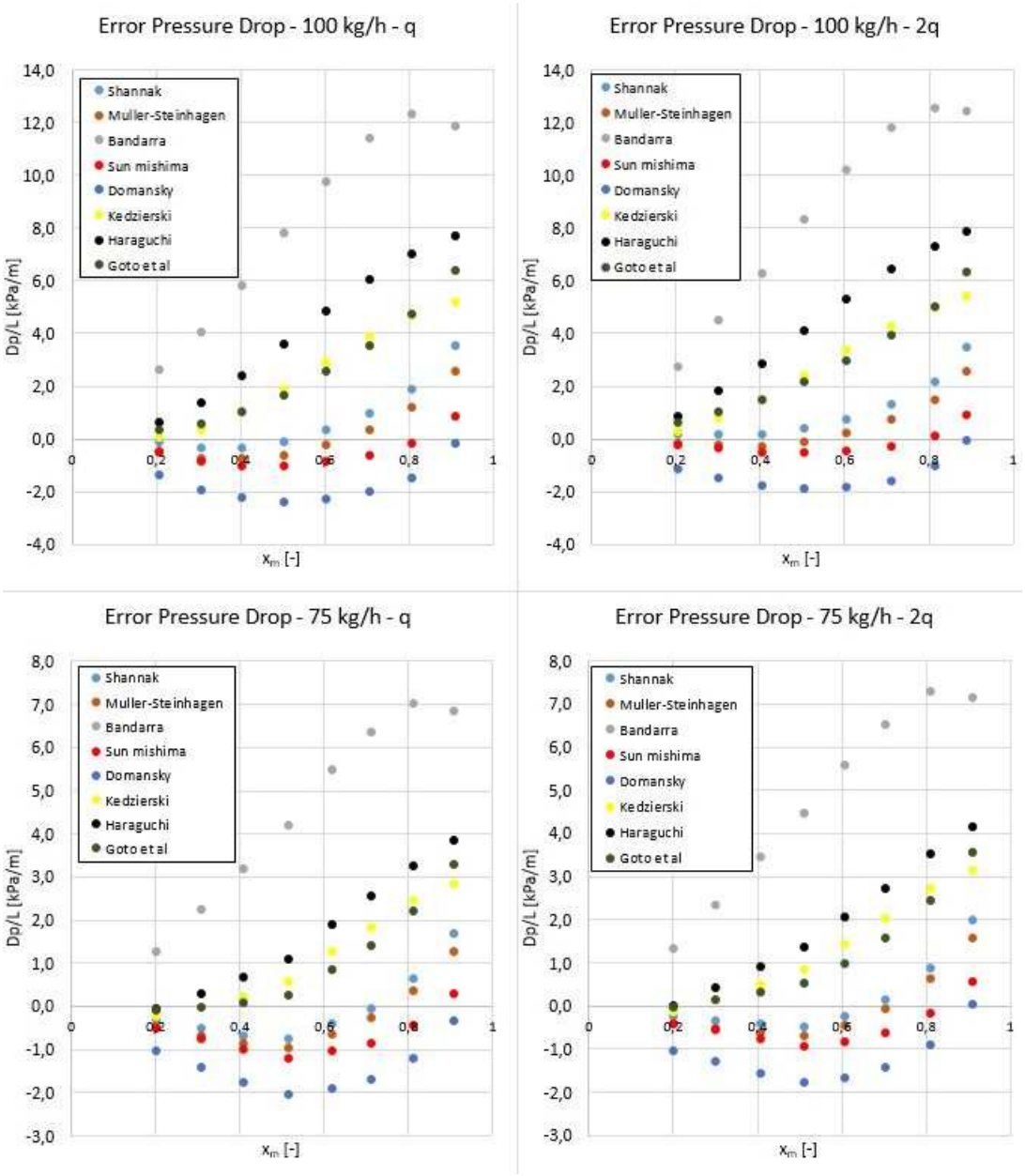

Figure 7.6: Error of predicted heat transfer coefficient with respect to the mean vapor quality at high mass flow rate $[75; 85] kg/h$.

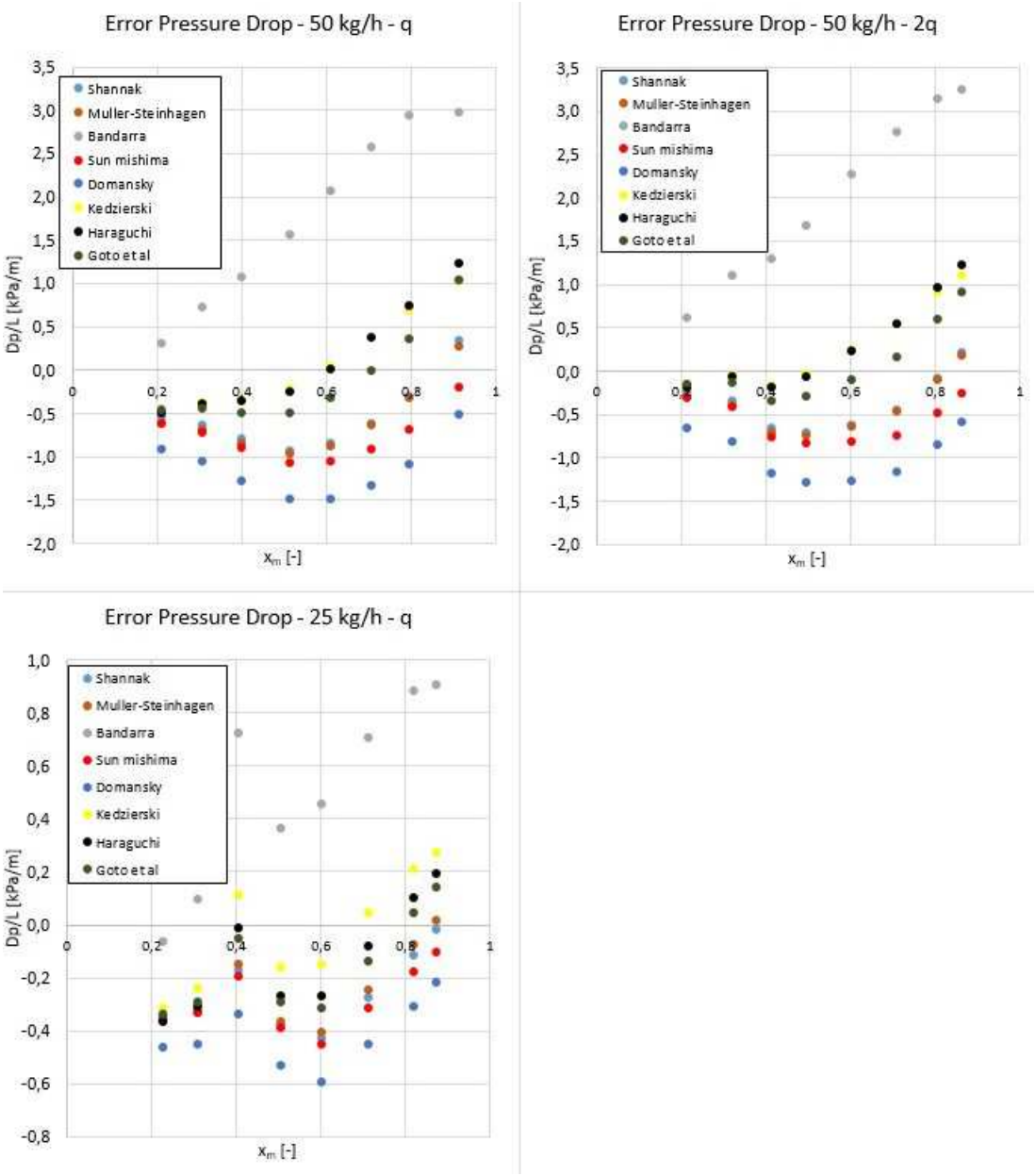

Figure 7.7: Error of predicted heat transfer coefficient with respect to the mean vapor quality at low mass flow rate $[25; 50] kg/h$.

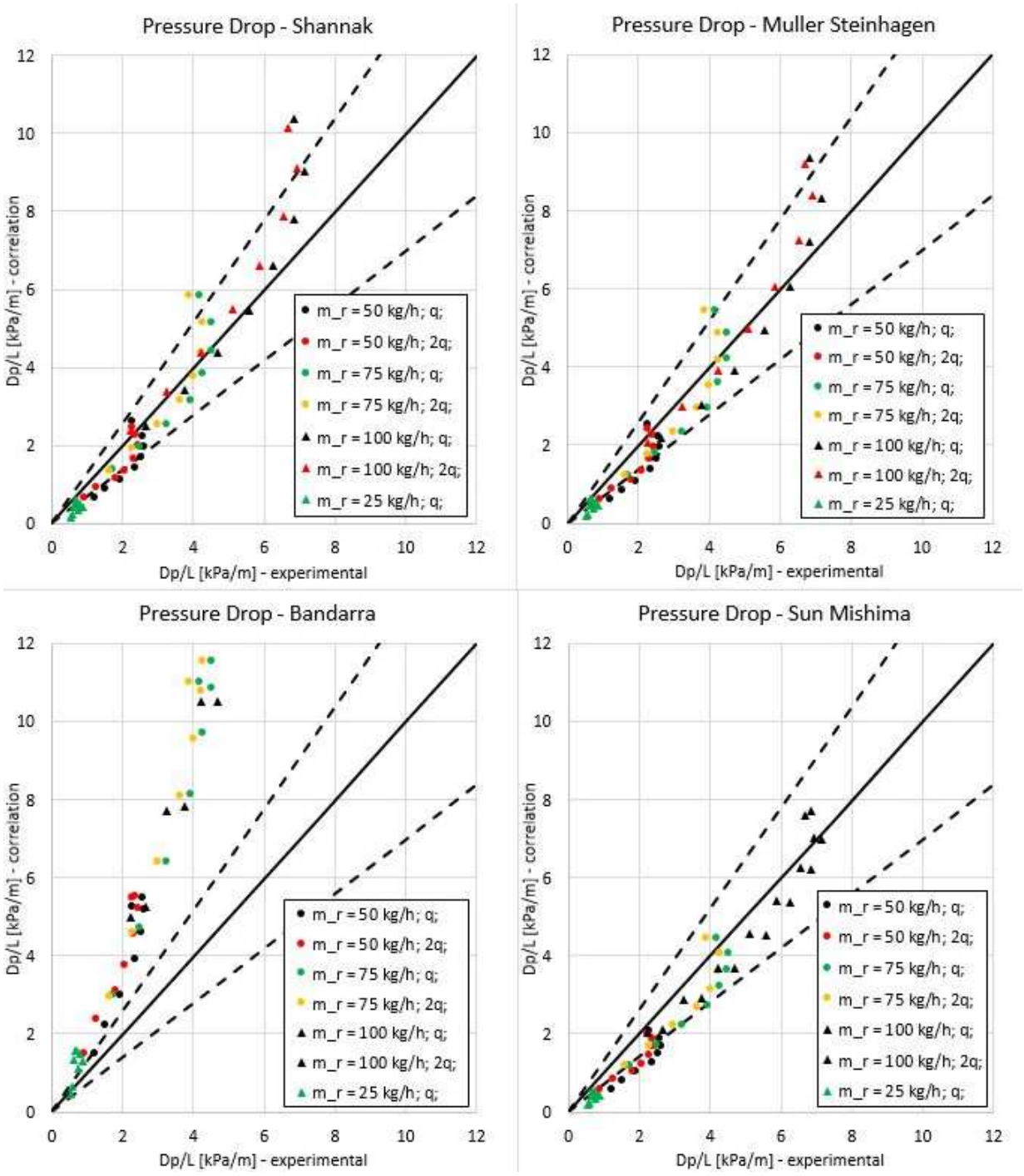

Figure 7.8: Parity plots of each single correlation for condensation heat transfer coefficient.

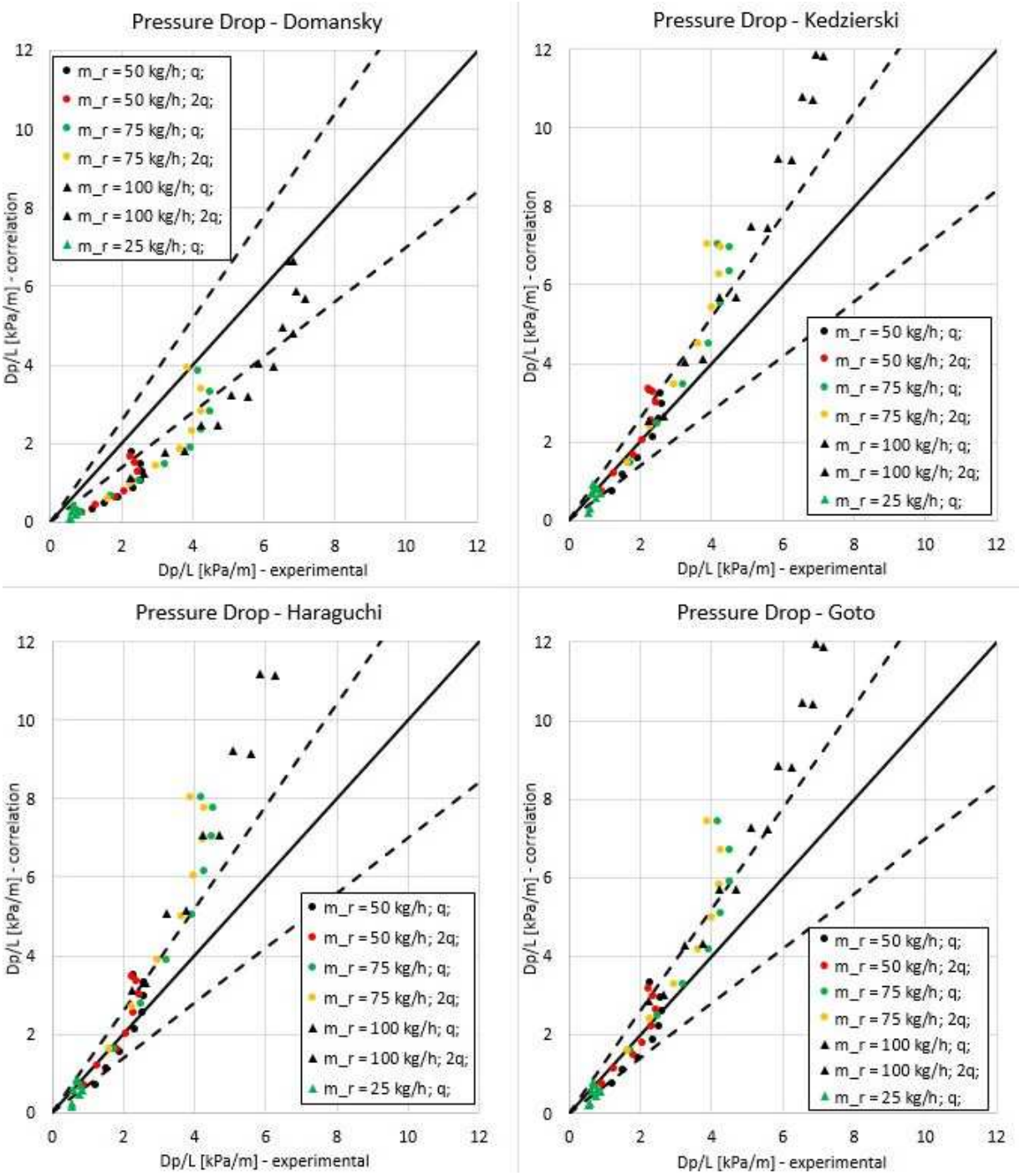

Figure 7.9: Parity plots of each single correlation for condensation heat transfer coefficient.

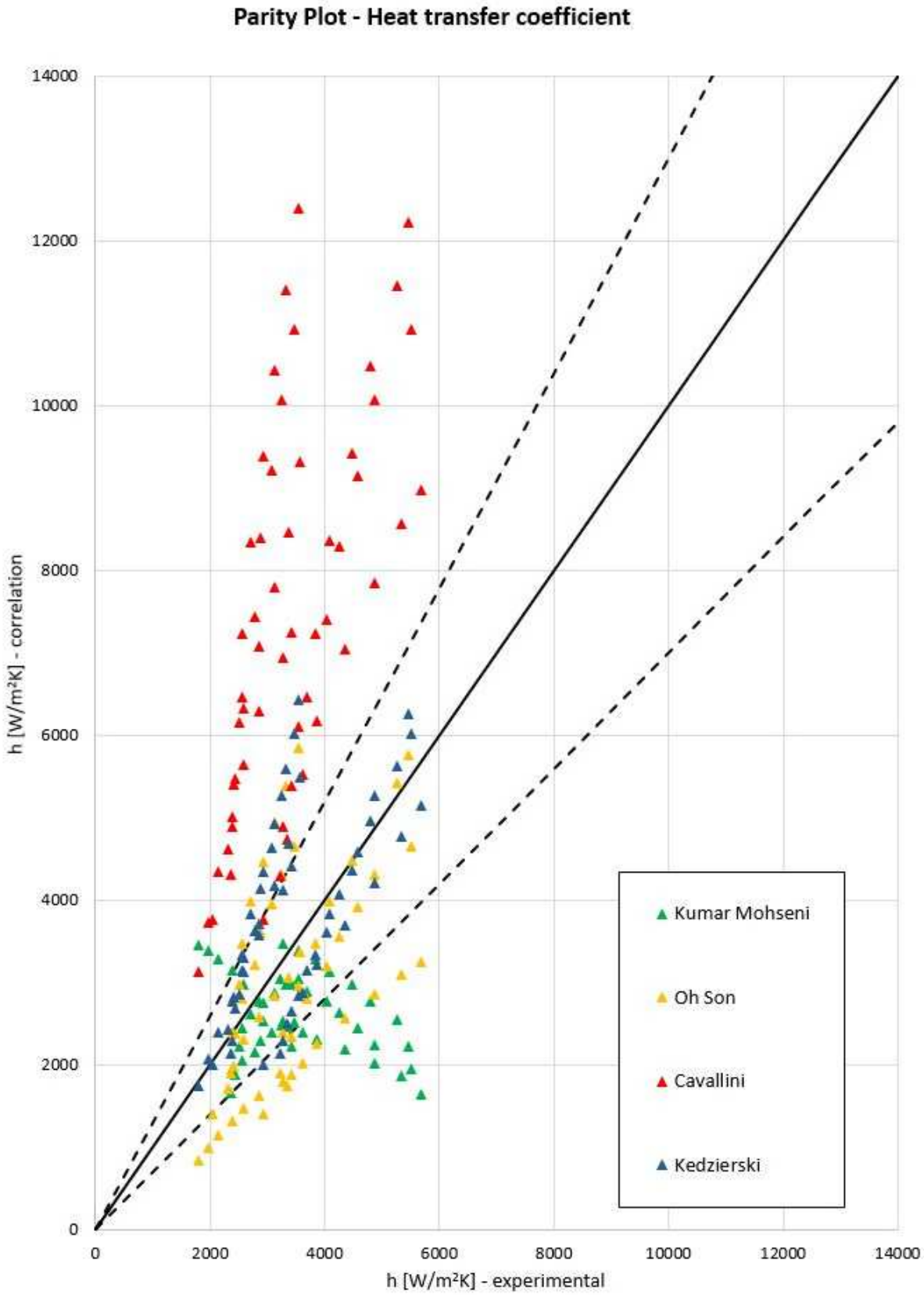

Figure 7.10: Comparison between data and correlation predictions for condensation heat transfer coefficient.

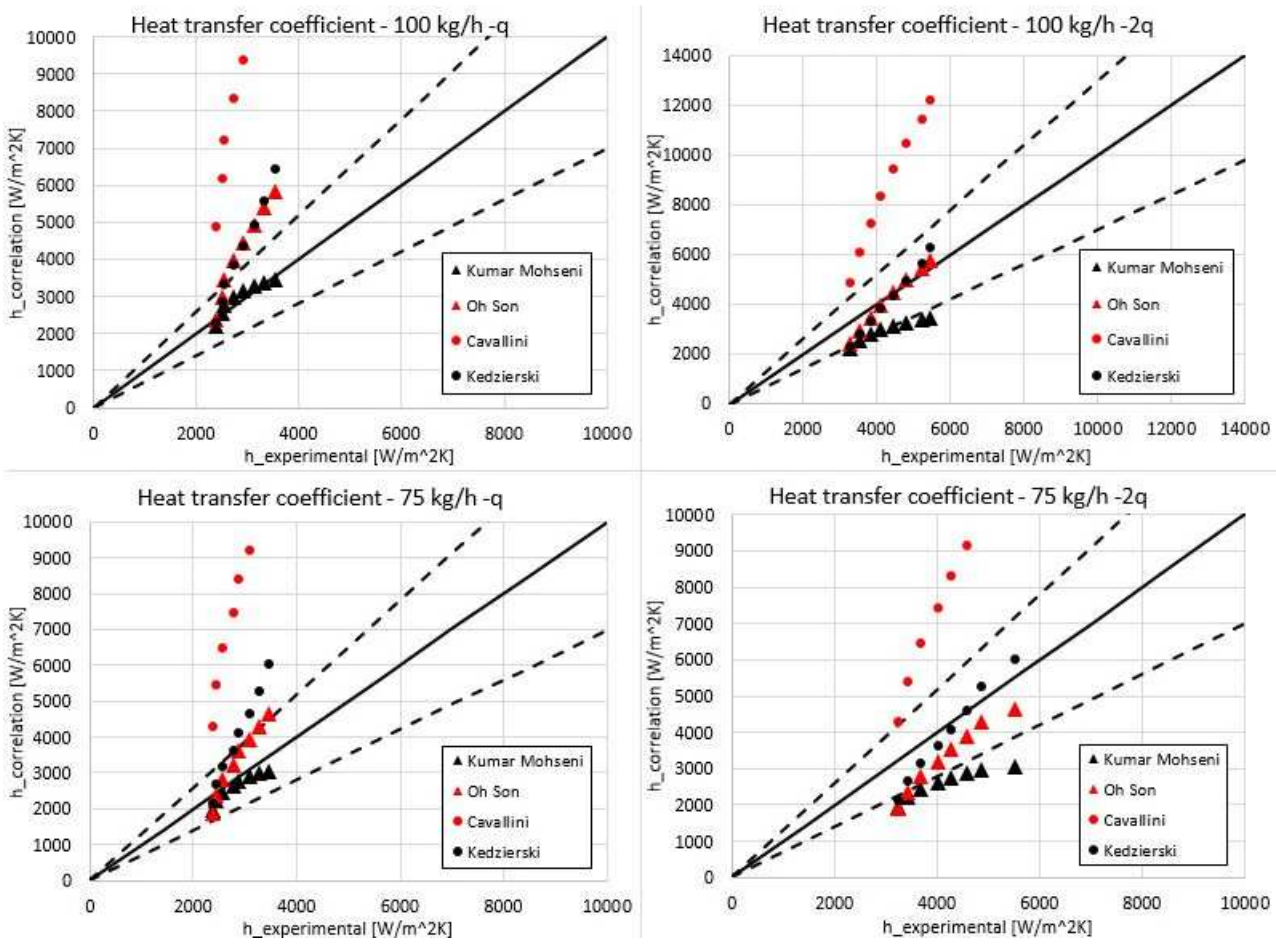

Figure 7.11: Comparison between data and correlation predictions for condensation heat transfer coefficient at high mass flow rate $[75; 100] kg/h$.

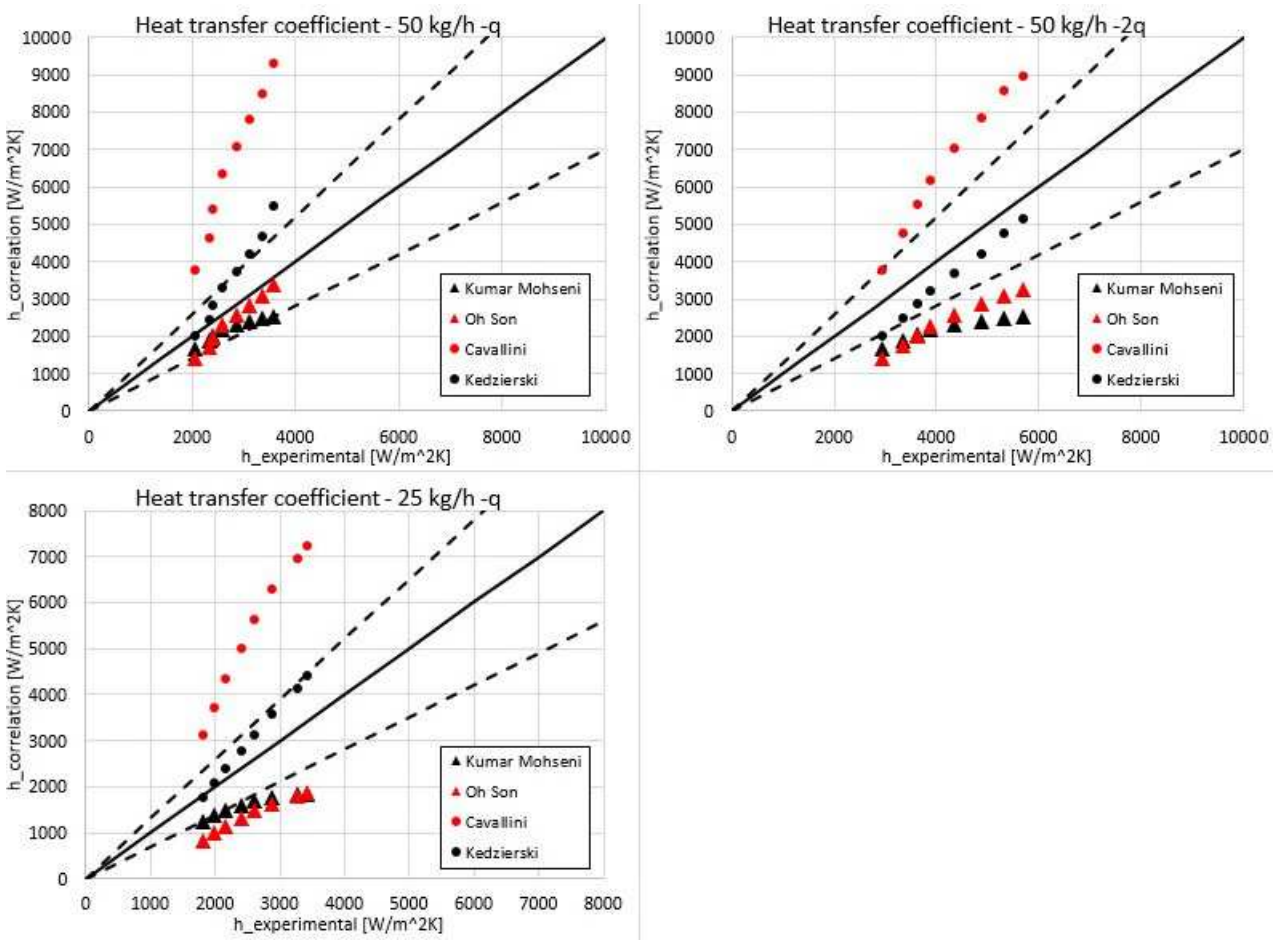

Figure 7.12: Comparison between data and correlation predictions for condensation heat transfer coefficient at low mass flow rate $[25; 50] kg/h$.

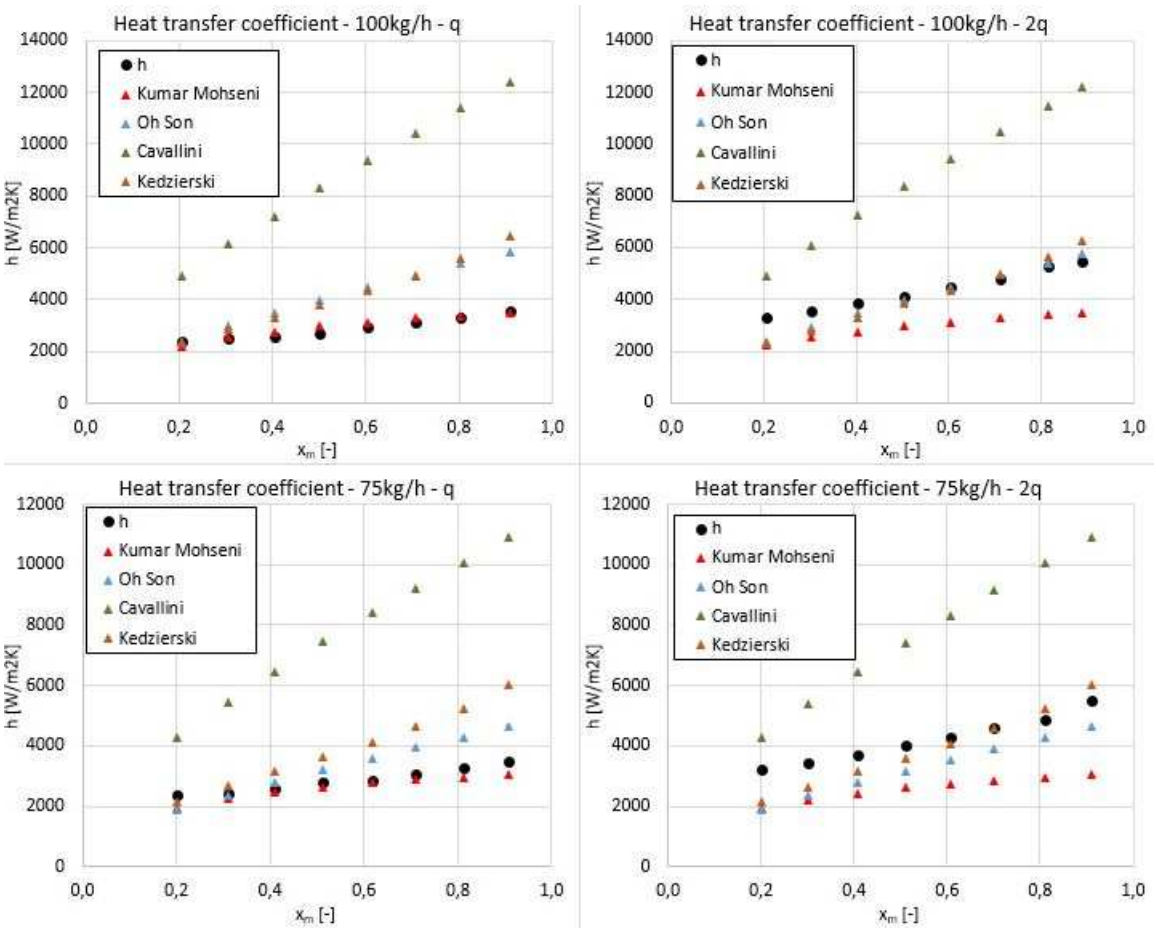

Figure 7.13: Predicted heat transfer coefficient trend with respect to the mean vapor quality at high mass flow rate $[75; 100] kg/h$.

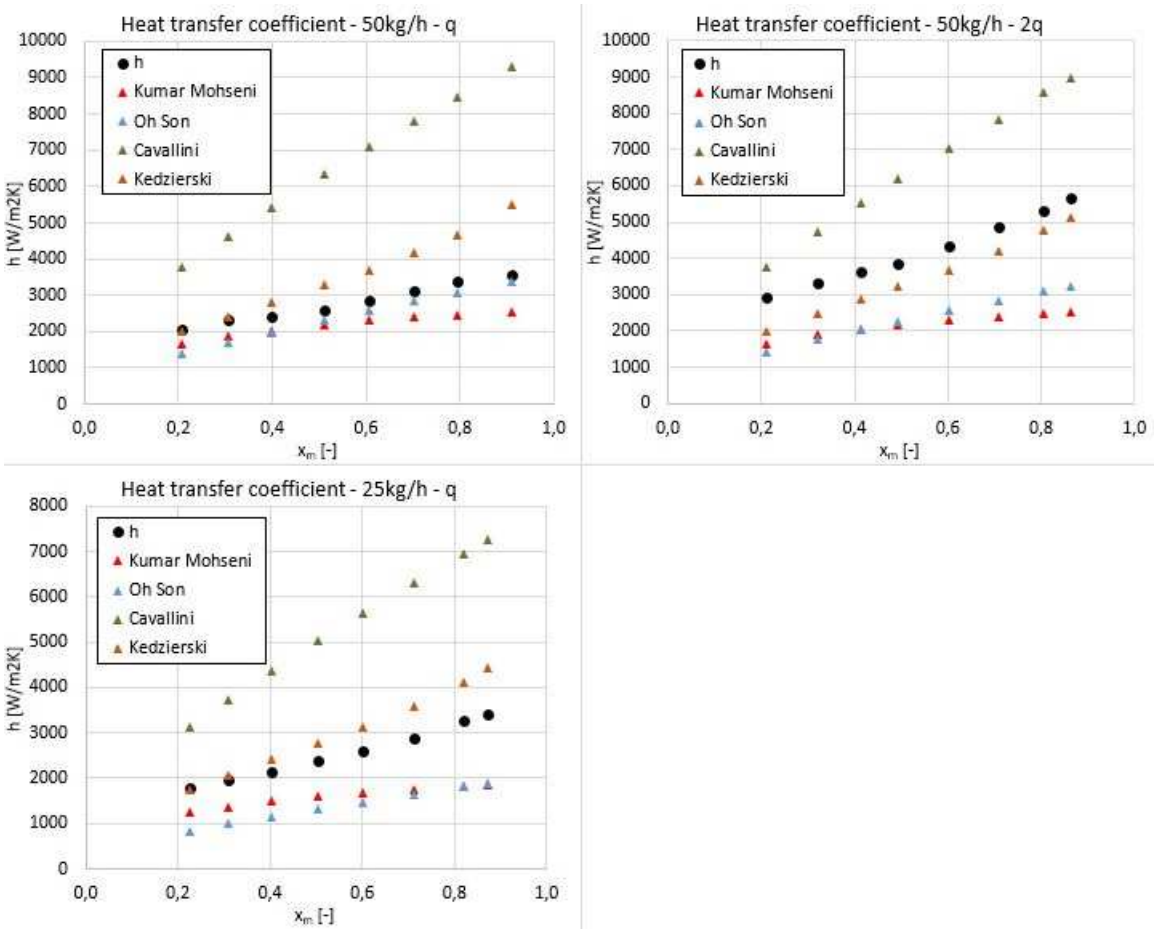

Figure 7.14: Predicted heat transfer coefficient trend with respect to the mean vapor quality at low mass flow rate $[25; 50] kg/h$.

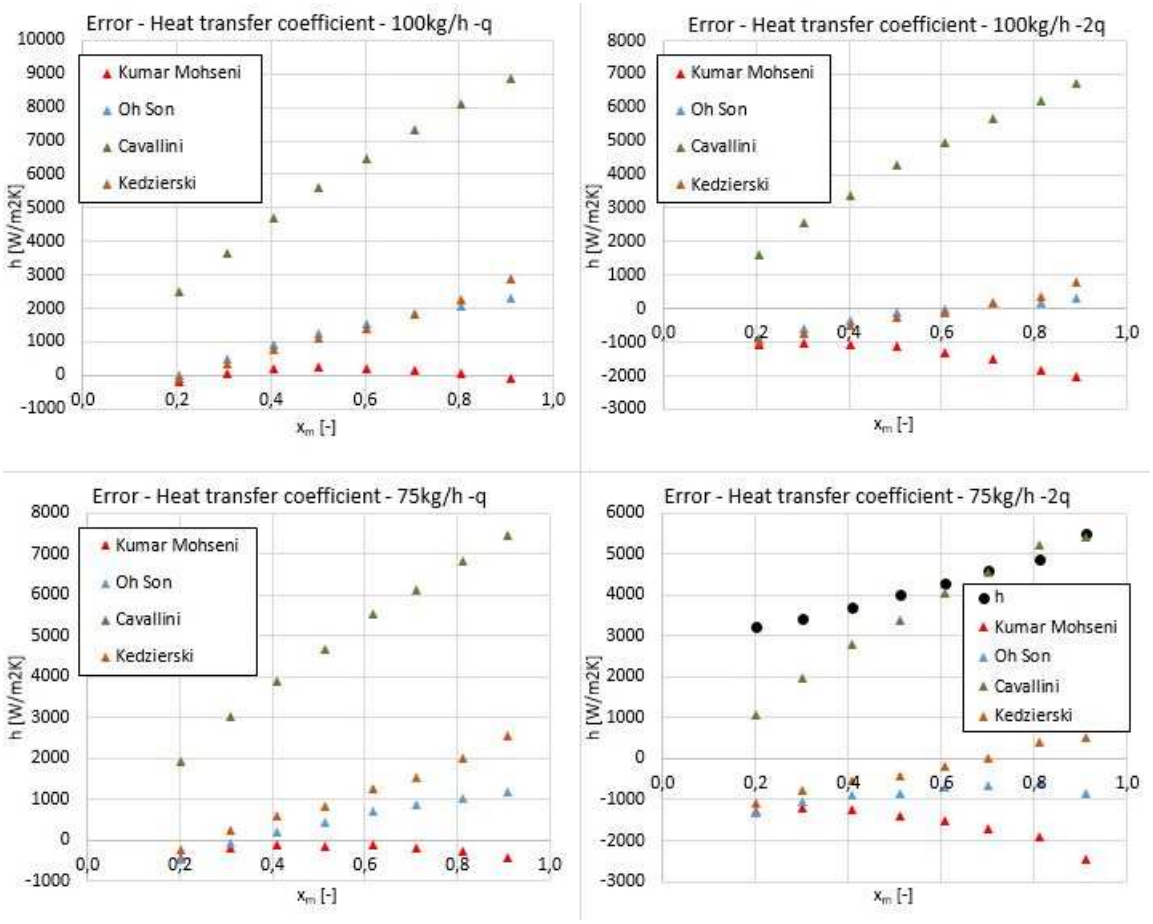

Figure 7.15: Error of predicted heat transfer coefficient with respect to the mean vapor quality at high mass flow rate $[75; 85] kg/h$.

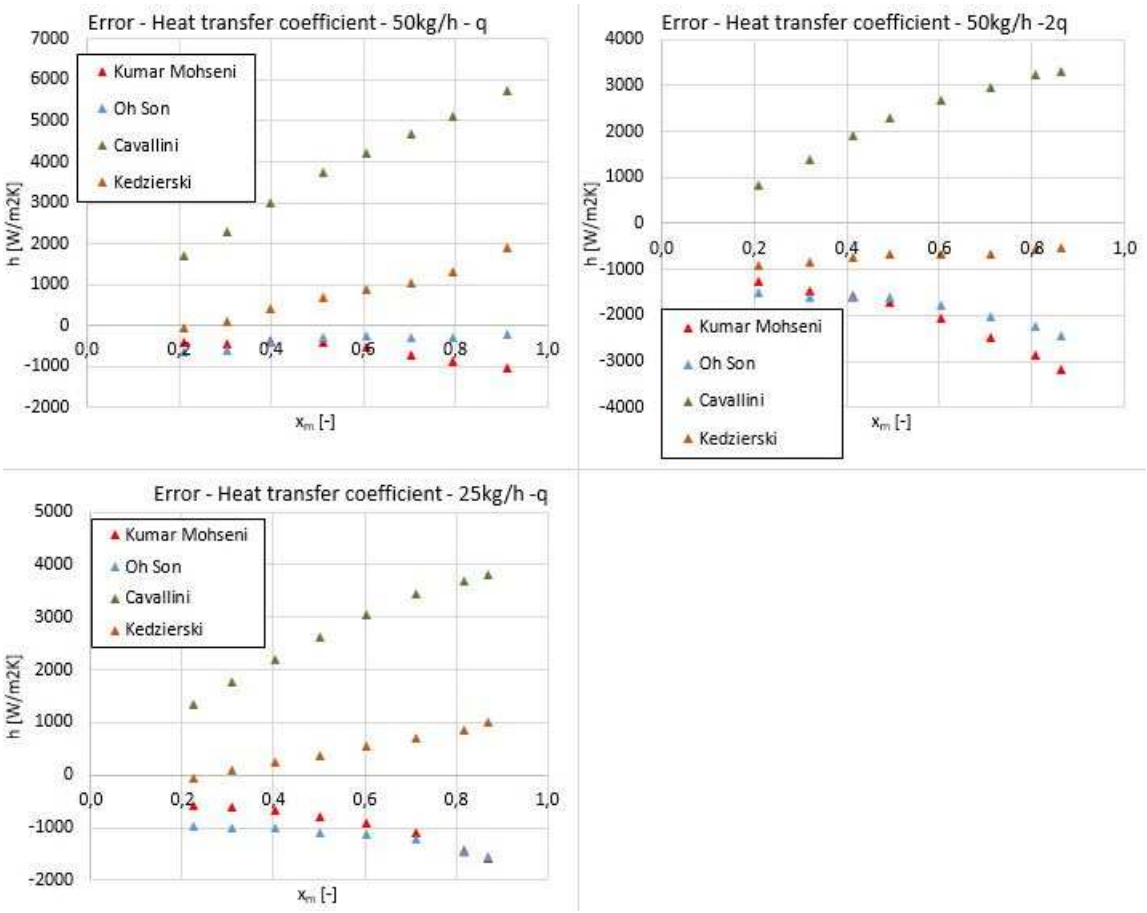

Figure 7.16: Error of predicted heat transfer coefficient with respect to the mean vapor quality at low mass flow rate $[25; 50] kg/h$.

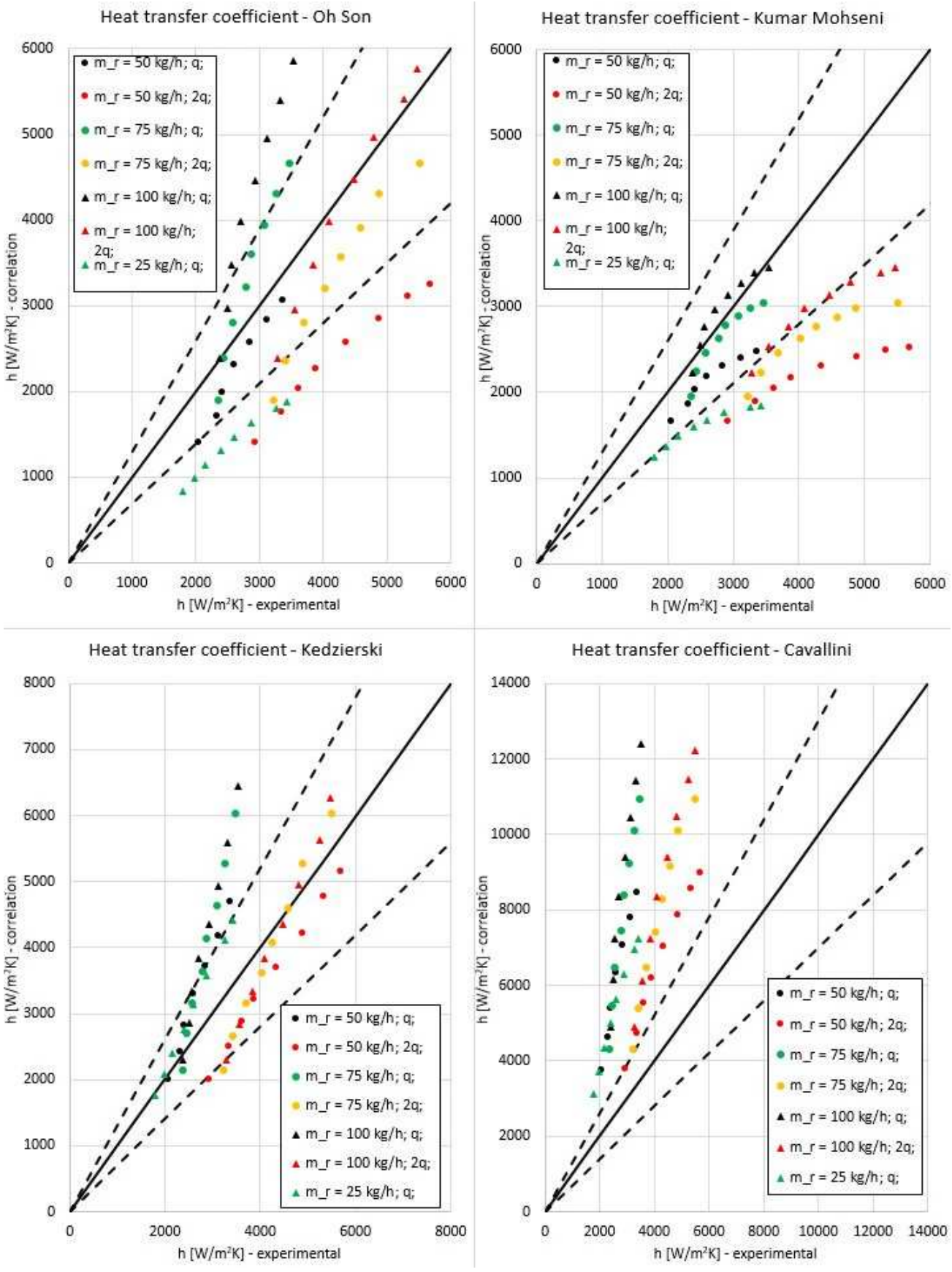

Figure 7.17: Parity plots of each single correlation for condensation heat transfer coefficient.

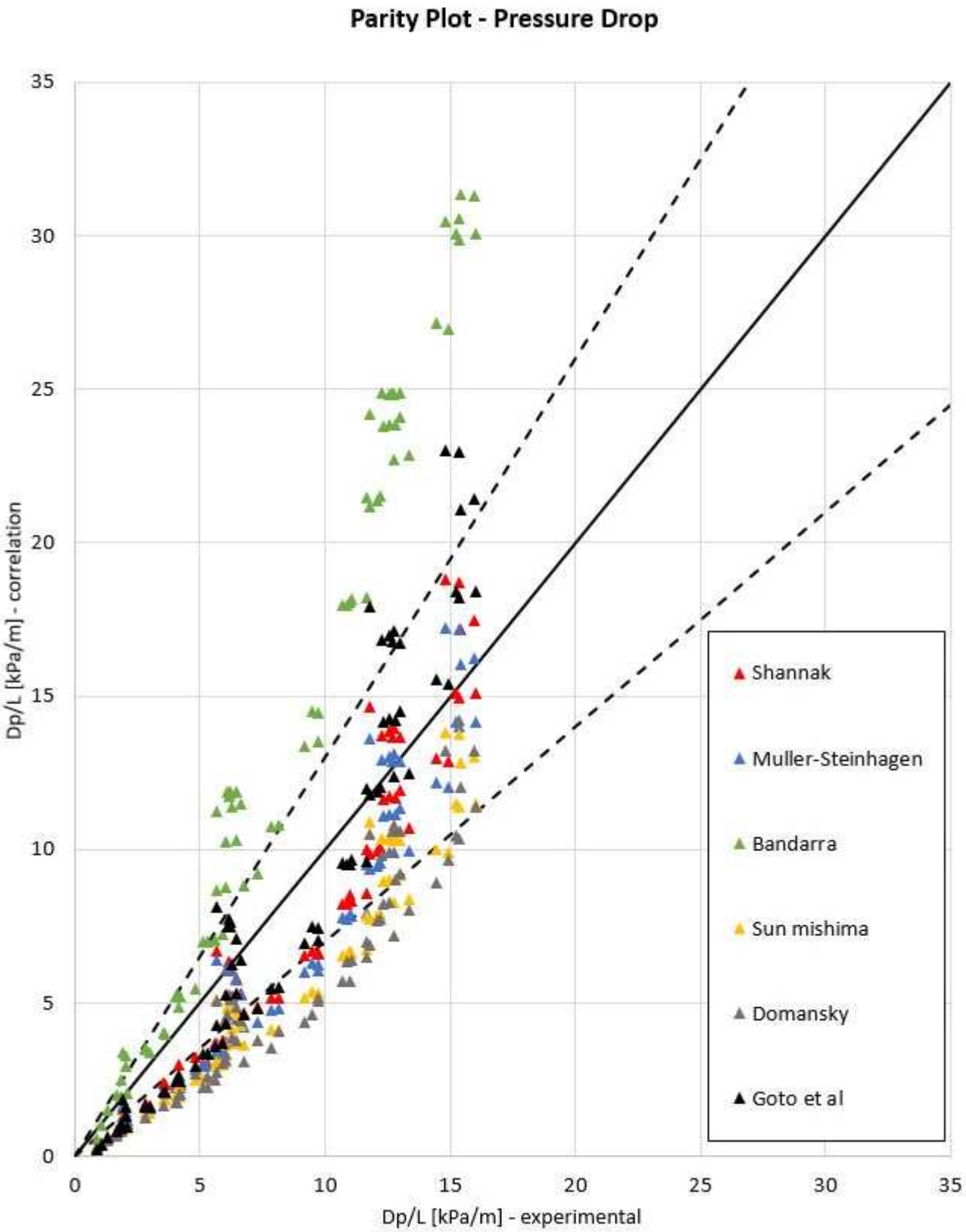

Figure 7.18: Comparison between data and correlation predictions for boiling pressure drop.

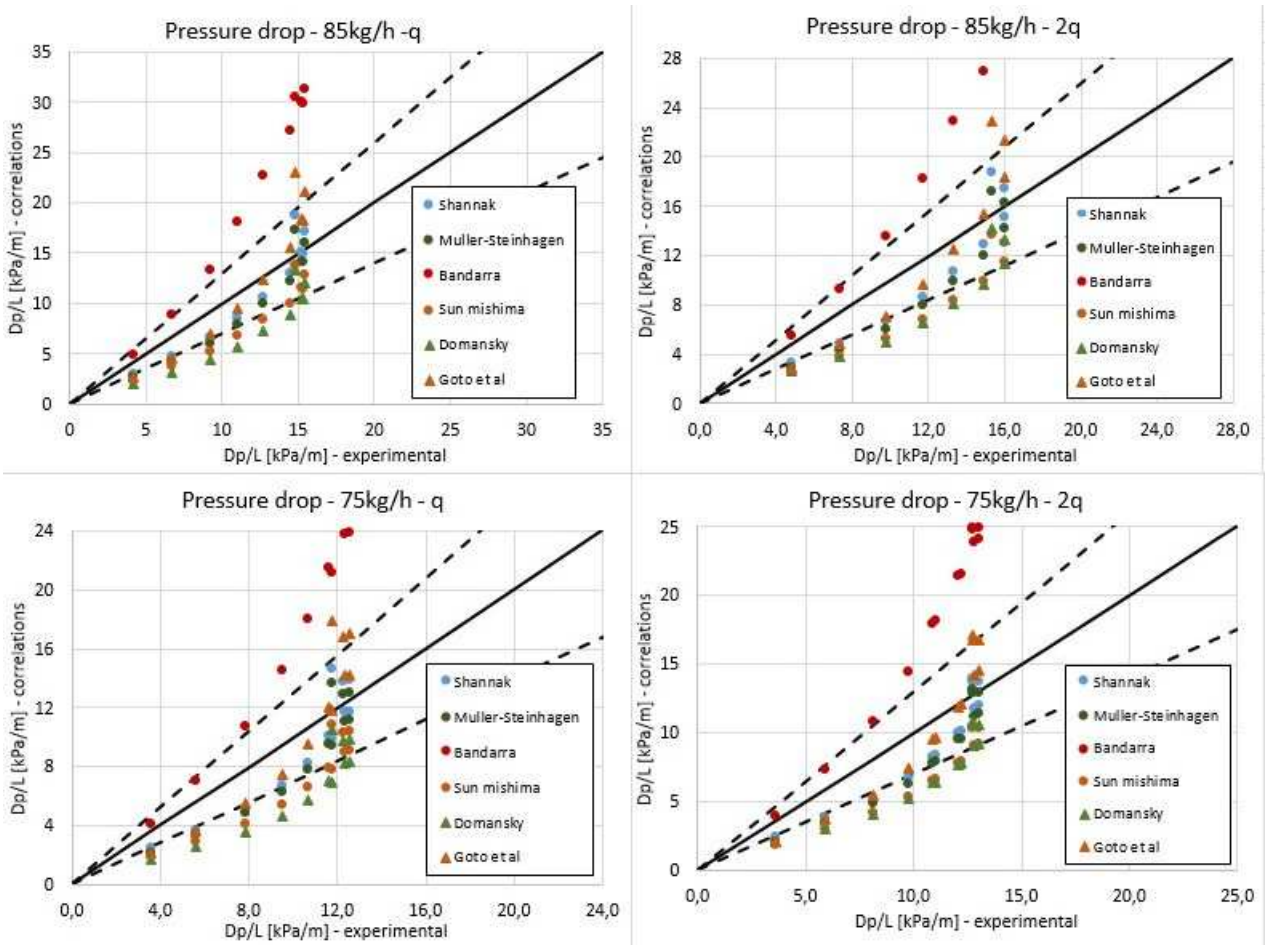

Figure 7.19: Comparison between data and correlation predictions for pressure drop at high mass flow rate $[75; 85] kg/h$.

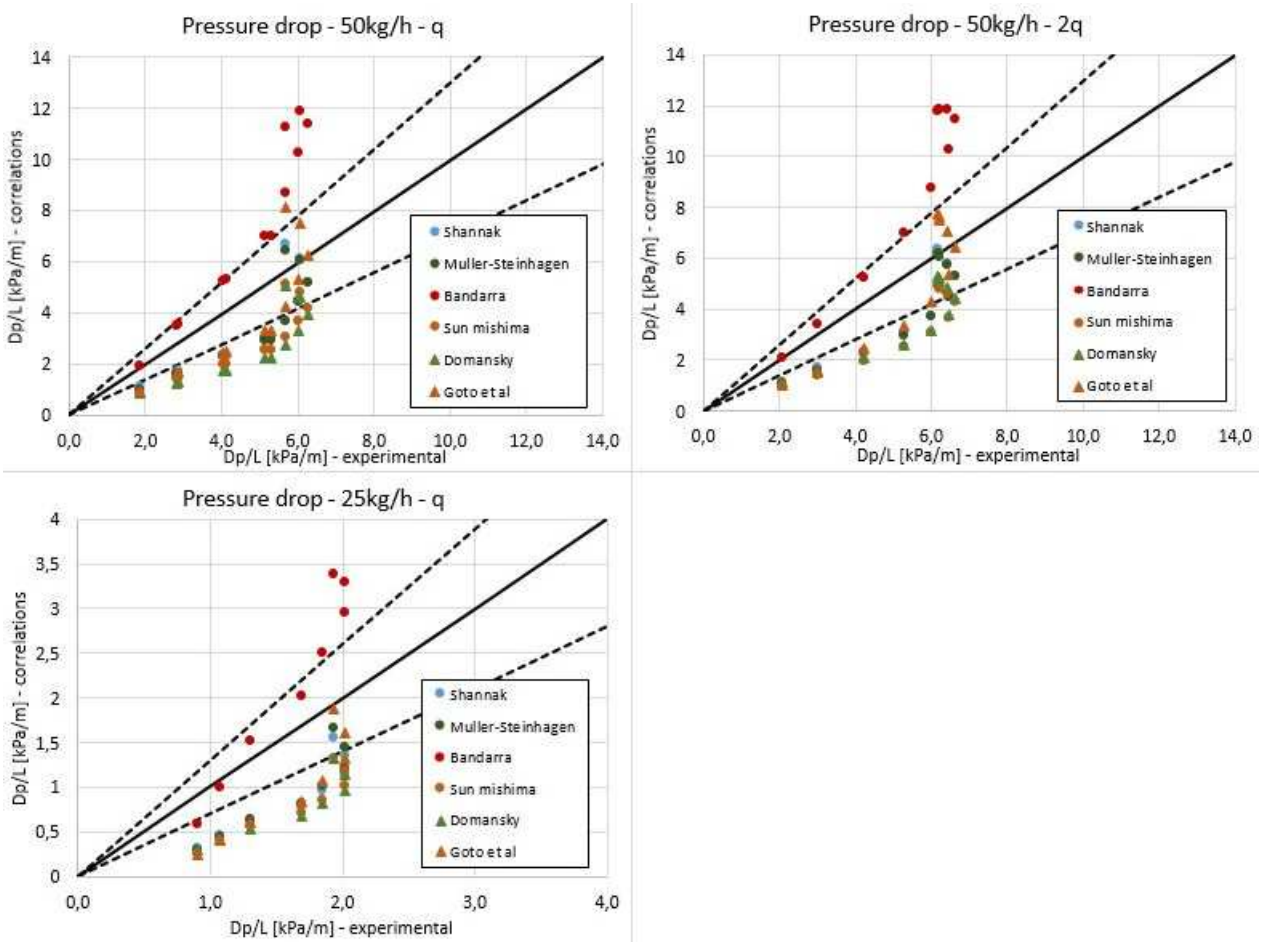

Figure 7.20: Comparison between data and correlation predictions for pressure drop at low mass flow rate $[25; 50] kg/h$.

fig. 7.20). Experimental pressure drop is lower with respect to Bandarra correlation prediction, so that the deviation of this correlation is between ±30% only for low mean vapor quality. All the other analyzed correlations tend to underestimate pressure drop at low vapor quality, while are quite accurate in high vapor quality region for any applied mass flow rate. The correlation that mostly fit with the measurements was developed by Goto et al., as highlighted by tab. 7.3.

From fig. 7.21 and fig. 7.22 the results of experimental pressure drop at low vapor quality is well predicted by many correlations, in particular by Shannak and Goto correlations. The decrease of pressure drop at high vapor quality is not predicted by any of them, since they assume an almost linear behavior for the considered experiments. Bandarra correlation is the only one that shows a similar pressure drop reduction, but it has also the worst predictive performances (see tab. 7.3).

Low deviation of the experimental curves is highlighted by fig. 7.23 and fig. 7.24, where low error values are evident in particular for low vapor quality. The errors of all the correlations are not constant, it means that the trend of pressure drop with the varying mean quality is not well predicted by any developed correlation. Parity plots depicted in fig. 7.25 highlight the relationship between experimental and predicted pressure drop for all the tested conditions.

7.4 Heat transfer coefficient in evaporation condition

Selected correlations for heat transfer coefficient in boiling condition are Murata [13], Yun [14], Han Chen [15], Rollmann and Spindler [16] and Cavallini [17]. An overview of all the predicted data with respect to the measurements is presented in fig. 7.26. The analysis has been performed only for $[25; 50] kg/h$ mass flow rate range, because higher mass flow rate experiments are affected by a discrepancy on the inlet refrigerant temperature (see section 6.2).

In fig. 7.26 is depicted an overview of the analyzed data with respect to their relative correlation predictions. From the chart is results evident the presence of two correlations (Yun [] and Murata []) that exhibit a very high average deviation.

In order to better analyze correlation results, in fig. 7.27are reported the predicted values of heat transfer coefficient in analyzed experimental conditions. From the charts and tab. 7.4 it follows that Han Chen and Rollmann Spindler correlations predict the experimental value with the lowest uncertainty. On the contrary, Cavallini correlation tends to overestimate the heat transfer coefficient, in any experimental condition but the case at $m_r = 50 kg/h$ and double heat flux. Yun and Murata correlation underestimate the heat transfer coefficient, so that their deviations are wider than 30% in any analyzed case. Predictive performances of chosen correlations are reported in tab. 7.4.

From fig. 7.28 the trend of experimental heat transfer coefficient at varying vapor quality is well predicted by Han Chen, Rollmann and Cavallini correlation. Their deviations tends to stay almost constant with mean vapor quality, while Yun and Murata errors increase at high vapor quality. It has to be noticed that Cavallini correlation presents the highest offset from measurements. At high mean quality, errors of correlation are generally greater than those shown at low vapor quality, as highlighted in fig. 7.29.

The fig. 7.30 highlights the performance of each single correlation. Han Chen correlation has best predictive performance, since for the whole range of experiments the deviation of predicted results is between 30%.

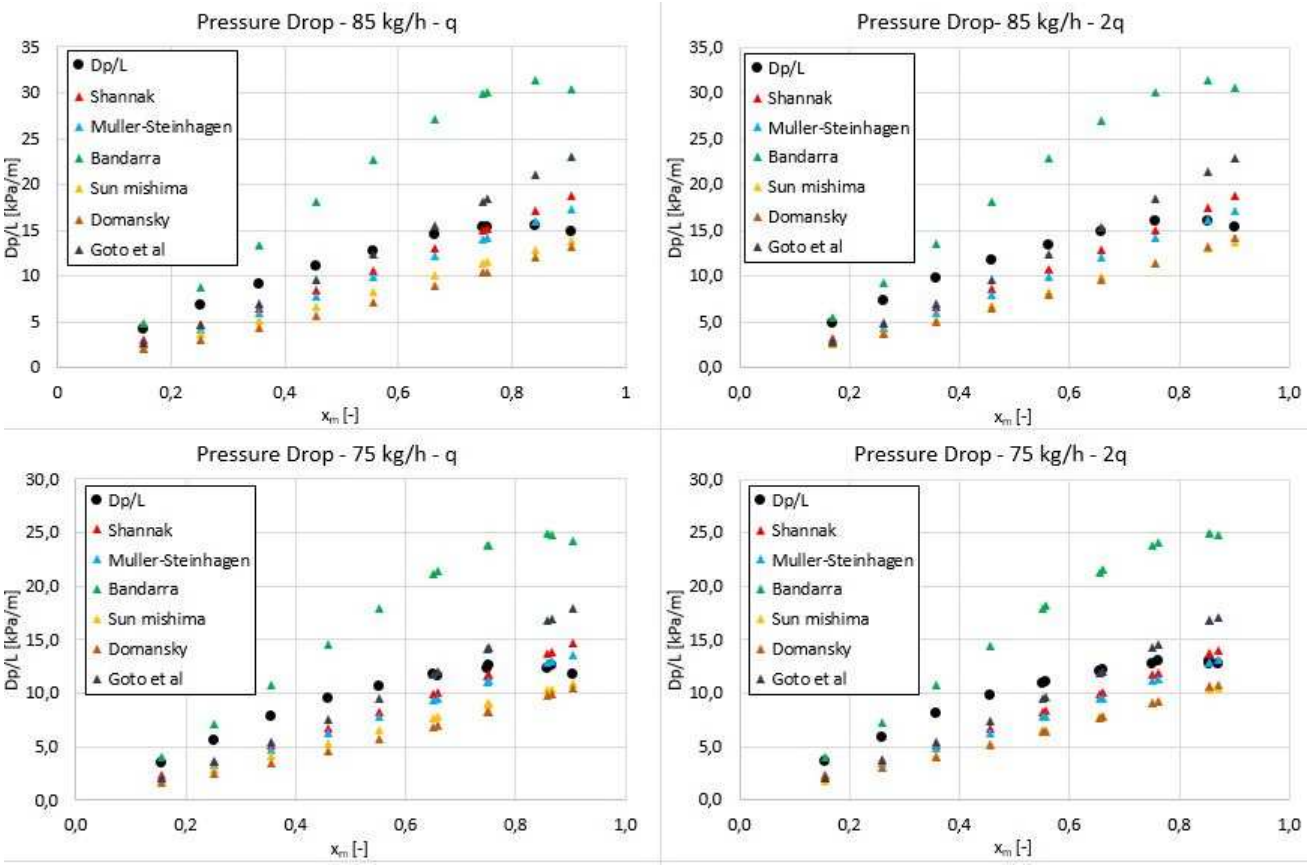

Figure 7.21: Predicted pressure drop trend with respect to the mean vapor quality at high mass flow rate $[75; 85] kg/h$.

	Heat transfer coefficient	
Correlation	$\sigma_{\%}$	$e_{\%}$
Murata	62.4	-62.3
Yun	64.2	-64.5
Han Chen	18.2	-9.3
Rollmann Spindler	24.9	21.6
Cavallini	56.7	52.4

Table 7.4: Mean percentage relative deviation and error of boiling heat transfer coefficient correlations.

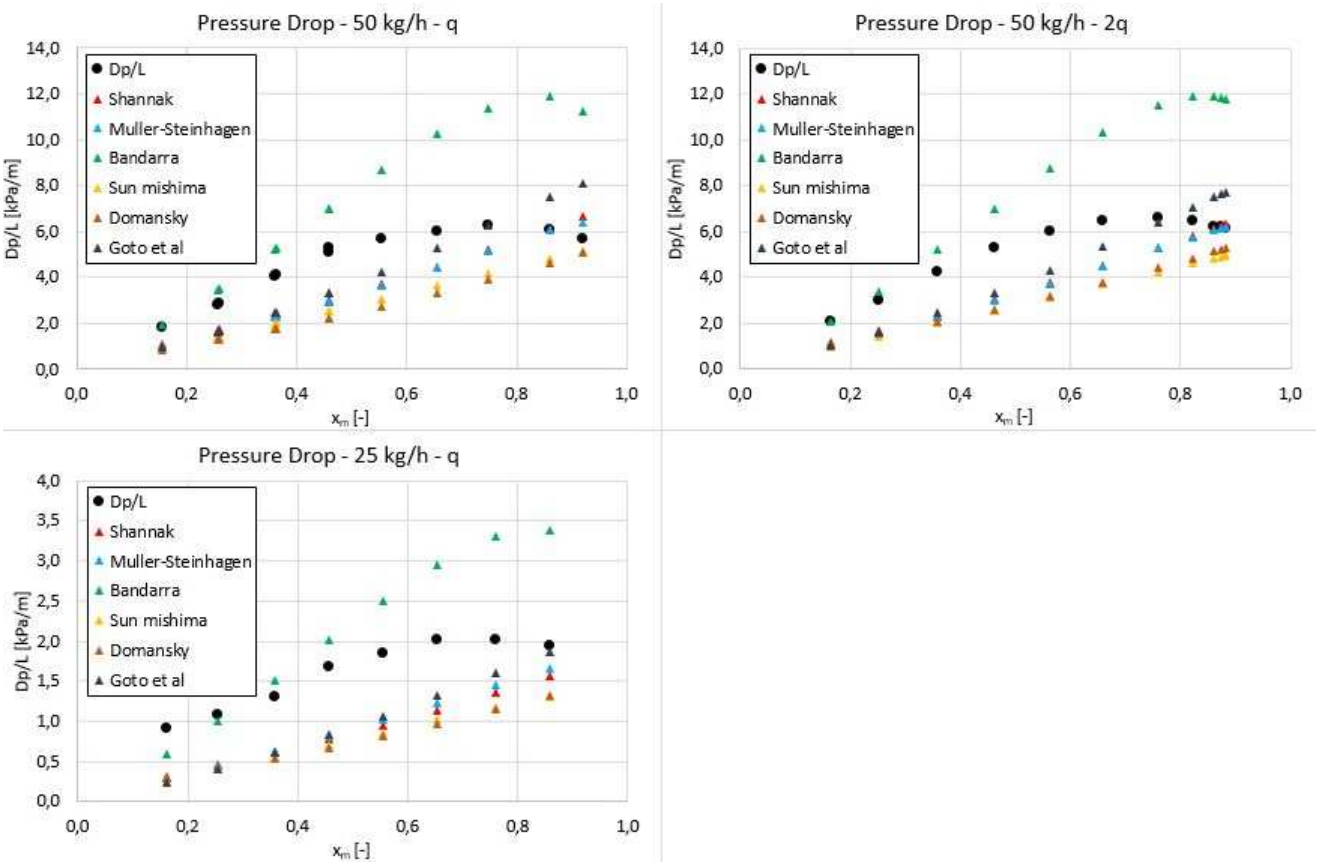

Figure 7.22: Predicted pressure drop trend with respect to the mean vapor quality at low mass flow rate $[25; 50] kg/h$.

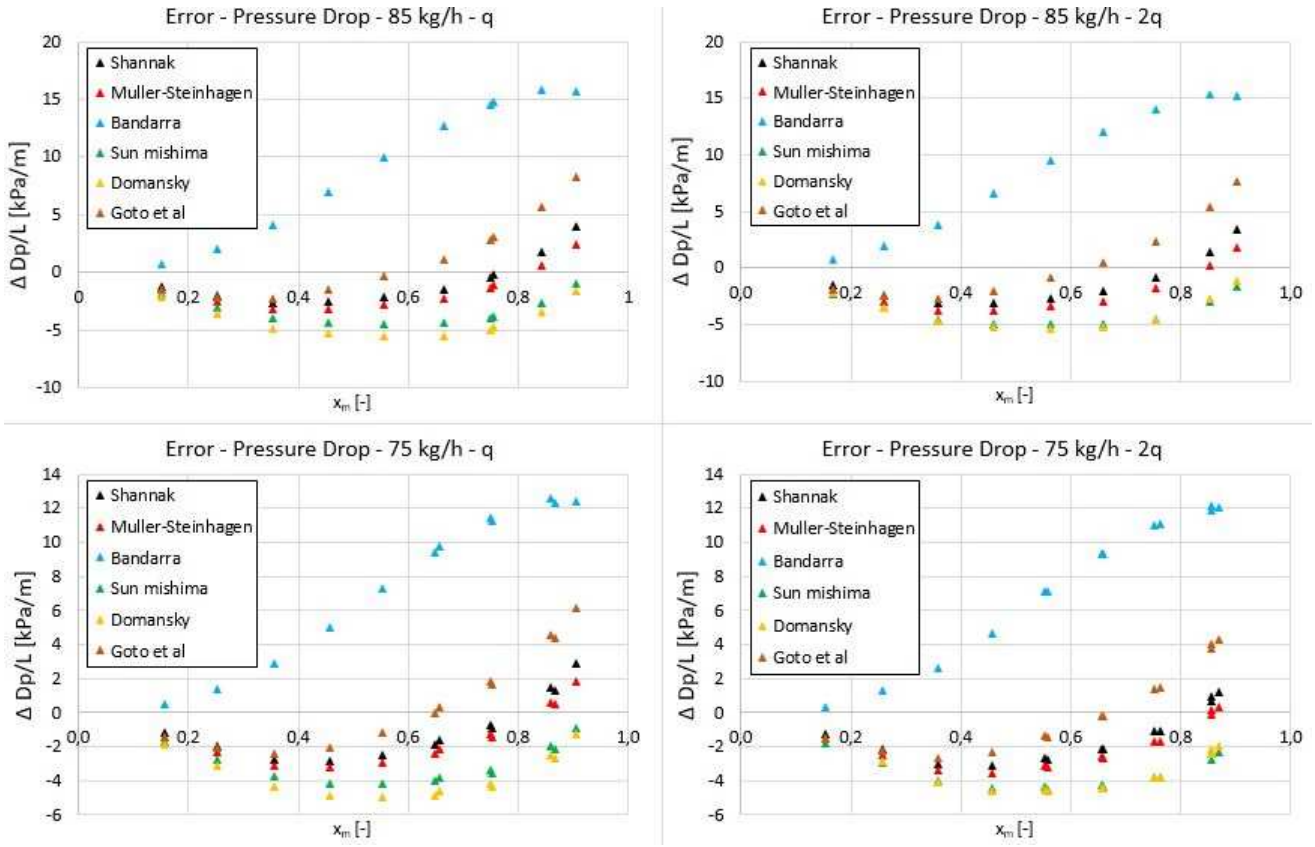

Figure 7.23: Error of predicted pressure drop with respect to the mean vapor quality at high mass flow rate $[75; 85] kg/h$.

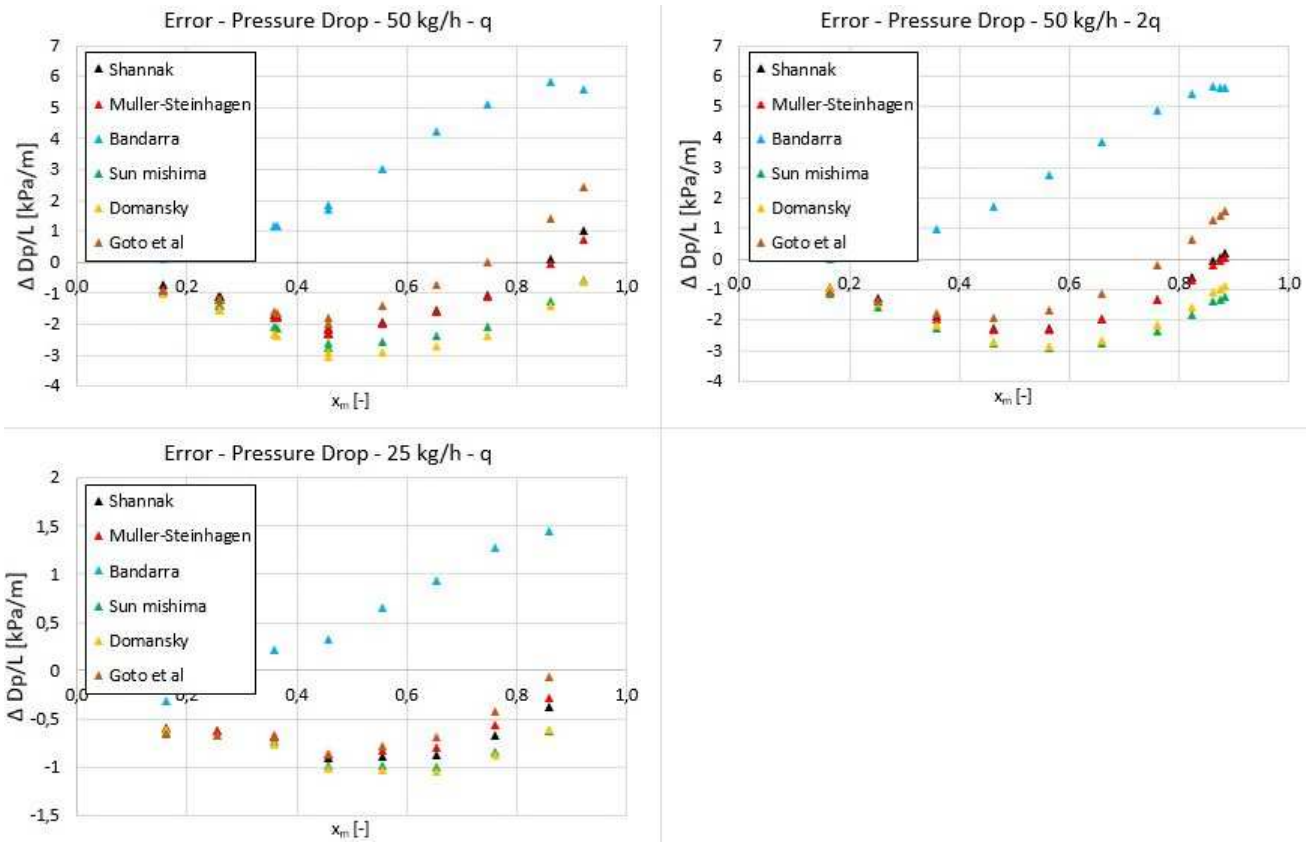

Figure 7.24: Error of predicted pressure drop with respect to the mean vapor quality at low mass flow rate $[25; 50] kg/h$.

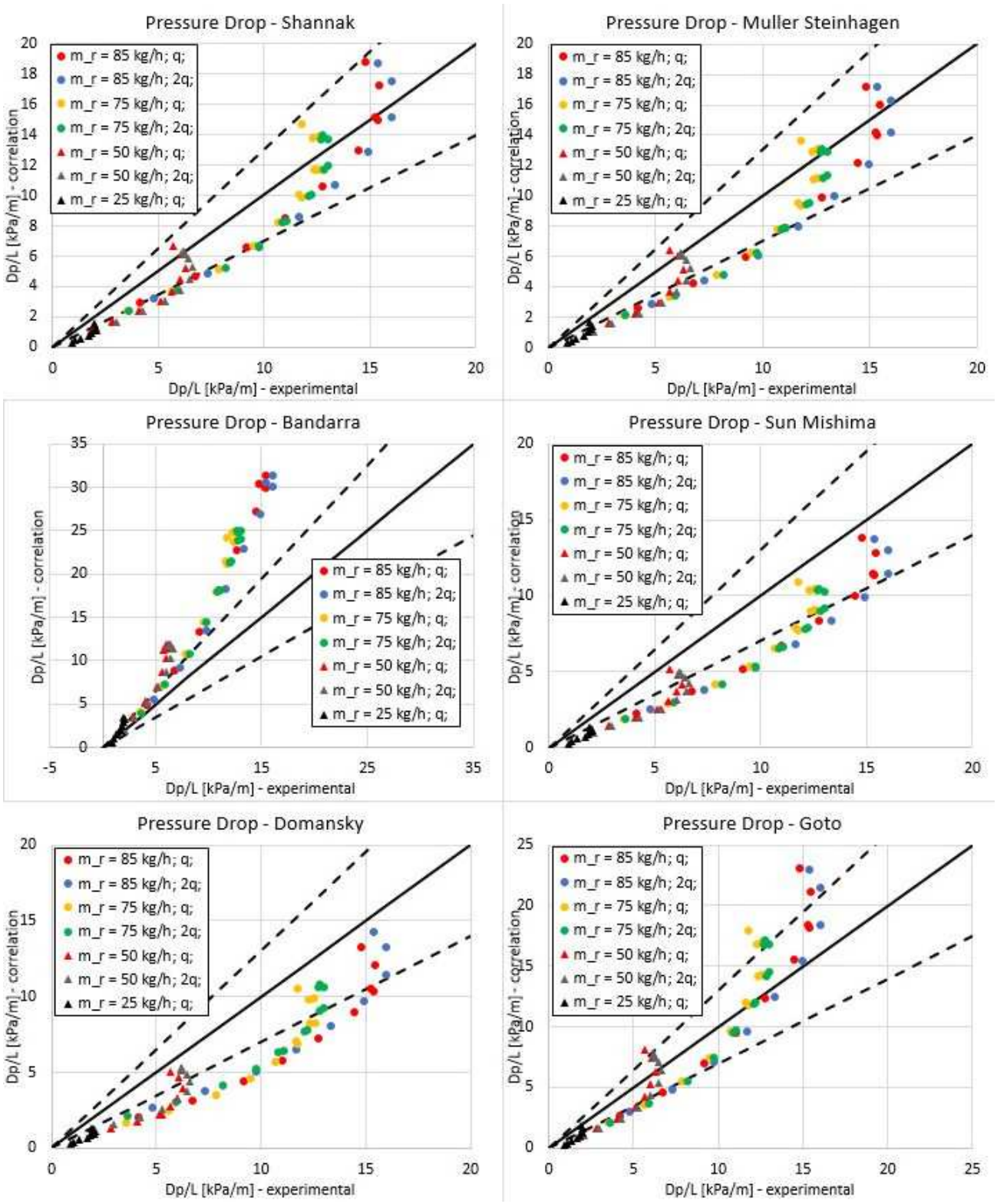

Figure 7.25: Parity plots of each single correlation for boiling pressure drop.

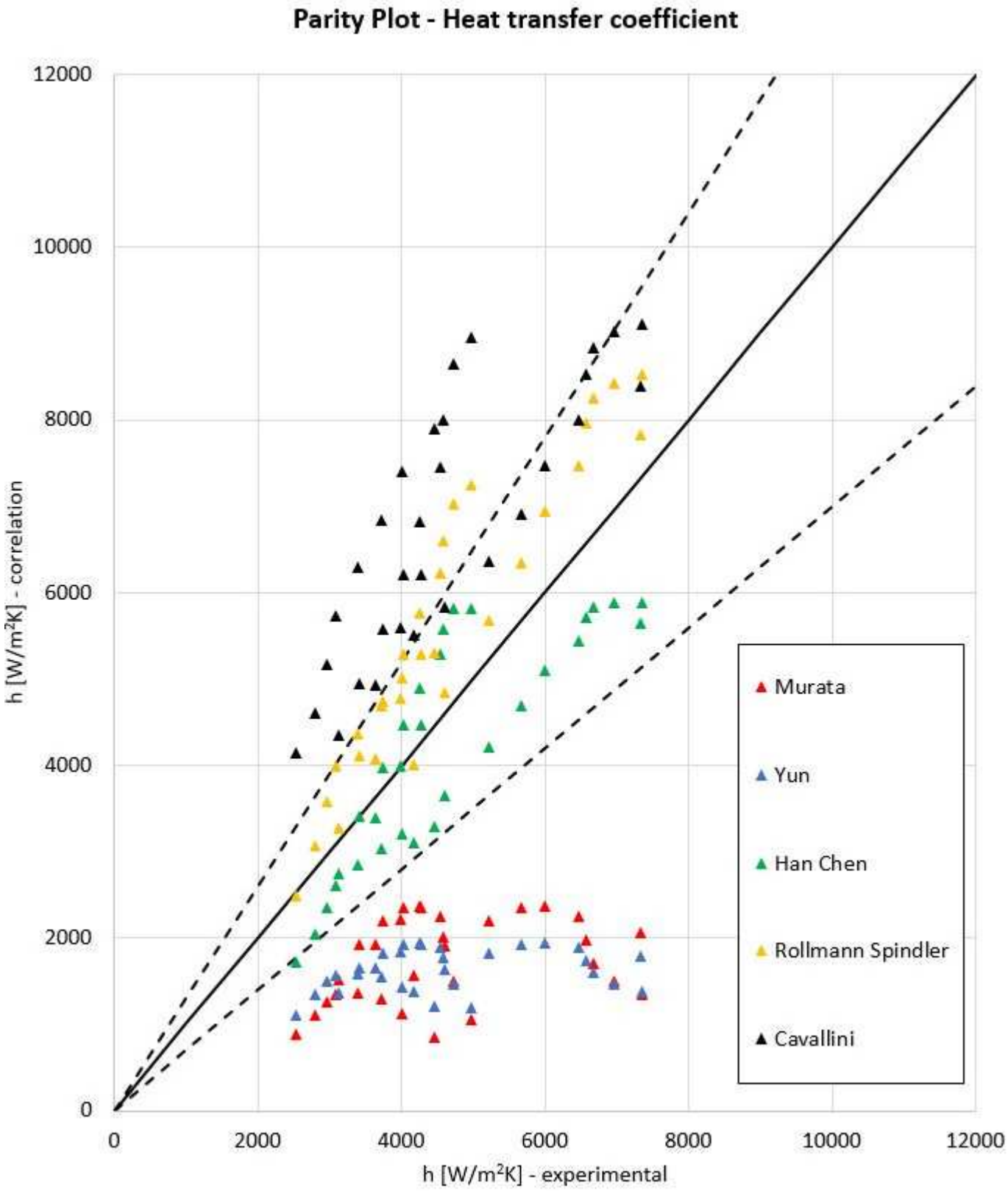

Figure 7.26: Comparison between data and correlation predictions for boiling heat transfer coefficient.

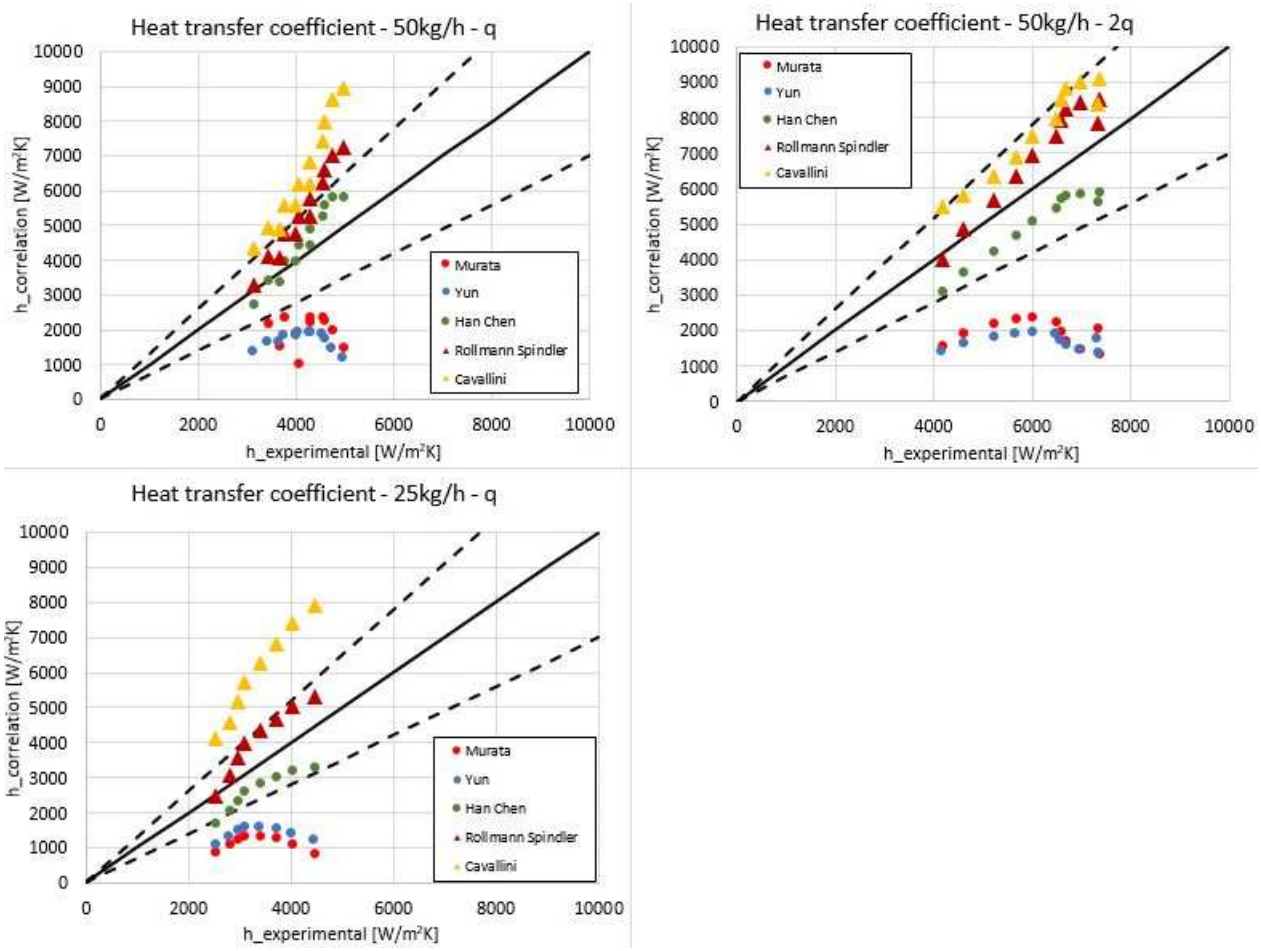

Figure 7.27: Comparison between data and correlation predictions for heat transfer coefficient at low mass flow rate $[25; 50] kg/h$.

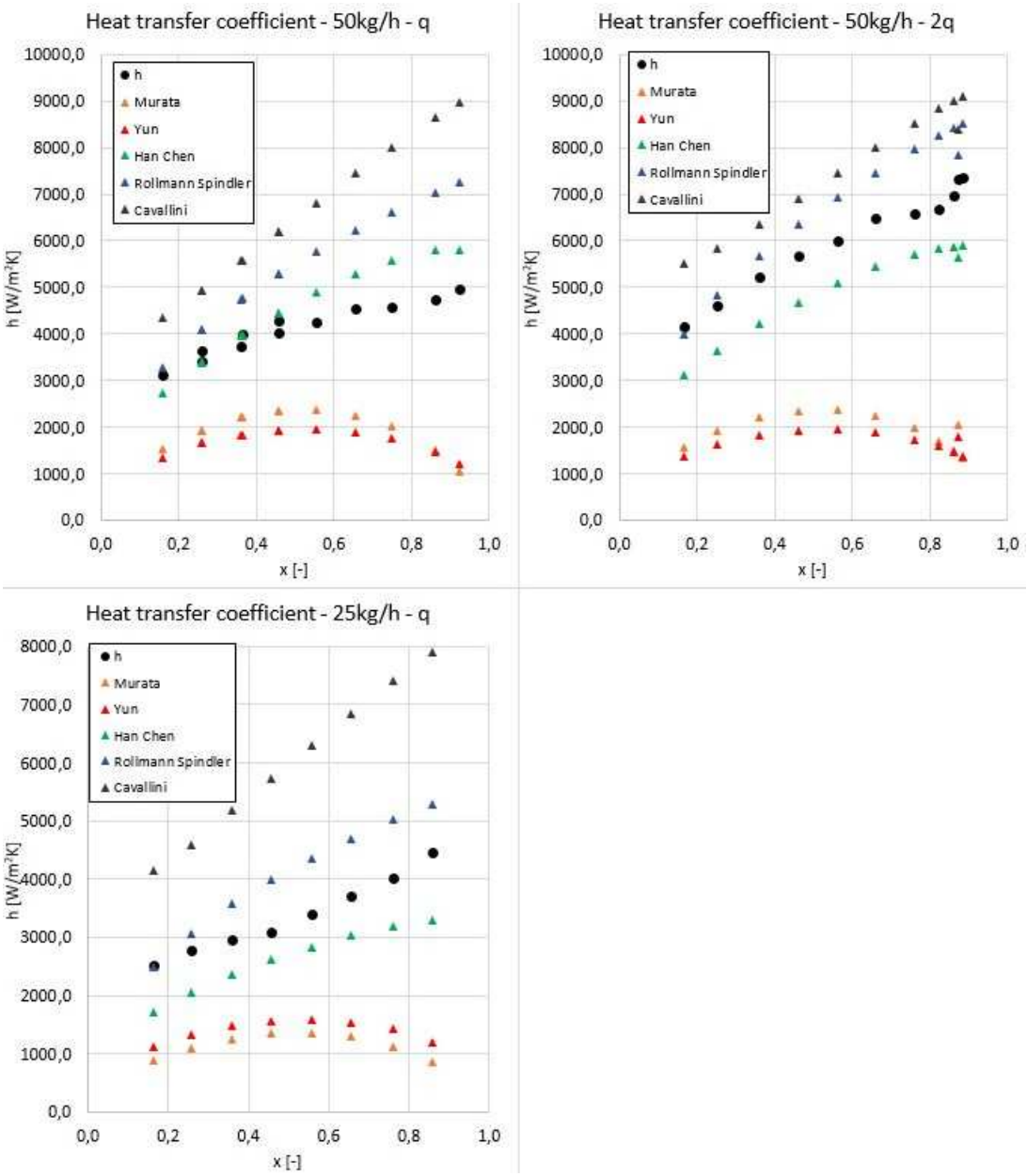

Figure 7.28: Predicted heat transfer coefficient trend with respect to the mean vapor quality at mass flow rate $[25; 50] kg/h$.

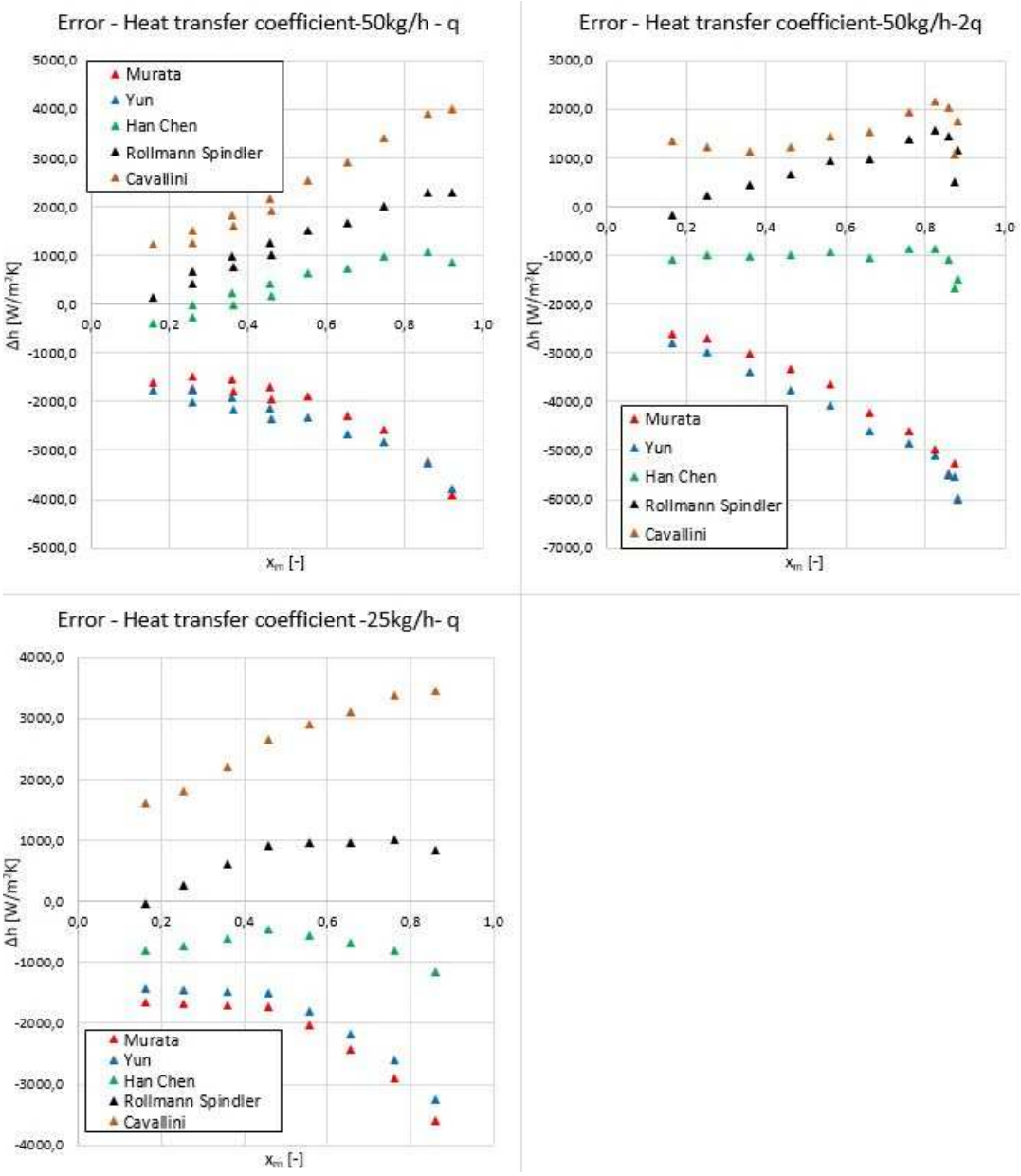

Figure 7.29: Error of predicted heat transfer coefficient with respect to the mean vapor quality at mass flow rate $[25; 50] kg/h$.

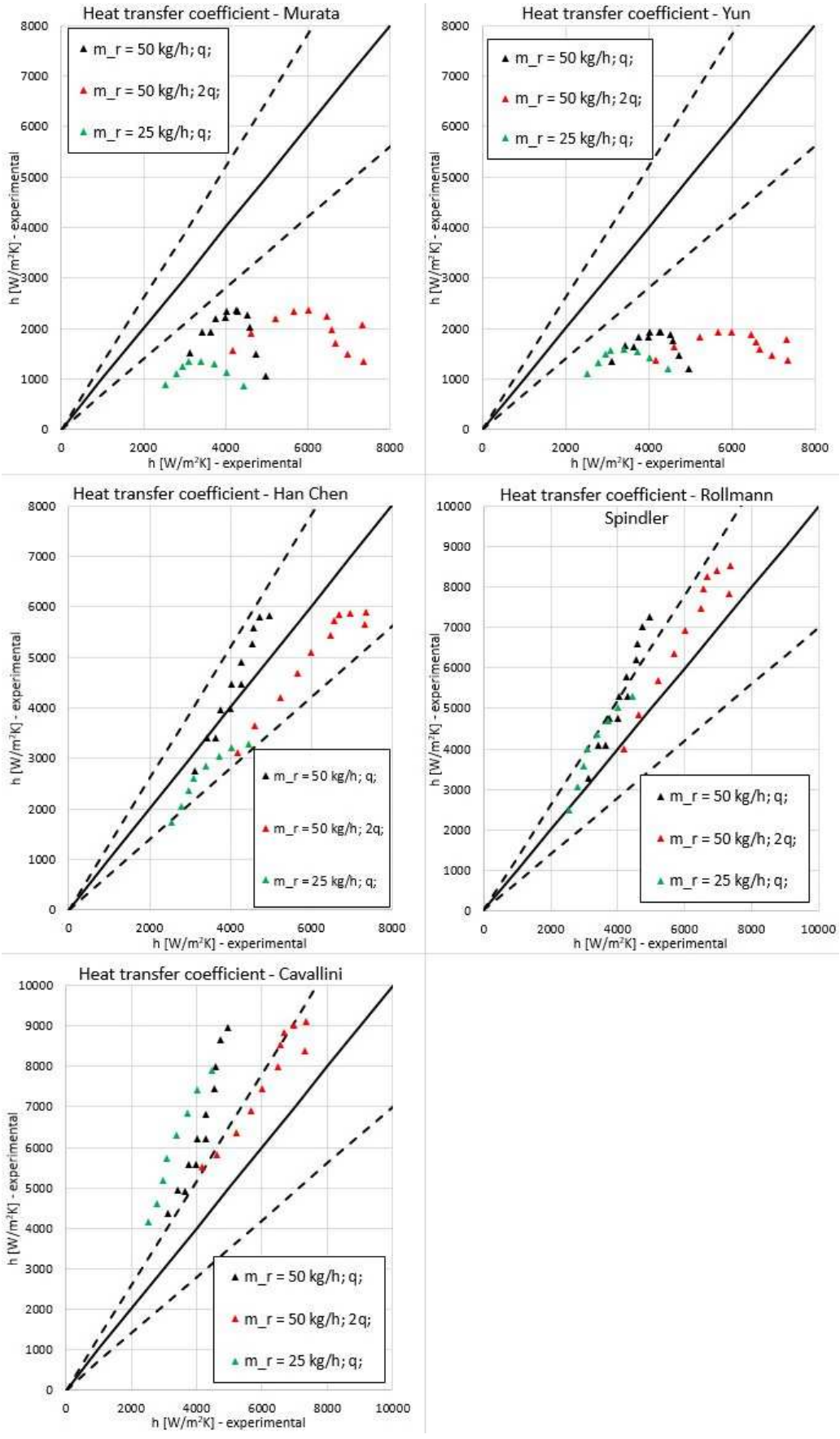

Figure 7.30: Parity plots of each single correlation for boiling heat transfer coefficient.

Chapter 8

Future developments

The thesis concerns the experimental analysis of heat transfer characteristics of microfin tubes and is aimed to combine them with the corresponding flow regimes, which establishes in the tube. The tests were performed, for both evaporation and condensation, to evaluate the heat transfer coefficient and the pressure drop of R134a flowing in a microfin tube. The experiments shows that in appropriate conditions microfin tube has better heat transfer coefficient than smooth tube, heat transfer process is mostly enhanced at high vapor qualities, where pressure drop are close to the smooth tube while heat transfer coefficient is increased.

In the future visualization and flow pattern recognition should be performed so that it would be possible to get information about the influence of microfin geometry on the flow regime transitions. The analysis should be integrated with the maps for the flow pattern condition and transition curves.

The analysis was limited on evaporation experiments, due to the non-equilibrium of the phases at the test section inlet. The discrepancy between the phases conditions leads to consider the data as unreliable, so evaporation heat transfer coefficient could not be investigated properly. In order to solve the problem it is advisable to install a heat exchanger at the test section inlet. The refrigerant will flow in the exchanger so to promote the mixing between the two phases and reach the equilibrium in the test section. A solution could be represented by a helical structure with horizontal axis, where centrifugal and gravity forces ensure the two phases to mix properly. It would be useful to expand the range of operating conditions of the facility, in particular to improve the plant stability at very low refrigerant mass flow rate. This would allow to study heat exchangers in the range of mass flow rate that is exploited usually to compare these devices.

R134a is going to be substituted due to more and more stringent regulation on environmental aspects. New refrigerants R1234ze and R1234yf have been developed to respond the environmental challenge, maintaining the same heat transfer performance of R134a. It would be interesting to perform analysis on these fluids, so that to evaluate their performances on heat transfer processes. The analysis of these innovative fluids on smooth tube could be taken as reference for a further study on microfin tubes.

Bibliography

[1] John G Collier and John R Thome. *Convective boiling and condensation*. Clarendon Press, 1994.

[2] Gad Hetsroni. *Handbook of multiphase systems*, pages 1–1–1–95. Taylor & Francis, 1982.

[3] Xiande Fang, Yu Xu, and Zhanru Zhou. New correlations of single-phase friction factor for turbulent pipe flow and evaluation of existing single-phase friction factor correlations. *Nuclear Engineering and Design*, 241(3):897–902, 2011.

[4] Yu Xu, Xiande Fang, Xianghui Su, Zhanru Zhou, and Weiwei Chen. Evaluation of frictional pressure drop correlations for two-phase flow in pipes. *Nuclear engineering and design*, 253:86–97, 2012.

[5] Licheng Sun and Kaichiro Mishima. Evaluation analysis of prediction methods for two-phase flow pressure drop in mini-channels. *International Journal of Multiphase Flow*, 35(1):47–54, 2009.

[6] H Müller-Steinhagen and K Heck. A simple friction pressure drop correlation for two-phase flow in pipes. *Chemical Engineering and Processing: Process Intensification*, 20(6):297–308, 1986.

[7] Enio P Bandarra Filho, José M Saiz Jabardo, and Paulo EL Barbieri. Convective boiling pressure drop of refrigerant r-134a in horizontal smooth and microfin tubes. *International journal of refrigeration*, 27(8):895–903, 2004.

[8] Benbella A Shannak. Frictional pressure drop of gas liquid two-phase flow in pipes. *Nuclear Engineering and Design*, 238(12):3277–3284, 2008.

[9] Jun-Young Choi, Mark A Kedzierski, and Piotr Domanski. *A generalized pressure drop correlation for evaporation and condensation of alternative refrigerants in smooth and microfin tubes*. US Department of Commerce, Technology Administration, National Institute of Standards and Technology, Building and Fire Research Laboratory, 1999.

[10] Jonathan A Olivier, Leon Liebenberg, Mark A Kedzierski, and Josua P Meyer. Pressure drop during refrigerant condensation inside horizontal smooth, helical microfin, and herringbone microfin tubes. *Journal of Heat Transfer*, 126(5):687–696, 2004.

[11] Hidetaka Haraguchi, Shigeru Koyama, and Tetsu Fujii. Condensation of refrigerants hcf c 22, hfc 134a and hcfc 123 in a horizontal smooth tube (1st report, proposals of empirical expressions for the local frictional pressure drop). *Nihon Kikai Gakkai Ronbunshu, B*

Hen/Transactions of the Japan Society of Mechanical Engineers, Part B, 60(574):2111–2116, 1994.

[12] M Goto, N Inoue, and N Ishiwatari. Condensation and evaporation heat transfer of r410a inside internally grooved horizontal tubes. *International Journal of Refrigeration*, 24(7):628–638, 2001.

[13] K Murata and K Hashizume. Forced convective boiling of nonazeotropic refrigerant mixtures inside tubes. *Journal of heat transfer*, 115(3):680–689, 1993.

[14] Rin Yun, Yongchan Kim, Kookjeong Seo, and Ho Young Kim. A generalized correlation for evaporation heat transfer of refrigerants in micro-fin tubes. *International journal of heat and mass transfer*, 45(10):2003–2010, 2002.

[15] XH Han, YB Fang, M Wu, XG Qiao, and GM Chen. Study on flow boiling heat transfer characteristics of r161/oil mixture inside horizontal micro-fin tube. *International Journal of Heat and Mass Transfer*, 104:276–287, 2017.

[16] P Rollmann, K Spindler, and H Müller-Steinhagen. Heat transfer, pressure drop and flow patterns during flow boiling of r407c in a horizontal microfin tube. *Heat and mass transfer*, 47(8):951, 2011.

[17] Andrea Padovan, Davide Del Col, and Luisa Rossetto. Experimental study on flow boiling of r134a and r410a in a horizontal microfin tube at high saturation temperatures. *Applied Thermal Engineering*, 31(17-18):3814–3826, 2011.

[18] MA Akhavan-Behabadi, Ravi Kumar, and SG Mohseni. Condensation heat transfer of r-134a inside a microfin tube with different tube inclinations. *International Journal of Heat and Mass Transfer*, 50(23-24):4864–4871, 2007.

[19] Hoo-Kyu Oh and Chang-Hyo Son. Condensation heat transfer characteristics of r-22, r-134a and r-410a in a single circular microtube. *Experimental Thermal and Fluid Science*, 35(4):706–716, 2011.

[20] A Cavallini, D Del Col, S Mancin, and L Rossetto. Condensation of pure and near-azeotropic refrigerants in microfin tubes: A new computational procedure. *International Journal of Refrigeration*, 32(1):162–174, 2009.

[21] Mark Kedzierski and JM Goncalves. Horizontal convective condensation of alternative refrigerants within a micro-fin tube. *Journal of Enhanced Heat Transfer*, 6(2-4), 1999.

[22] R.L.Simpson. A generalized correlation of roughness density effect on the turbulent boundary layer. *AIAA Journal*, 11, 1973.

[23] J.Weisman, D.Duncan, J.Gibson, and C.Crawford. Effects of fluid properties and pipe diameter on two phase flow pattern in horizontal lines. *International Journal of Multiphase Flow*, 5:437–462, 1979.

[24] LPM Colombo, A Lucchini, and A Muzzio. Flow patterns, heat transfer and pressure drop for evaporation and condensation of r134a in microfin tubes. *International Journal of Refrigeration*, 35(8):2150–2165, 2012.